4ème Ligne de Lumière CRG-FAME à l'ESRF

Sommaire

Résumé

La qualité scientifique et technique de la ligne est mise en avant par les 18 publications, 14 actes de colloques et 42 communications orales pour 2003 et 2004. La demande croissante en temps faisceau (+6% en 2005 par rapport à 2004, +44% par rapport à 2003) est également symptomatique de ce bon fonctionnement. Deux exemples scientifiques sont mis en exergue, dans le domaine des sciences de l'univers (G. Pokrovski *et al.*) et de l'environnement (A. Manceau *et al.*), domaine de recherche représentant la moitié environ des activités de la ligne.

L'année 2004 a été marquée par de nombreuses améliorations techniques, la plus importante financièrement parlant étant la mise en place et le pilotage d'une vanne cryogénique motorisée. Cette installation, couplée à la réalisation d'un système de régulation de la température du 1er cristal du monochromateur, a permis d'améliorer très nettement la stabilité de la ligne. Nous disposons maintenant de 2 montages complet (Si(111) et Si(220)) du 2nd cristal du monochromateur avec dans chaque cas un 2ème courbeur complet.

Les expériences sur la ligne FAME nécessitent de plus en plus l'utilisation du cryostat à hélium liquide, afin de protéger les échantillons des dégâts d'irradiation dans la plupart des cas : 18% des

expériences en 2003, environ 30% en 2004 soit une consommation de 15 bouteilles de 100 litres à raison de 5€/l. Pour limiter les effets du faisceau à moindre coût, nous avons mis en place en amont de l'échantillon un « shutter » expérimental pour le protéger pendant les phases de réglage et ne l'irradier que pendant les acquisitions.

Les demandes d'investissement pour 2005 visent toutes à continuer l'amélioration de la stabilité de la ligne. Une 2nde vanne pointeau motorisée permettra de finaliser la régulation du débit d'azote liquide dans le monochromateur. Le remplacement du bloc support du 1er cristal du monochromateur par un pont thermique plus rigide améliorera encore l'amortissement des vibrations éventuelles. Enfin, la mise en place d'un XBPM, pour mesurer la position (hauteur et angle) du faisceau X incident sur la ligne, permettra de corriger et donc de s'affranchir des variations de la position du faisceau d'électrons dans l'anneau.

Le détecteur de fluorescence Canberra 30-éléments est réparé. Le coût de la réparation est pris partiellement en charge par l'assurance, la partie restant à notre charge étant de 46k€. Cet incident a nécessité l'annulation de quelques expériences en septembre 2004. A cette période en effet, il n'a pas été possible de se faire prêter un autre détecteur multi-éléments. D'avril à juillet, nous avons utilisé le détecteur de la ligne CRG-SNBL, pour la dernière expérience d'août celui de la ligne ID26 et pour la première semaine d'octobre celui de la ligne BM29.

L'électronique analogique du détecteur nécessite des frais (réparations de cartes électroniques) et n'est pas complètement adapté pour la future station de micro-faisceau (il n'est pas possible d'enregistrer simultanément plus de 2 raies de fluorescence, ce qui est incompatible avec la mesure de cartes de fluorescence X). Nous avons donc, comme l'année passée, déposé une demande de financement dans le cadre des mi-lourds CNRS-SDU, pour une électronique numérique de type XIA (identique à celles opérationnelles sur les lignes BM29, ID26, BM01 de l'ESRF et la ligne µfaisceau 10.3.2 de l'ALS). Cette demande financière pourrait bien sûr compléter un financement spécifique pour cette opération attribué par le CA.

Le projet micro-faisceau avance également bien du point de vue de la conception de l'optique et de l'environnement échantillon : un état des lieux du projet est présenté ici. Les premiers essais devraient avoir lieu fin 2005.

Un autre projet nous tient particulièrement à cœur pour 2005, l'organisation d'une formation pour les utilisateurs de la ligne, FAME+ (Formation en Absorption X pour la Maîtrise de l'Expérience et le Pilotage d'une Ligne Utilisant un Synchrotron). Un dossier a été monté dans ce sens avec la formation permanente du CNRS.

Côté personnel, Vivian Nassif (post-doc CEA/Grenoble) a rejoint l'équipe en juin. Olivier Proux a réussi le concours ITA du CNRS et est maintenant en CDI (IR CNRS, LGIT). En 2005, un nouveau post-doc du CEA/Cadarache va rejoindre l'équipe FAME (Hervé Palancher). Jean-Jacques Menthonnex partira en retraite en septembre 2005. Son remplacement est impératif afin de ne pas handicaper le fonctionnement de la ligne.

Statistiques

Répartition du temps de faisceau sur FAME en 2004

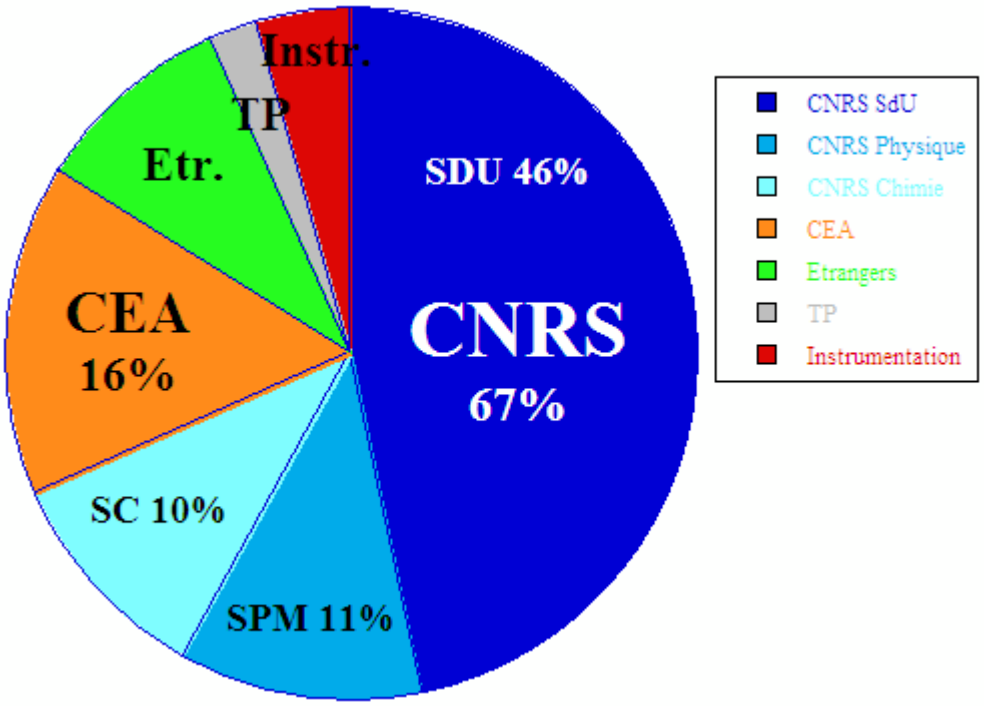

Figure 1: Répartition du temps de faisceau sur la ligne FAME pour l'année 2004 (comités de programme CRG et ESRF, instrumentation et enseignement)

Evolution de l'attribution et des demandes de temps de faisceau :

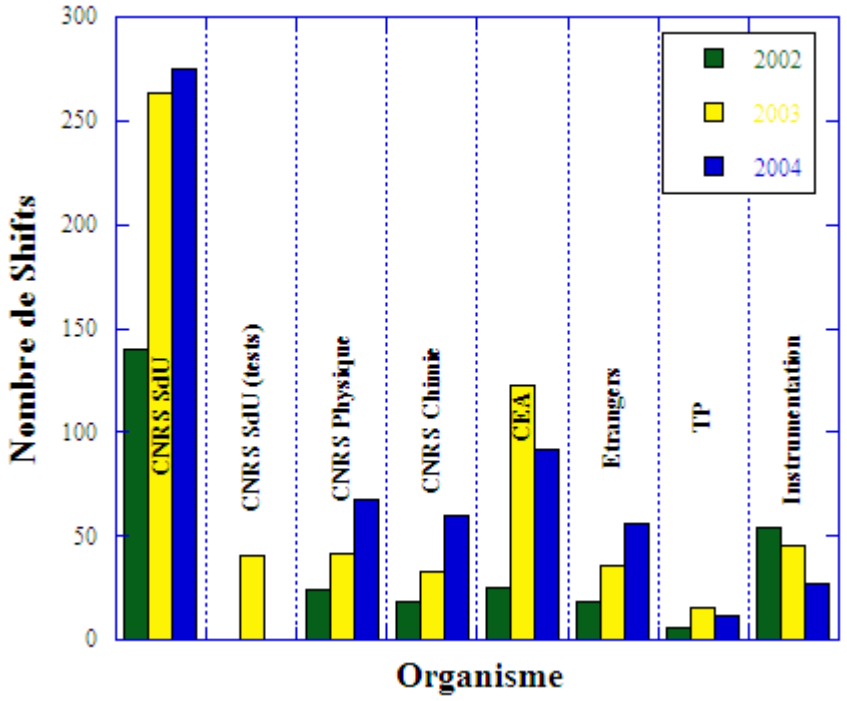

Figure 2 : Evolution de la répartition du temps de faisceau sur la ligne FAME entre 2002 et 2004 en fonction des organismes de recherche

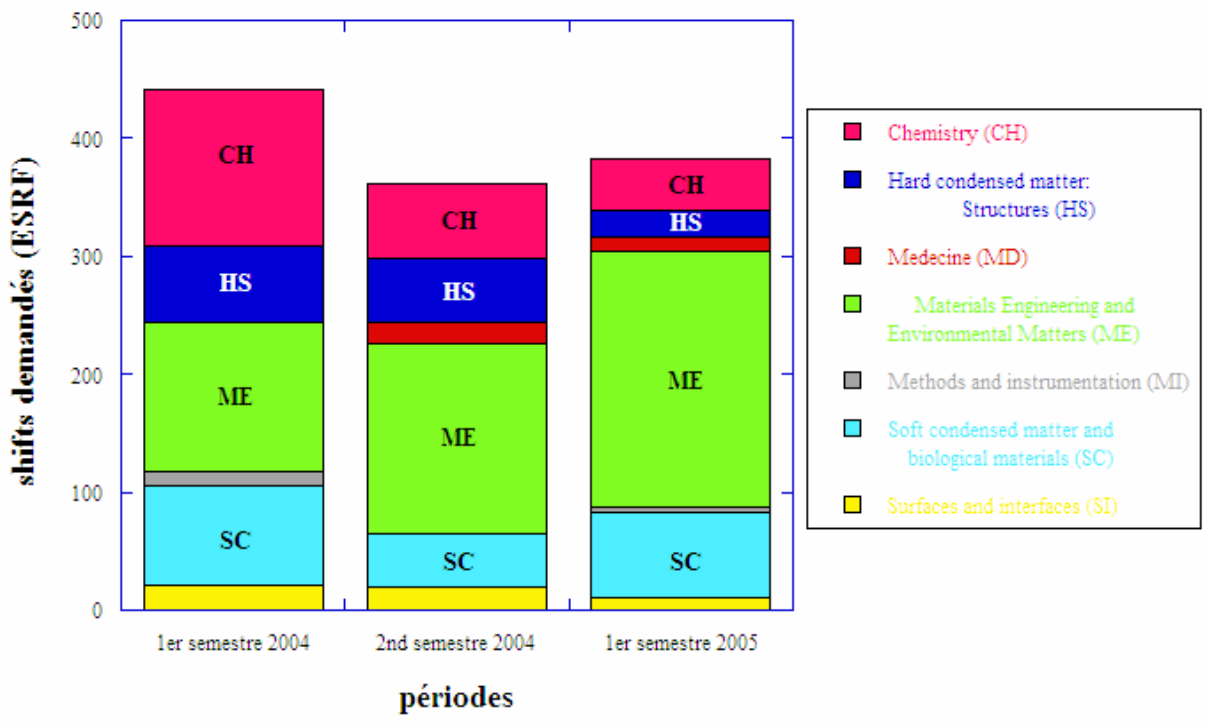

Figure 3 : Evolution des shifts demandés aux différents comités ESRF

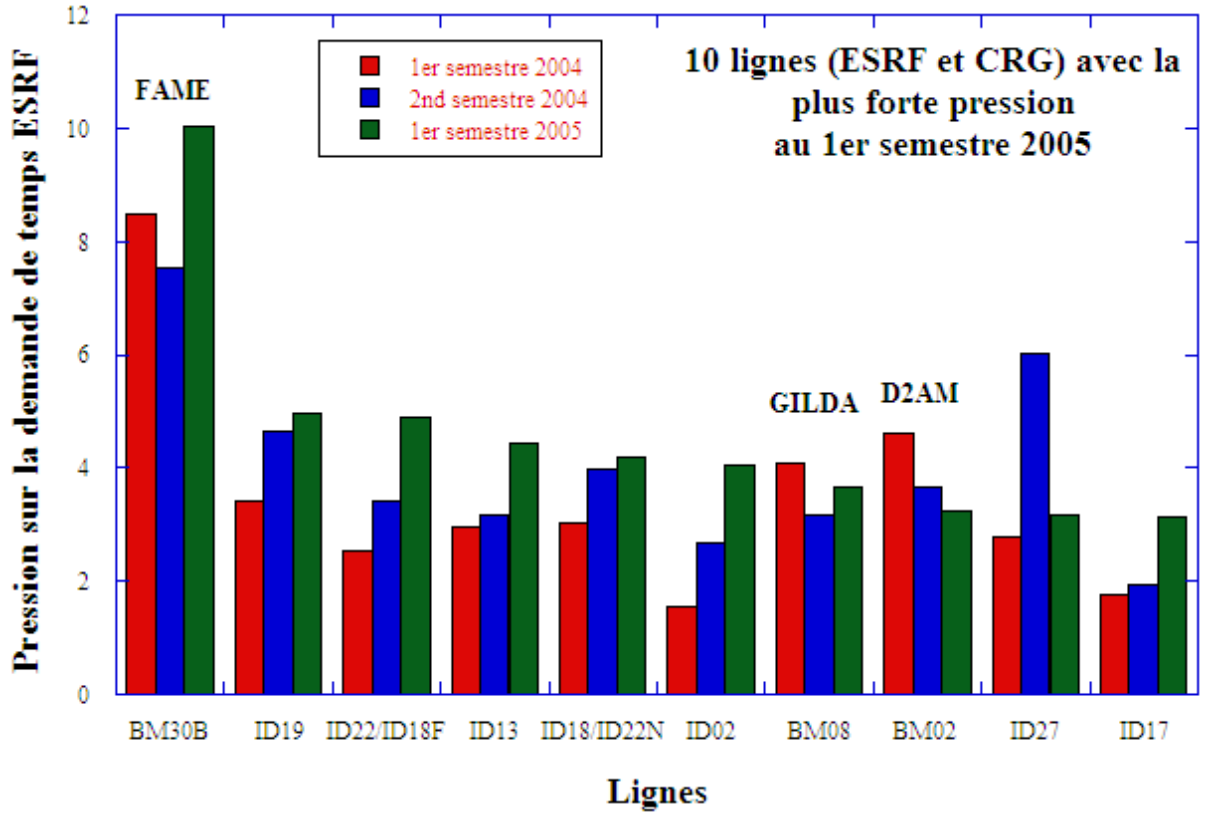

Figure 4 : Evolution de la pression (shifts demandés sur shifts disponibles sur le temps ESRF) sur les différentes lignes de l'ESRF

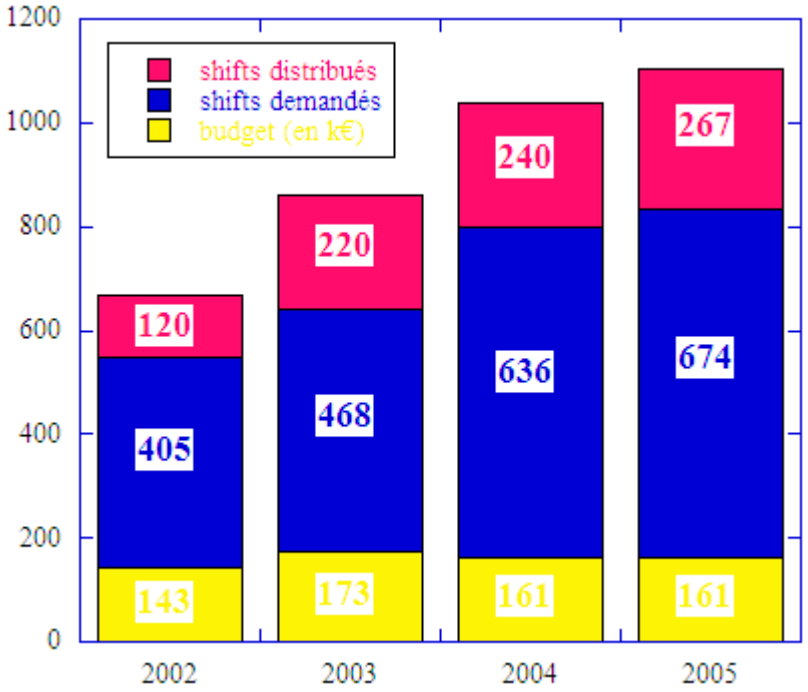

Figure 5 : Evolutions du budget (en k€) et du nombre de shifts demandés et distribués par le comité CRG français

Exemples scientifiques

La présentation des résultats des expériences est résumée dans les rapports d'expérience joints en annexe et les articles de la ligne regroupés dans la bibliographie.

A XAFS spectroscopy study of local environment around gold in high T/P aqueous sulfide and chloride solutions Implications for the mechanisms of gold deposits formation

Gleb Pokrovski[1], Jacques Schott[1], Boris Tagirov[2], Jean-Louis Hazemann[3]

1 Laboratoire des Mécanismes & Transferts en Géologie, LMTG-OMP-CNRS, Toulouse
2 Institute of Mineralogy and Petrology, ETHZ Zürich Switzerland
3 Laboratoire de Cristallographie, ESRF-CNRS, Grenoble

The dissolution and atomic structure of gold in chloride and sulfide aqueous solutions were examined by XAFS spectroscopy at Au L_3-edge at temperatures to 400°C and pressures to 100 MPa, using an X-ray cell recently developed at the Laboratoire de Cristallographie. This cell allows simultaneous measurement of the absolute concentration of the absorbing element in the fluid (from edge-step height in transmission mode, fluid density and absorption cross-section of the element), and atomic environment around the absorber (from analysis of XANES and EXAFS spectra in fluorescence mode). Details about the cell operation and spectra analysis can be found in refs. 1 & 2. An improved cell design used for the present experiment utilizes a piston equipped with Viton joints and inserted into a thin-wall mono-crystalline sapphire tube. This construction avoids solutes precipitation in the colder parts of the cell.

Results on the gold-chloride system. Four experiments were performed in the system $HAu^{(III)}Cl_4$-NaCl-HCl±Au(metal) at 60 MPa as a function of temperature and time. It was found that below 200°C, the XANES spectra of Au in solution exhibit a strong before-edge feature (Fig. 1, A) corresponding to 2p-5d electronic transitions characteristic of tri-valent Au in the plane square $Au^{(III)}Cl_4^-$ complex reported in previous low-temperature XAFS and Raman studies[3,4]. At 200°C, this feature rapidly disappears indicating a reduction of this species, presumably into $Au^{(I)}Cl_2^-$ [4, 5]. However, at higher temperature, the absorption-edge height shows rapid gold precipitation (Fig. 2). XANES spectra above 250°C display features characteristic of metallic gold (Fig. 1). The very narrow temporal and temperature interval of the Au(I) appearance in solution (Fig. 1 & 2) contradicts to the previous batch-reactor solubility studies which indicate that above 250°C, $AuCl_2^-$ should be the dominant species, and attain concentrations 10 times higher than measured in our experiments[4,5]. This discrepancy might be attributed to a leak of oxygen through or reaction with the Viton seals, thus destabilizing Au(I) chloride species in favor of metallic gold. Another possibility[3] could be the beam-induced reduction of $AuCl_2^-$ into Au^0.

Results on the gold-sulfide system. An experiment was performed in the system Au-NaOH-S by allowing a foil of metallic gold and sulfur crystals to react with a NaOH aqueous solution at elevated temperature. The complete dissolution of sulfur occurs above 100°C and produces sulfide (H_2S, HS^-) and sulfate (HSO_4^-, SO_4^{2-}) species. Fig. 3 shows that at 300°C and 60 MPa, gold rapidly dissolves, resulting in a spectrum similar to that of Au_2S (Fig. 1) and $Na_3Au(S_2O_3)_2$ (not shown) in which $Au^{(I)}$ is linearly coordinated by two sulfur atoms. This indicates that dissolved $Au^{(I)}$ is likely to be surrounded by two sulfide ligands in this solution by forming $Au(HS)_2^-$, as was suggested by solubility studies. Au concentrations attain a steady-state after about 4 hours of dissolution at 300°C (Fig. 3). At 400°C, however, a regular drop of Au concentration with time is observed. The before-edge absorption in transmission mode also shows a significant decrease which can be attributed to a loss of sulfur (the major contributor to the absorption below the Au L_3 edge in this solution). This could be due to a leak of the volatile and reactive H_2S through the Viton seals out of the cell. Nevertheless, such a leak does not occur at lower temperatures, and the absorption edge heights measured at steady-state at 300°C/60 MPa allow reliable determination of Au concentration in solution in equilibrium with metallic gold: 0.091±0.020 mol/kg H_2O. This value is in agreement with that predicted using the thermodynamic properties of $Au(HS)_2$- obtained from our recent batch-reactor solubility study.

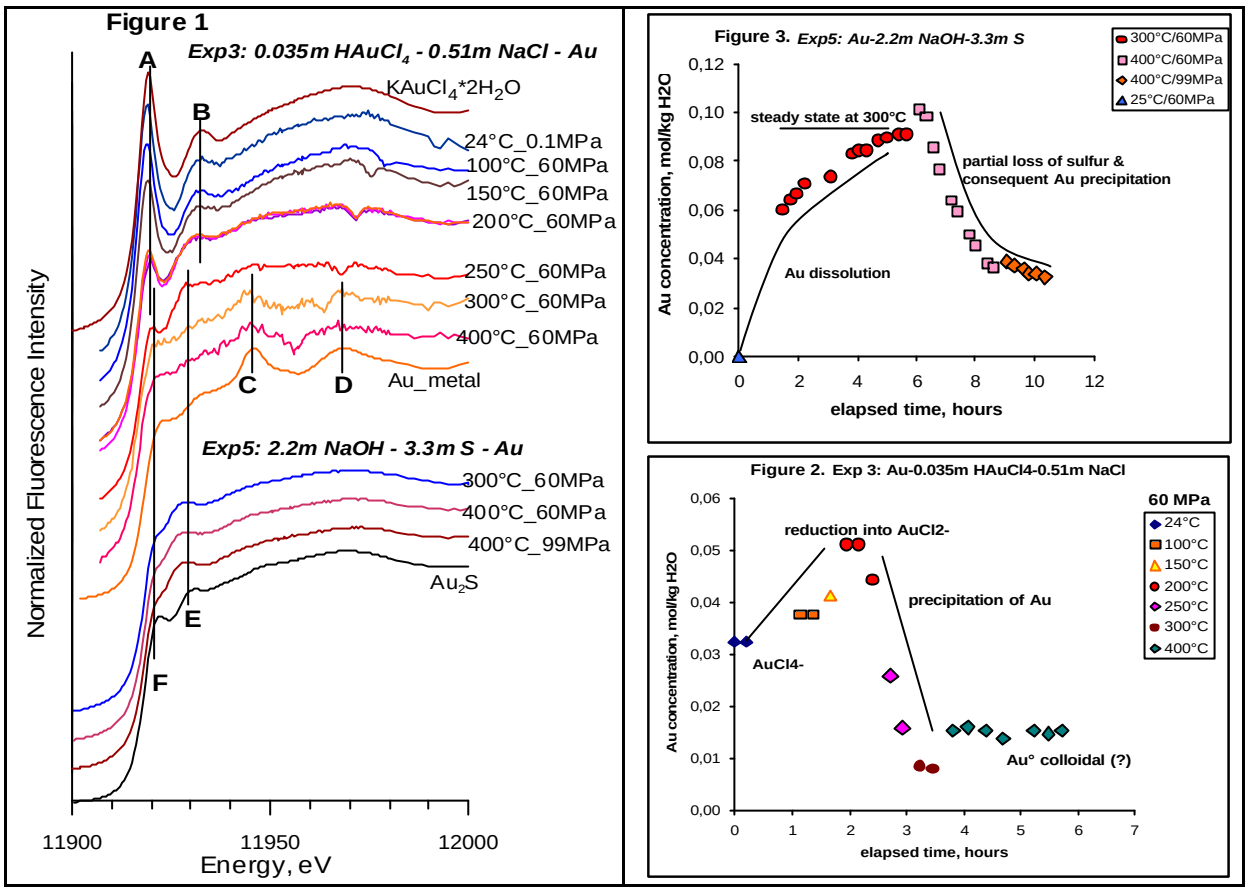

Fig. 1. Normalized near-edge fluorescence spectra of Au-bearing solids and experimental solutions at indicated conditions (concentrations in molalities). Vertical lines show features characteristic of the square $Au^{(III)}Cl_4$ cluster (A & B), metallic gold (C & D), and linear $Au^{(I)}S_2$ and $Au^{(I)}Cl_2$ (E & F) configurations.

Fig. 2 & 3 Total dissolved concentration of gold as a function of time and temperature for the experiments in the systems $HAuCl_4$-NaCl-Au (Fig. 2) and Au-NaOH-S (Fig. 3) shown in Fig. 1.

Conclusions & perspectives. To our knowledge, this experiment is the first measurement of gold solubility and structure of Au(I) chloride and sulfide complexes at hydrothermal conditions using *in situ* XAFS spectroscopy. Our results demonstate the feasability of XAFS measurements of this extremely inert and weakly soluble noble metal. The ultimate goal of our future experiments will be to access, via EXAFS spectra, quantitative structural parameters of the $Au^{(I)}$ complexes dominant in natural ore-forming fluids, and to measure Au solubilities over a wide range of magmatic-hydrothermal conditions. This will be achieved using an improved cell construction (polycristalline sapphire avoiding diffraction, high-temperature joints with improved seal properties), and the high X-ray flux and sensitive detection provided by the ESRF.

References

1. Pokrovski G.S., Zakirov I.V., Roux J., Testemale D., Hazemann JL., Bychkov A.Y., & Golikova G.V., *Geochim. Cosmochim. Acta* **66**, 3453-3480 (2002)
2. Pokrovski G.S., Roux J., Hazemann JL., & Testemale D., *Chem. Geology (submitted)* (2004)
3. Berrodier I., Farges F., Benedetti M., Winterer M., Brown G.E., Jr., Deveughèle M., *Geochim. Cosmochim. Acta* **68**, 3019-3042 (2004)
4. Murphy P.J., Stevens G., & LaGrange S., *Geochim. Cosmochim. Acta* **64**, 479-494 (2000)
5. Gammons C.H. & Willams-Jones A.E., *Geochim. Cosmochim. Acta* **61**, 1971-1983 (1997)

Natural speciation of Mn, Ni and Zn at the micrometer scale in a clayey paddy soil by polarized X-ray Absorption Spectroscopy

Manceau A.[1], Tommaseo C.[1], Geoffroy N.[1], Schlegel M.[2], Chen Z.S.[3],

1 Environmental Geochemistry Group, LGIT, CNRS, Grenoble
2 DEN/DPC/SCP, CEA-Saclay
3 Department of Agricultural Chemistry, National Taiwan University, Taipei, Taiwan

During the last two years, great strides in our knowledge of the sequestration mechanism of zinc and nickel in soils have been made, despite the generally low concentration of these elements in the analyzed matrices and the high proportion of iron, which gives a parasitic fluorescence signal that is quite intense at the Ni and Zn K-edges[1-6]. Among all the experiments, I think that the most novel has been, and still is, the development of polarized EXAFS on highly textured (single crystal-like) self-supporting films from the clayey fraction of natural soils and from clay standards[7]. These experiments are technically challenging in many respects (elaboration of high quality films, quality-control by texture goniometry, availability of a focused X-ray beam for grazing-incidence measurements, high stability of the spectrometer during the scans at varying incidence angle, 30-Ge detector for Fe Ka rejection and high flux) and have led to several groundbreaking, and even flabbergasting, results. This research work on P-EXAFS still is completely original and has been a shoo-in for acceptance in premier journals in our field.

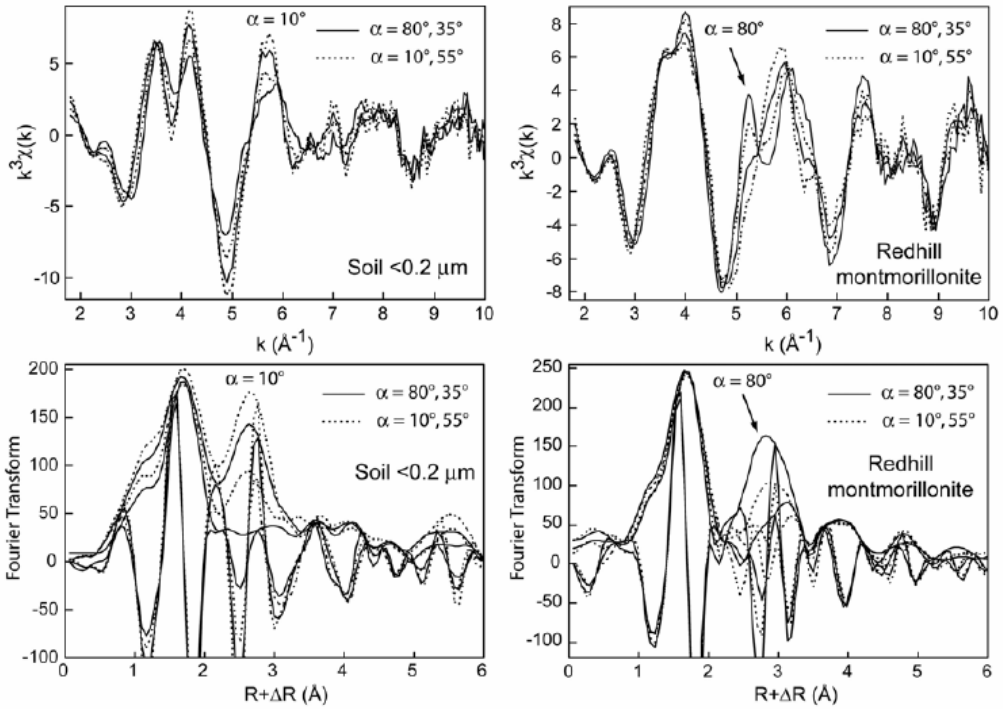

Fig. 1 Polarized EXAFS and Fourier transforms from the <0.2 µm soil fraction and the Redhill montmorillonite reference.

A glimpse of this accomplishment is shown below with the P-EXAFS data obtained on Zn in a clayey paddy soil from Taïwan ([Zn] = 42 ppm) and on Zn in substitution to Al in the octahedral sheet of montmorillonite ([Zn] = 85 ppm)[8]. The two samples exhibit a reversed polarization dependence, although Zn is surrounded by Al in the two samples (fig. 1). This difference is due to the fact that Zn occupies two distinct crystallographic sites (fig. 2): it is located in the octahedral sheet sandwiched between two tetrahedral Si sheets in montmorillonite, and it is located in the vacancy sites of an $Al(OH)_3$ layer in the soil sample. The two local environments, not only are highly anisotropic, but also dissimilar, thus enabling their differentiation. We believe that the new coordination chemistry of zinc discovered in the paddy soil from Taïwan is ubiquitous, and is the main sequestration mechanism of zinc in acidic to near-neutral aluminium-rich clayey soils at the earth's surface.

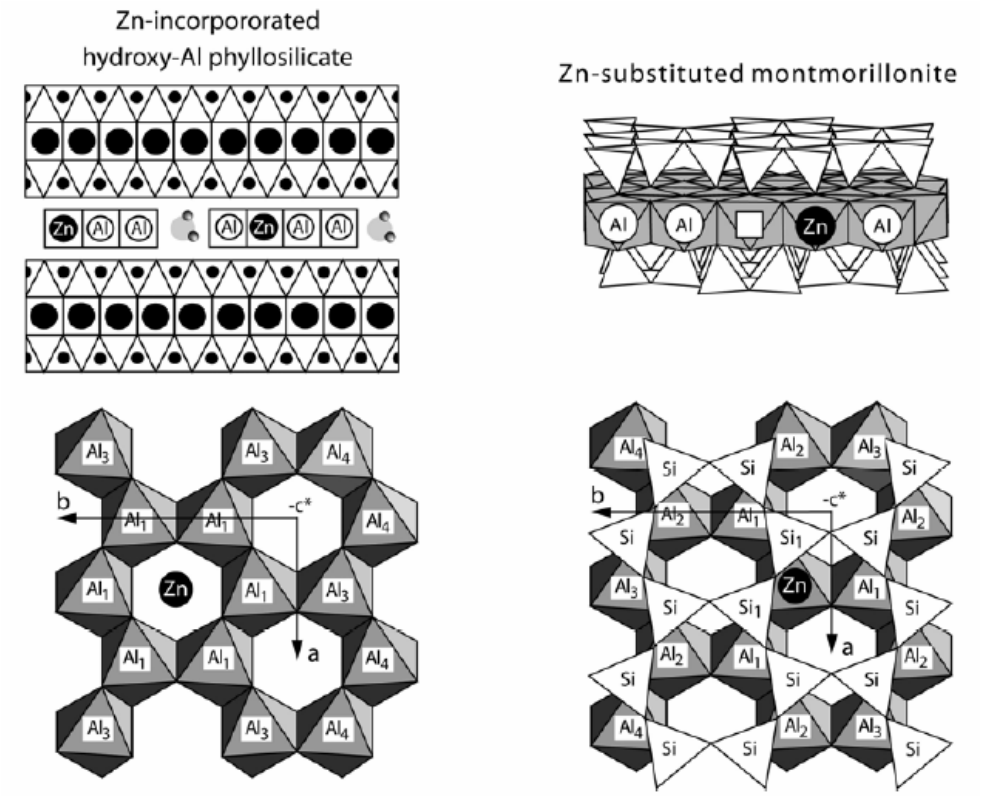

Fig. 2. Schematic representation of the site occupancy of Zn in Zn-substituted montmorillonite and hydroxy-Al phyllosilicate.

References

[1] Manceau A., Marcus M.A., Tamura N., "Quantitative speciation of heavy metals in soils and sediments by synchrotron X-ray techniques", *Reviews in Mineralogy and Geochemistry*, Mineralogical Society of America, Washington, DC., **49** (2002) 341-428

[2] Manceau A. *et al.*, "Molecular-scale speciation of Zn and Ni in soil ferromanganese nodules from loess soils of the Mississippi basin" *Environmental Science & Technology*, **37** (2003) 75-80

[3] Manceau A. *et al.*, **"**Zn speciation in a soil of the Ohio River basin by combining x-ray fluorescence, absorption and diffraction at micrometer scales of resolution", *Geochimica et Cosmochimica Acta* **68** (2004) 2467-2483

[4] Marcus M. A., Manceau A., Kersten M., "Mn, Fe, Zn and As speciation in a fast-growing ferromanganese marine nodule" *Geochimica et Cosmochimica Acta* **68** (2004) 3125-3136

[5] Isaure M.P. *et al.*, "Zinc mobility and speciation in soil covered by contaminated dredged sediment using micrometer-scale and bulk-averaging X-ray fluorescence, absorption and diffraction techniques", in press in *Geochimica et Cosmochimica Acta*

[6] Panfili F. *et al.*, "The effect of phytostabilization on Zn speciation in a dredged contaminated sediment using scanning electron microscopy, X-ray fluorescence, EXAFS spectroscopy and principal components analysis", in press in *Geochimica et Cosmochimica Acta*

[7] Manceau A., Lanson B., Drits V.A., "Structure of heavy metal sorbed birnessite. Part 3. Results from powder and polarized EXAFS spectroscopy" *Geochimica et Cosmochimica Acta*, **66** (2002) 2639-2663

[8] Manceau A. *et al.*, "Natural speciation of Mn, Ni and Zn at the micrometer scale in a clayey paddy soil using X-ray fluorescence, absorption, and diffraction", submitted to *Geochimica et Cosmochimica Acta*

Bilan du personnel impliqué dans la gestion de la ligne

Depuis décembre 2003, trois points sont à noter concernant le personnel impliqué sur FAME.

- Olivier Proux, ingénieur de recherche CNRS (LGIT SDU), est maintenant en CDI depuis le concours de juin 2004. Sa prise de fonction dans ce cadre est effective depuis le 1er décembre 2004
- Vivian Nassif est ingénieur post-doctoral CEA (DRFMC/SP2M, CEA/Grenoble) depuis le 14 juin 2004. Son rôle s'articule autours de l'accueil des utilisateurs et du développement de l'environnement échantillon dans le cadre du projet micro-faisceau
- Hervé Palancher commencera un stage post-doctoral CEA (DES/SESC, CEA/Cadarache) début 2005. Une partie de son activité consistera à préparer et à accueillir sur FAME les expériences du groupe de Carole Valot, une autre partie consistera en sa participation au projet micro-faisceau.

Un point important est le départ à la retraite de Jean-Jacques Menthonnex en septembre 2005. Afin de ne pas handicaper le fonctionnement de la ligne, son remplacement est indispensable.

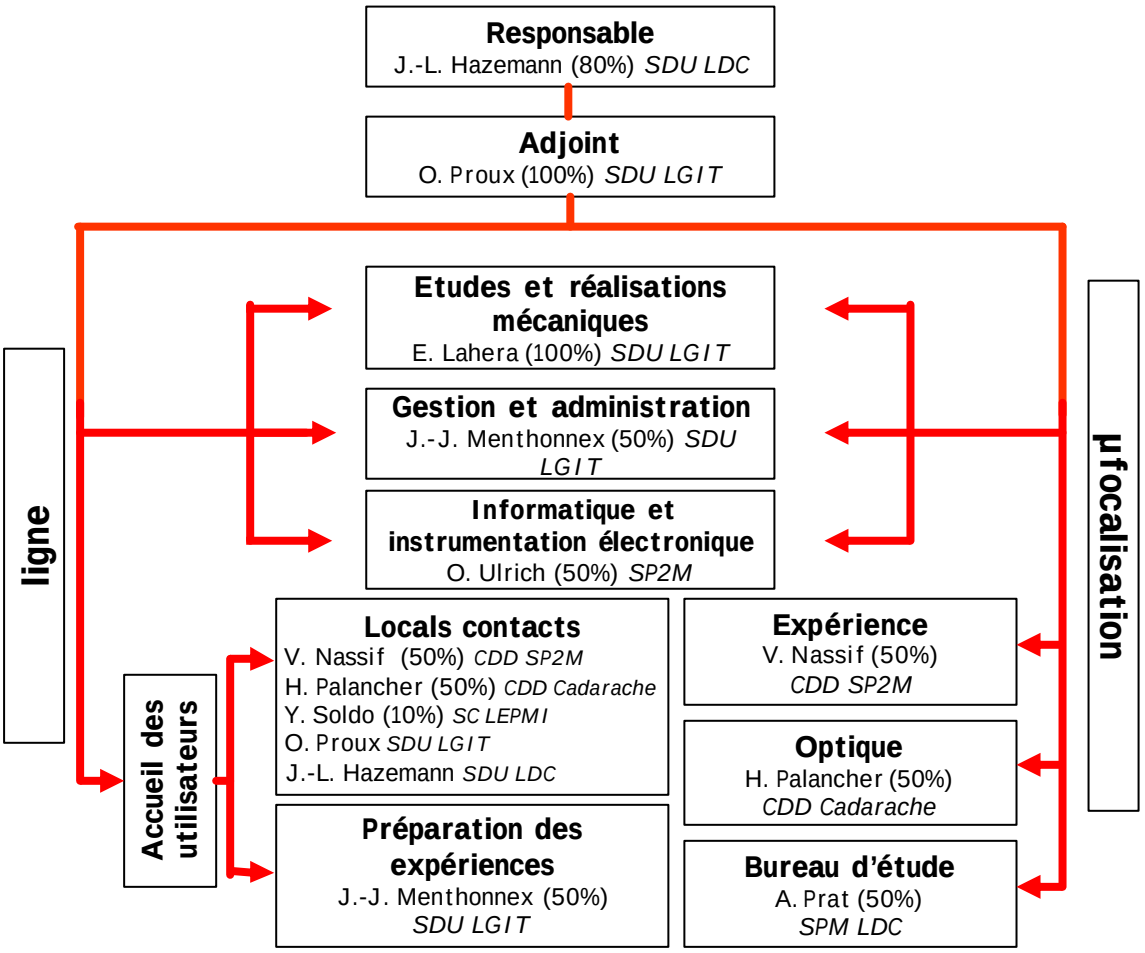

Figure: Organigramme de la ligne FAME

Evolutions techniques

Domaine en énergie et résolution

Les expériences à hautes énergies se font maintenant facilement avec les cristaux Si(220). Une expérience au seuil K du Xenon (34.5-35.5 keV) a été de nouveau réalisée par P. Martin (CEA Cadarache). Pour les basses énergies, le seuil K du Titane (4.9-5.6 keV) a été étudié avec ces mêmes cristaux par l'équipe A. Sadoc (LPMS Paris). A l'exception du Calcium et du Scandium, tous les éléments (pour Z=22) peuvent donc être étudiés avec les cristaux Si(220), *i.e.* avec une très bonne résolution en énergie, particulièrement pour les éléments légers.

Systèmes de détection

Détection de fluorescence

Le détecteur Canberra 30-éléments est revenu de réparation mi-octobre. L'ensemble des cristaux de Germanium a été changé, de même que certains étages de la chaîne de pré-amplification (7 penta-fet). L'ensemble des 30 éléments fonctionne de nouveau correctement.
Les tests effectués sur la ligne montrent que la résolution en énergie des éléments est de nouveau très bonne, comparable aux autres multi-éléments (13 éléments discrets) de différentes lignes d'absorption X de l'ESRF, testés sur FAME avec la même électronique analogique, même les plus récents (BM1).

détecteurs	30 éléments *BM30 CRG-FAME*		13 éléments		
	avant réparation	*après réparation*	*BM1*	*ID26*	*BM29*
résolution moyenne	**337.5 eV**	**297.5 eV**	**302.0 eV**	**283.9 eV**	**290.5 eV**
écart à la moyenne	42.4 eV	25.8 eV	17.1 eV	24.6 eV	27 eV
éléments efficaces	26	30	13	13	13

Tableau : résolutions moyennes et écarts à la moyenne de différents détecteurs solide Germanium multi-éléments, mesurés avec la source de Fe^{55} pour un temps de mise en forme de 125ns.

Mesure de l'intensité des faisceaux transmis :

Des supports de diodes avec une nouvelle géométrie ont été conçus. Deux diodes en silicium encadrent une feuille diffusante à 45° par rapport au faisceau incident (figure 1). Ce design, beaucoup plus compact que le précédent, a permis d'augmenter de manière très significative le taux de comptage :

- avant : kapton à 90° du faisceau incident, diodes Si à 45°

$I_0 = 0{,}34\ 10^{-8}$A pour une épaisseur de kapton de 50µm (absorption : 1,5% @11,7keV)

- maintenant : kapton à 45° du faisceau incident, diodes Si // au faisceau

$I_0 = 1{,}50/2{,}00\ 10^{-8}$A pour une épaisseur de kapton de 25µm (absorption : 1,1% @11,7keV)

On peut donc diminuer l'épaisseur du diffuseur tout en gardant un courant de diode très correct et supérieur à ce que l'on avait. Cette diminution de la fraction du faisceau absorbée pour la mesure de l'intensité des faisceaux transmis, permet d'augmenter la qualité des mesures, notamment la bonne compensation entre les détecteurs (mesures en transmission principalement).

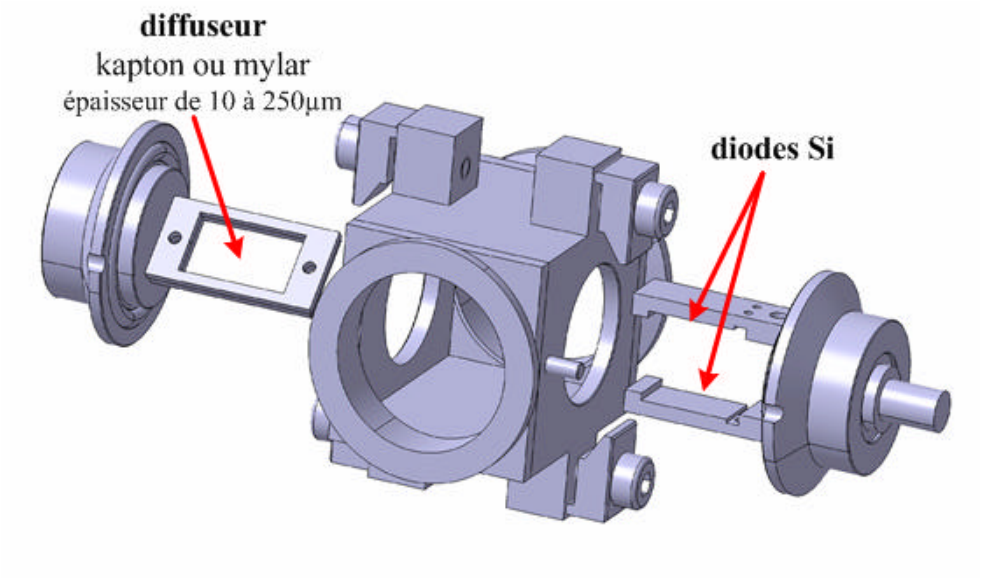

Figure 1 : visualisation 3D du nouveau montage des diodes Si. Conception et réalisation : E. Lahera

Stabilité de la ligne

Optimisation du parallélisme entre les deux cristaux du monochromateur

L'installation d'un piezoélectrique permettant de faire varier le parallélisme du deuxième cristal est effective depuis janvier 2004. Sa mise en œuvre permet l'asservissement automatique de sa position au maximum de la rocking curve (figure 2).
En effet, les températures du 1er et du 2nd cristal du monochromateur sont différentes (respectivement autours de 120K et de 300K). De ce fait leurs distances inter-planaires différent sensiblement : à énergie diffractée équivalente, les angles de Bragg sont donc légèrement différents pour les deux cristaux. Au cours d'un spectre EXAFS, il est donc impératif d'ajuster la position angulaire du 2nd cristal pour garder toujours un flux maximum.

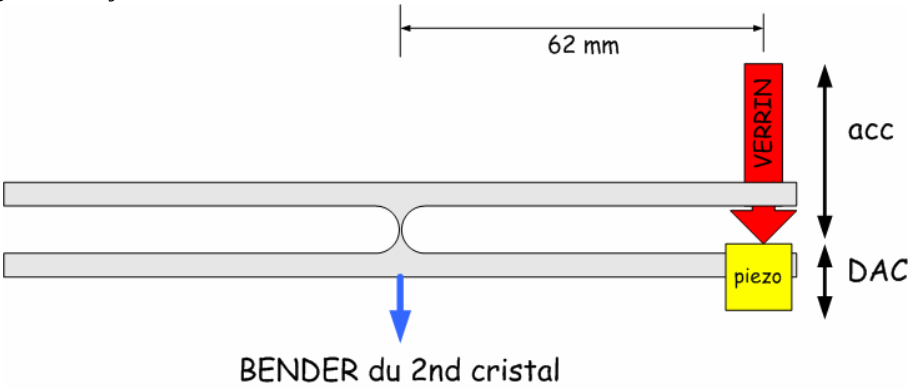

Figure 2 : Figure de principe du montage du piezoélectrique du 2nd cristal du monochromateur. Conception et réalisation mécanique : E. Lahera et A. Prat.

L'implantation du piezoélectrique (figure 2) permet de garder le verrin (moteur acc) pour les réglages grossiers (retrouver le faisceau), le piezo permettant d'affiner et d'optimiser automatiquement le flux, sans aucun jeu, *via* le système de détection synchrone.

Lorsque le faisceau est trouvé, l'asservissement automatique permet de se maintenir au maximum du flux (figure 3) :

- fréquence d'oscillation du piezo (F_{OSC}) aux alentours de 400-440 Hz
- amplitude d'oscillation du piezo : 1-2 mV RMS (soit 4-8 nm ou 0, 1 µrad)
- fréquence de mesure du flux : 1 kHz (limite des MCCE)

L'ajustement se fait en minimisant l'amplitude du signal à 1 fois FOSC. L'intérêt de minimiser la valeur est qu'en cas de perte de faisceau (déplacement de la table ou des fentes pendant les réglages, perte de faisceau dans l'anneau…) le système ne se dérègle pas.

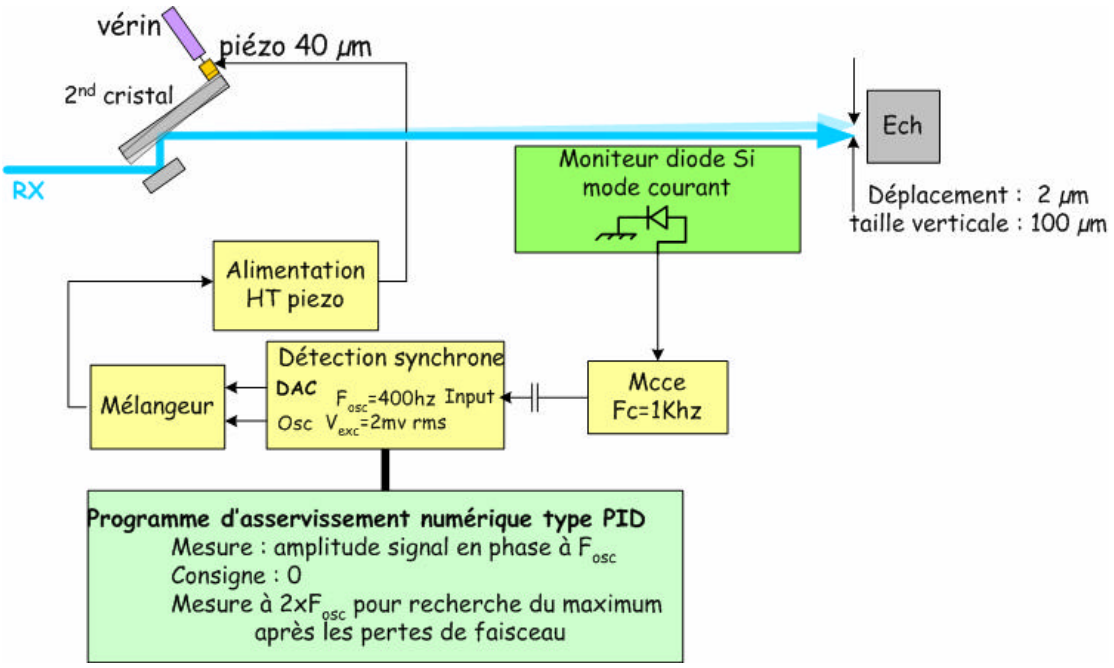

Figure 3 : Schéma de fonctionnement de l'asservissement angulaire du 2nd cristal. Conception et réalisation électronique : O. Ulrich.

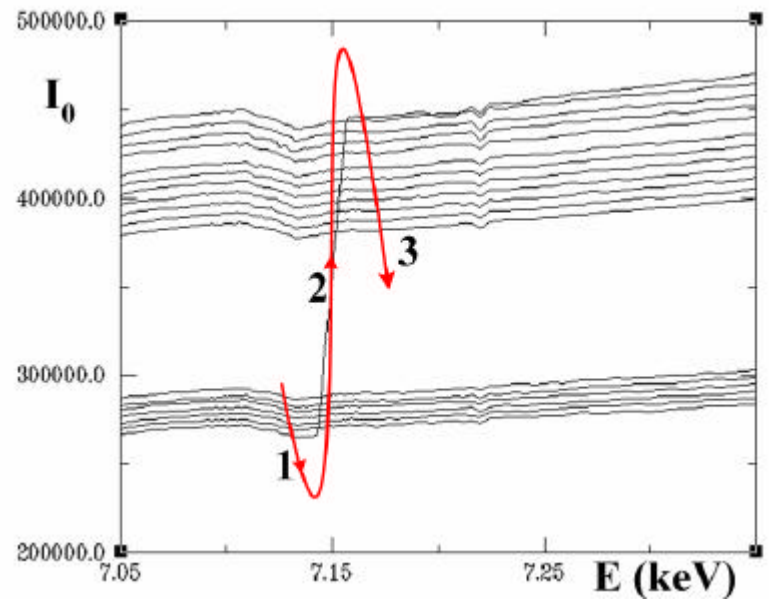

Figure 4 : Evolution de l'intensité du faisceau X (I_0) au cours de la décroissance de l'intensité du faisceau d'électrons dans l'anneau (séquences 1 et 3) de part et d'autre d'une réinjection (séquence 2) - seuil K du Fe, 16 bunchs

Stabilité de la cryogénie

Les instabilités liées à la cryogénie du monochromateur ont été fortement diminuées avec :

1) La mise en place d'une vanne pointeau motorisée permettant la régulation du débit d'azote liquide à la sortie du séparateur de phase. Le pilotage de la vanne motorisée par un Eurotherm permet

maintenant la gestion complète et précise du remplissage du séparateur, sans variation de pression à l'intérieur de la circulation d'azote liquide.

2) L'installation d'un système de régulation de la température du 1er cristal (au 1/100ème de degré), permettant de s'affranchir de la variation de charge thermique sur ce cristal et de donc d'augmenter stabilité en énergie de la ligne. La régulation permet de rendre indépendante la température de l'ouverture des fentes et du remplissage de l'anneau (modes ou taux de remplissage) (figure 5).

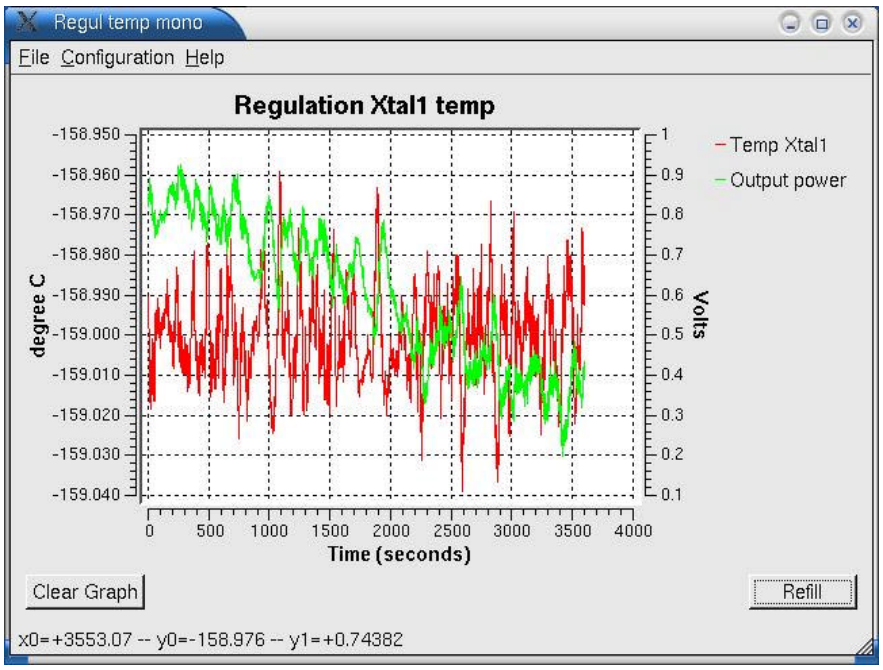

Figure 5 : fenêtre de visualisation et de dialogue permettant de choisir la température de régulation du 1er cristal et de gérer l'ouverture de la vanne pointeau motorisée (réalisation : O. Ulrich). La température (trait rouge) reste constante tandis que la charge apportée (trait vert) pour chauffer augmente progressivement, l'intensité du faisceau dans l'anneau décroissant (sens de défilement de la droite vers la gauche).

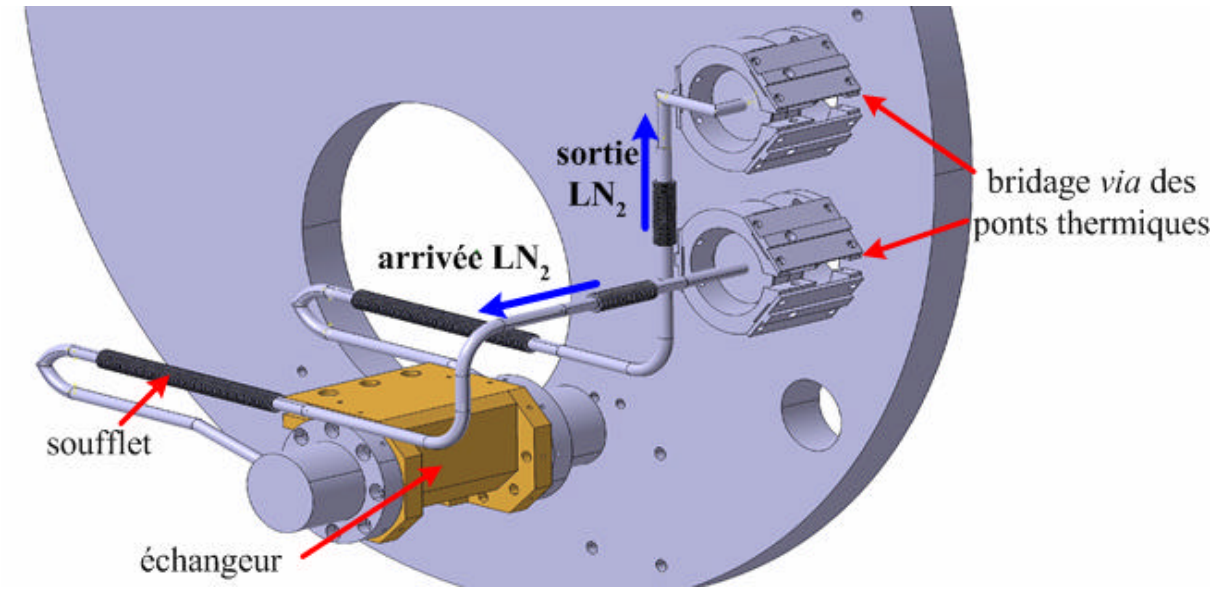

Figure 6 : représentation 3D du nouveau système de circulation d'azote liquide (LN_2) dans le monochromateur (dessin et réalisation : E. Lahera)

3) Le bridage des connecteurs via des ponts thermiques pour limiter les vibrations amenées à l'échangeur par l'arrivée et la sortie d'azote liquide (figure 6)

4) L'utilisation de soufflets ultra-souple (épaisseur des parois de 15/100ème de mm) pour la circulation interne (figure 6)

L'écoulement d'azote liquide reste toutefois fortement non-laminaire si la vanne manuelle, située à l'intérieur de la cabane optique, n'est pas correctement ouverte. Sa conception même fait cependant qu'il est impossible de réguler correctement le débit d'azote par son biais. Son remplacement par une 2ème vanne pointeau motorisée à l'entrée du monochromateur permettrait de diminuer très nettement les vibrations du 1er cristal, et donc le bruit absolu de la ligne.

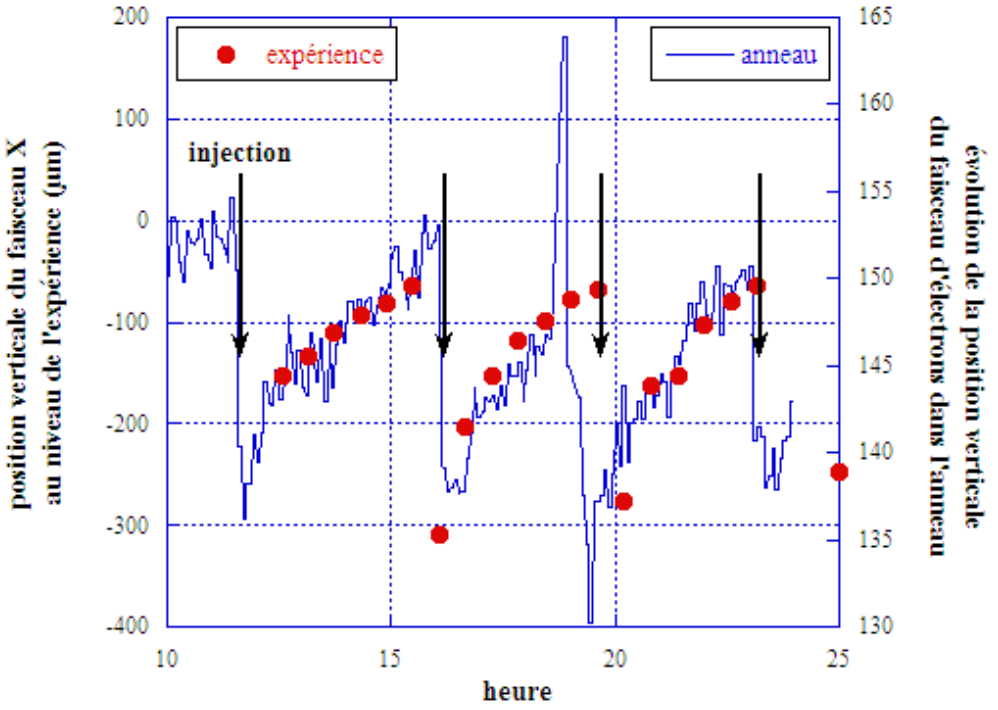

Figure 7 : évolutions de la position verticale du faisceau au niveau de l'expérience EXAFS (points rouges) et de celle du faisceau d'électrons dans l'anneau (traits bleus), en fonction du temps et des injections

Stabilité de la source

Afin de diagnostiquer précisément l'évolution au cours du temps de la hauteur du faisceau au niveau de l'expérience EXAFS, deux séries de mesure ont été menées, avec et sans les miroirs. Avec les miroirs, la hauteur du faisceau évolue de 125µm entre le début et la fin de vie du faisceau, de 30µm après l'injection (2 injections). Sans miroir, la hauteur du faisceau évolue de 240µm entre le début et la fin de vie du faisceau, au maximum 145µm après l'injection (6 injections).

Les évolutions de la hauteur du faisceau sont donc importantes, quel que soit la configuration. La régulation de la température du 1er cristal étant effective au 1/100 de degré, les différences de hauteur de faisceau observées ne sont pas *a priori* dues à des effets thermiques, mais peuvent être corrélées à la variation de la hauteur du faisceau d'électrons dans l'anneau (figure 7)
Après discussion avec les services correspondants de l'ESRF, une solution a été trouvée pour pouvoir suivre précisément l'évolution (hauteur et angle) du faisceau d'électrons au niveau de notre aimant de courbure, en utilisant les valeurs :

- du BPM 5 (faisceau d'électrons avant le BM)
- d'un XBPM (faisceau de rayons X au niveau du front-end)

Un XBPM (X-ray Beam position monitor) sera installé par les services techniques de l'ESRF (groupe « anneau de stockage ») au cours de l'arrêt d'hiver, en janvier. Pour des raisons de configuration (la sortie BM30 est double), cet appareillage sera positionné dans la première enceinte après l'aimant de courbure, à 5m environ de la source.

Expérience

Modification de l'équerre supportant la tête goniométrique

Cette modification répond à un double objectif :
1) Optimiser l'accès à l'échantillon (figure 13)
2) Permettre un rapprochement plus important entre la table EXAFS et le tube de FIP, dans l'optique d'un déplacement de la table en tête de cabane d'expérience (*cf.* le projet microfaisceaux)

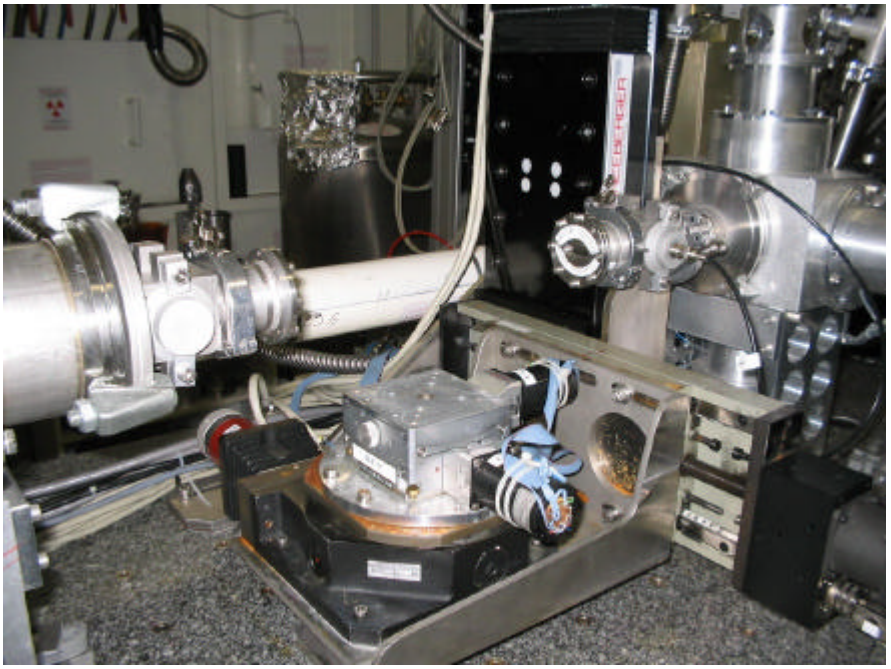

Figure 8 : nouvelle configuration de la tête goniométrique porte-échantillon (conception et suivi de la réalisation : P. Trévisson)

Shutter expérimental

Dans certains cas, les dégâts d'irradiation subits par les échantillons sont préjudiciables à la qualité des mesures, les évolutions structurales étant conséquentes. L'installation d'un shutter d'expérience, conçu et monté par P. Trévisson, en amont de l'échantillon permet de protéger l'échantillon lorsqu'il n'est pas nécessaire de l'irradier (optimisation de la ligne, rampe en température pour des études de cinétique…). Ce shutter est installé depuis novembre 2004.

Formation FAME : FAMEPLUS

Formation en Absorption X pour la Maîtrise de l'Expérience et le Pilotage d'une Ligne Utilisant un Synchrotron

En janvier 2004, une formation interne à la ligne a regroupé 9 utilisateurs (CNRS-SdU) de FAME. Ces trois jours ont permis de voir à quel point une telle formation répondait à une attente et des besoins réels. Nous avons de plus pu nous rendre compte directement de ses conséquences positives lorsque les personnes «formées» sont revenues pour leurs propres expériences au cours de l'année écoulée.
En collaboration avec le service de la formation permanente de la délégation Rhône-Alpes du CNRS à Grenoble, et plus particulièrement Elisabeth Rochas, nous avons monté un dossier en vue d'organiser un atelier (Action Nationale à Gestion Déconcentrée) sur cette thématique pour le printemps 2005, FAME+ (Formation en Absorption X pour la Maîtrise de l'Expérience et le Pilotage d'une Ligne Utilisant un Synchrotron). Un budget de 3.5 k€ vient d'être alloué en février 2005 pour cette opération.

Pourquoi un tel projet ?
De part la complexité de l'environnement synchrotron et la difficulté à obtenir du temps de faisceau *via* les différents comités de programme CRG et ESRF, peu de nouvelles équipes ayant des problématiques scientifiques en adéquation avec ces instruments utilisent la ligne d'Absorption X FAME. Le but de cette formation est donc d'ouvrir l'instrument à l'ensemble de notre communauté, par une familiarisation avec les aspects techniques de l'expérience et des différents moyens d'analyse.
L'autre constat est que les chercheurs-utilisateurs de l'appareillage d'absorption X de FAME ne sont pas familiarisés avec les réglages optiques de la ligne. Il est difficile pour eux de faire le moindre changement seul et donc impossible de faire, par exemple, des tests de faisabilité.
Une formation explicitant le fonctionnement de FAME aurait donc plusieurs intérêts :

- ouvrir la ligne à l'ensemble de la communauté SdU
- rendre plus autonomes les utilisateurs et futurs utilisateurs sur les différents aspects techniques de la ligne,
- augmenter la sécurité sur la ligne, des personnes et du matériel,
- donner aux utilisateurs un regard critique sur tous les points importants qui permettent la réalisation d'une expérience dans de bonnes conditions.

Interdisciplinarité du projet
Ce projet, axé autours de la technique XAS, est dans un premier temps réservé à la communauté des sciences de l'univers. Il peut être toutefois, dans un second, ouvert aux autres départements scientifiques. Le Rayonnement Synchrotron est en effet un outil très fédérateur, qui réunit autour d'un même instrument des communautés à la fois différentes par leur problématique scientifique, et très inter-dépendantes dans leur démarche expérimentale auprès du synchrotron. L'interdisciplinarité s'effectue naturellement par l'investissement très fort de la communauté des physiciens, des sciences de l'univers, chimiques et biologiques, sur les thèmes et outils utilisés.

Site internet de FAME

Le site internet de la ligne (http://www.esrf.fr/exp_facilities/BM30B/BM30Bb-en.html) a été remanié. L'ancienne version, très technique, illustrait bien la phase de construction mais ne répondait pas trop aux attentes des utilisateurs. La nouvelle version est plus conviviale, la navigation simplifiée. Deux nouvelles rubriques ont été écrites :

- « Thématiques scientifiques », qui regroupe de nombreux exemples d'expériences réalisées sur la ligne et classées par domaine de recherche
- « Biblio », qui regroupe l'ensemble des articles publiés ayant trait à des expériences réalisées sur FAME. Des liens permettent dans chaque cas de naviguer vers le site du journal concerné.

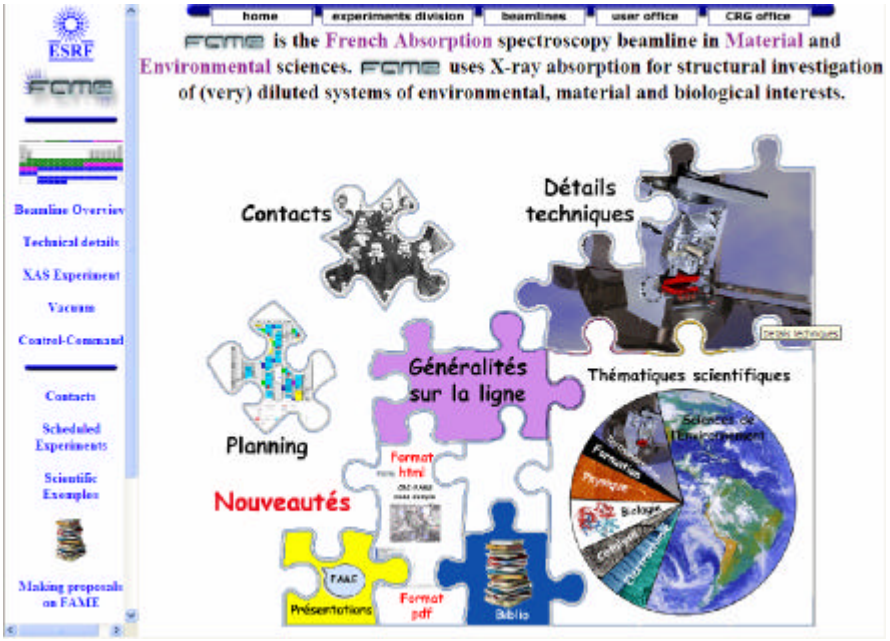

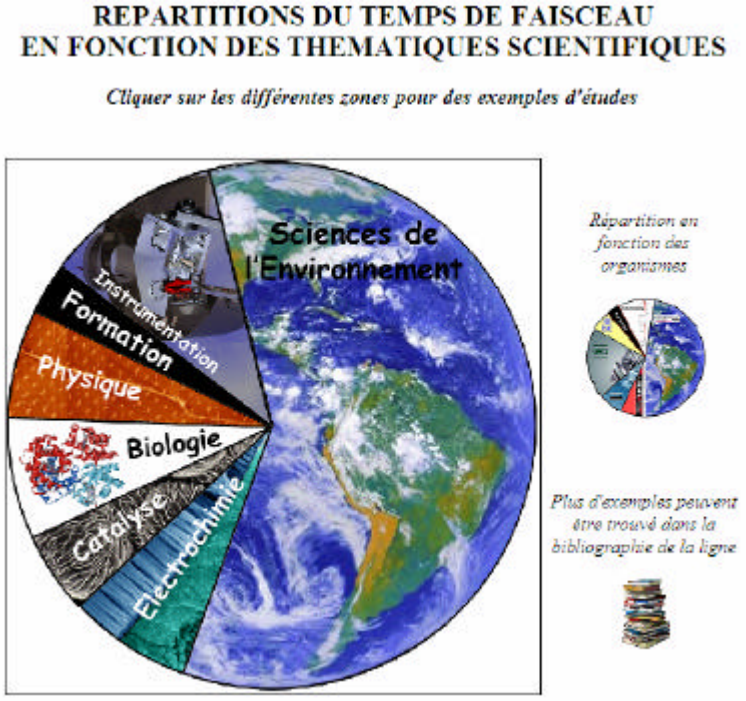

Micro-focalisation sur FAME

Contexte

L'implantation d'un système optique de micro-focalisation sur FAME doit répondre à un double objectif d'un point de vue technique : 1) avoir un faisceau le plus petit et le plus stable possible et 2) pouvoir travailler à des énergies comprises entre 4 et 22 keV. Un système de type miroirs « Kirkpatrick-Baez » est le mieux adapté pour une telle application, également le plus fréquemment rencontré sur de nombreux synchrotron.
Des tests ont été réalisés sur la ligne, pour vérifier la faisabilité d'une expérience de micro-focalisation sur FAME et se rendre compte des besoins et des contraintes techniques que cela impose.
Les premières séries de tests a été réalisée en collaboration avec S. Lequien (Lab. Pierre Süe, CEA-Saclay), en utilisant deux miroirs KB optimisés pour la ligne D15 du LURE (P. Chevallier). Une taille minimale de faisceau de $19\times19\mu m^2$ a été obtenue sans collimater le faisceau incident.
Une deuxième série de test a été réalisé en utilisant un seul miroir (ID1, ESRF) et en focalisant verticalement la nappe (cf. détails dans le rapport d'activités 2003). Pour une ouverture des fentes de 50 µm (50% du flux), la taille obtenue est de 5,8 µm. Pour une ouverture des fentes de 10 µm (10% du flux) la taille chute à 3,6 µm.
Ces différentes données nous ont permis de définir les conditions d'implantation des miroirs KB et de choisir la divergence interceptée par les miroirs, de manière à garder une taille des éléments optiques raisonnable.

Définition des éléments optiques

Positions des éléments et divergences interceptées pour (10µm×10µm)

Pour avoir une taille de 10 par 10 µm avec une taille de source secondaire de 150 par 80 µm :
Ratio en H : 15 Ratio en V : 8

Focalisation Verticale : distance source V - miroir V / miroir V - échantillon = 8 d'où :
distance miroir V – échantillon = 1/9 × distance source V - échantillon

Focalisation Horizontale : distance source H - miroir H / miroir H - échantillon = 15 d'où :
distance miroir H – échantillon = 1/16 × distance source H - échantillon

Source verticale à **3.5m** de l'éch. : distance centre miroir vertical – éch. : **0.390m**
Source horizontale à **2.5m** de l'éch. : distance centre miroir horizontal – éch. : **0.156m**

Soit des tailles de miroirs de **200mm** pour le 1er (V) et **150mm** pour le 2nd (H).

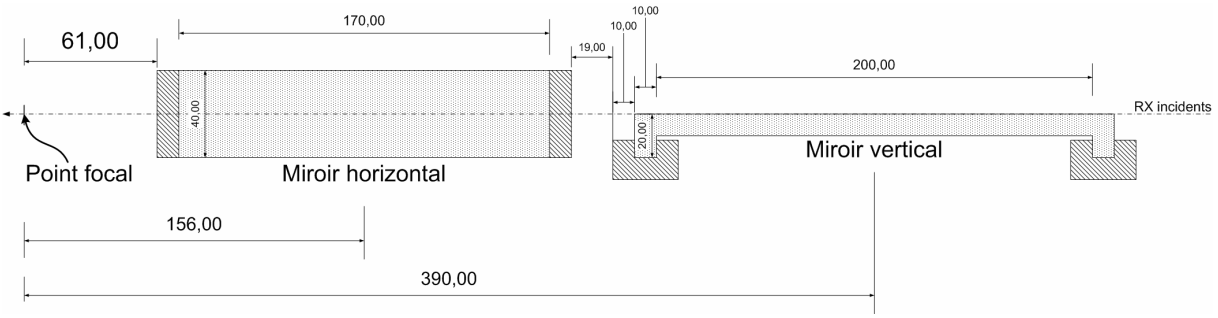

Figure 1 : Schéma de principe des miroirs KB (distances en mm)

Rayons de courbure et flèches des miroirs

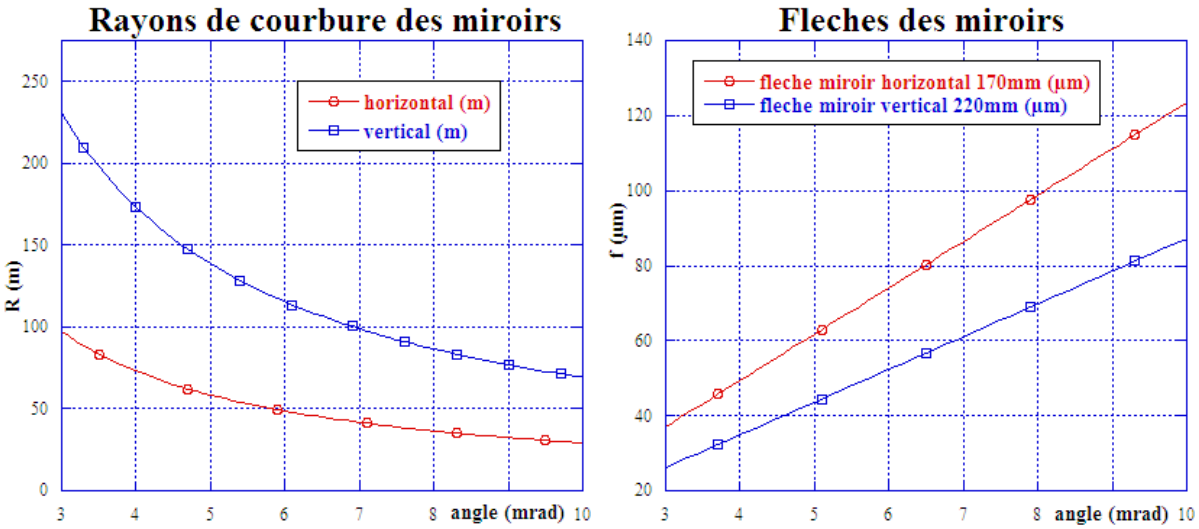

Figure 2 : rayons de courbure et flèches des miroirs dans le cas d'une tâche focale de 10µm×10µm

Gammes de déplacement et incertitudes

Miroirs	déplacement angulaire	précision max.
1er miroir (focalisation vertic.)	de -0.5 à 10.5 mrad	2.5 µrad
2nd miroir (focalisation horiz.)	de -0.5 à 10.5 mrad	6.5 µrad

Tableau 1 : gammes et précision des déplacements angulaires

Miroirs	déplacement vertical	déplacement horizontal
1er miroir (focalisation verticale)	Gamme : de -0.5 à 10.5 mm Précision : 1µm	pas nécessaire
2nd miroir (focalisation horizontale)	Gamme : de -0.5 à 3 mm Précision : 1µm	Gamme : de -0.5 à 6.5 mm Précision : 1µm

Tableau 2 : gammes et précision des déplacements linéaires

Courbeurs

L'étude technique des courbeurs est bien avancée (Figure 3). Les grands principes sont les mêmes que ceux mis en œuvre pour le courbeur du 2nd cristal du monochromateur :

- mouvements angulaires via des points faibles
- miroir en forme de U pour pouvoir le coller sur les mâchoires et ainsi limiter au maximum les contraintes
- utilisation du même type de vérins, associés dans certains cas à des systèmes piezoélectrique pour les mouvements les plus précis (courbure)

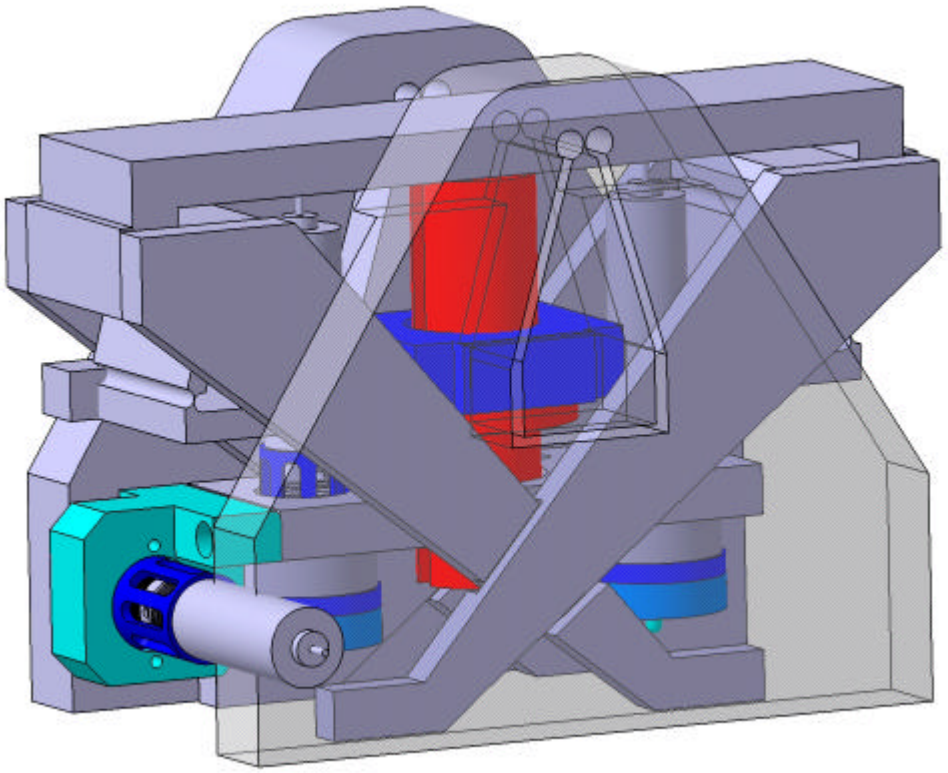

Figure 3 : plan 3D d'un courbeur.

Table KB

La table «KB » supporte à la fois l'optique et l'échantillon, pour qu'en cas de vibrations ces deux éléments vibrent ensemble.

Hauteur de la table

La hauteur du faisceau, au niveau de la cabane d'expérience, varie de 1414mm (pas de miroir) à 1500mm (7mrad). Pour pouvoir aligner le KB à la fois en conditions de mesure (avec les miroirs) et avec un faisceau «hautes énergies » (au cas où), la hauteur moyenne du faisceau au niveau de la table serait idéalement de **1460±50mm**

Déplacement latéral de la table

Pour un alignement correct de la table, son déplacement latéral motorisé doit être possible, avec une amplitude d'environ ±**50mm**

Précisions

Comme pour la table EXAFS « classique », la précision dans le positionnement de la table doit être de 1µm

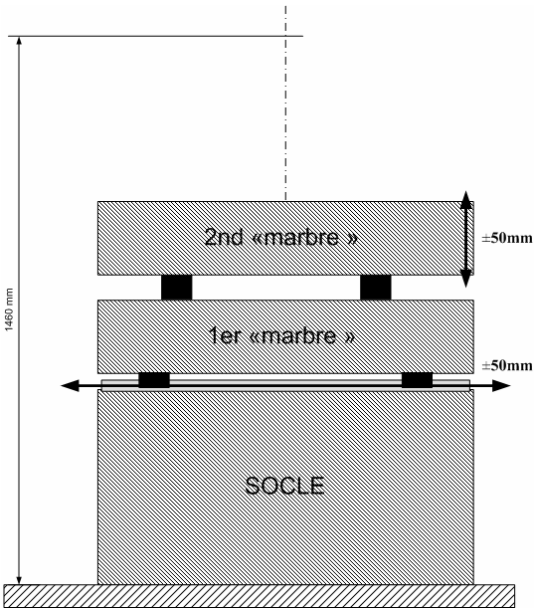

Figure 4 : schéma de principe de la table

Manipulateur d'échantillons

Gamme de déplacement de l'échantillon

Pour pouvoir étudier des échantillons très divers, la course des moteurs assurant les translations horizontale et verticale doit être assez importante, de l'ordre de 100mm, de manière à choisir la zone plus réduite à analyser en fluorescence X puis en XAS.

Modes de déplacement X, Z

Pour minimiser la durée d'acquisition des cartes de fluorescence, le mode de déplacement choisi est similaire à celui de la ligne 10.3.2 de l'ALS :

- pour le déplacement horizontal: moteur continu avec contrôle de position intégré
- pour le déplacement vertical: moteur pas à pas
- résolution : 0.1µm

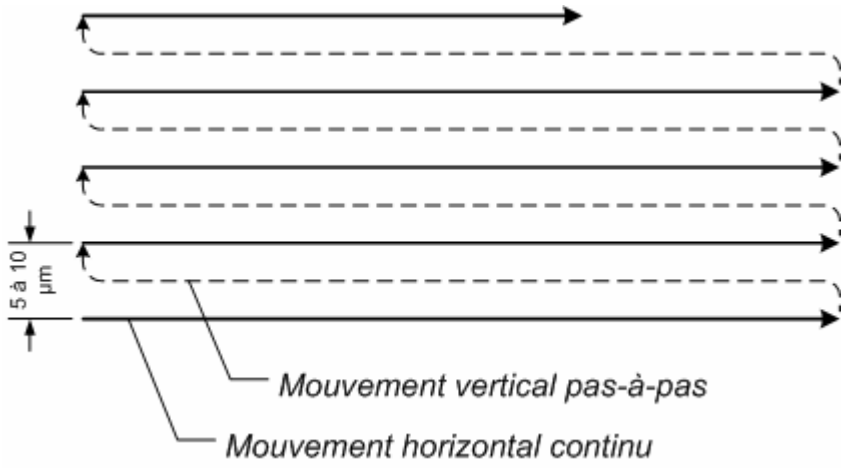

Figure 5 : schéma de principe du balayage de l'échantillon pour les cartes de fluorescence X

Mise au point

Pour s'assurer que la surface de l'échantillon est au niveau de l'échantillon, il est nécessaire de faire la mise au point. Une translation longitudinale au faisceau permet d'effectuer ce régalage. Le microscope étant réglé pour que son point focal soit au niveau de l'axe optique, il faut que l'image de l'échantillon dans le microscope soit nette. Le réglage est alors correct à la profondeur de champ près.

Disposition des éléments dans la cabane d'expérience

La disposition des éléments dans la cabane d'expérience (figure 6) est imposée par la configuration choisie pour la microfocalisation au vue des différentes expériences préliminaires effectuées sur FAME depuis 2 ans, à savoir la création d'une source secondaire réelle grâce à l'optique « initiale » de la ligne, source imagée par l'optique « microfocalisante ».

Cette configuration présente les avantages suivants :

- possibilité de d'imager la source secondaire sans déplacer les KB, et donc de re-régler rapidement la ligne en cours d'expérience,
- possibilité de collimater la source secondaire,
- aucun déplacement des 2 tables, « EXAFS » et « KB », entraînant un gain de temps entre les différentes expériences.

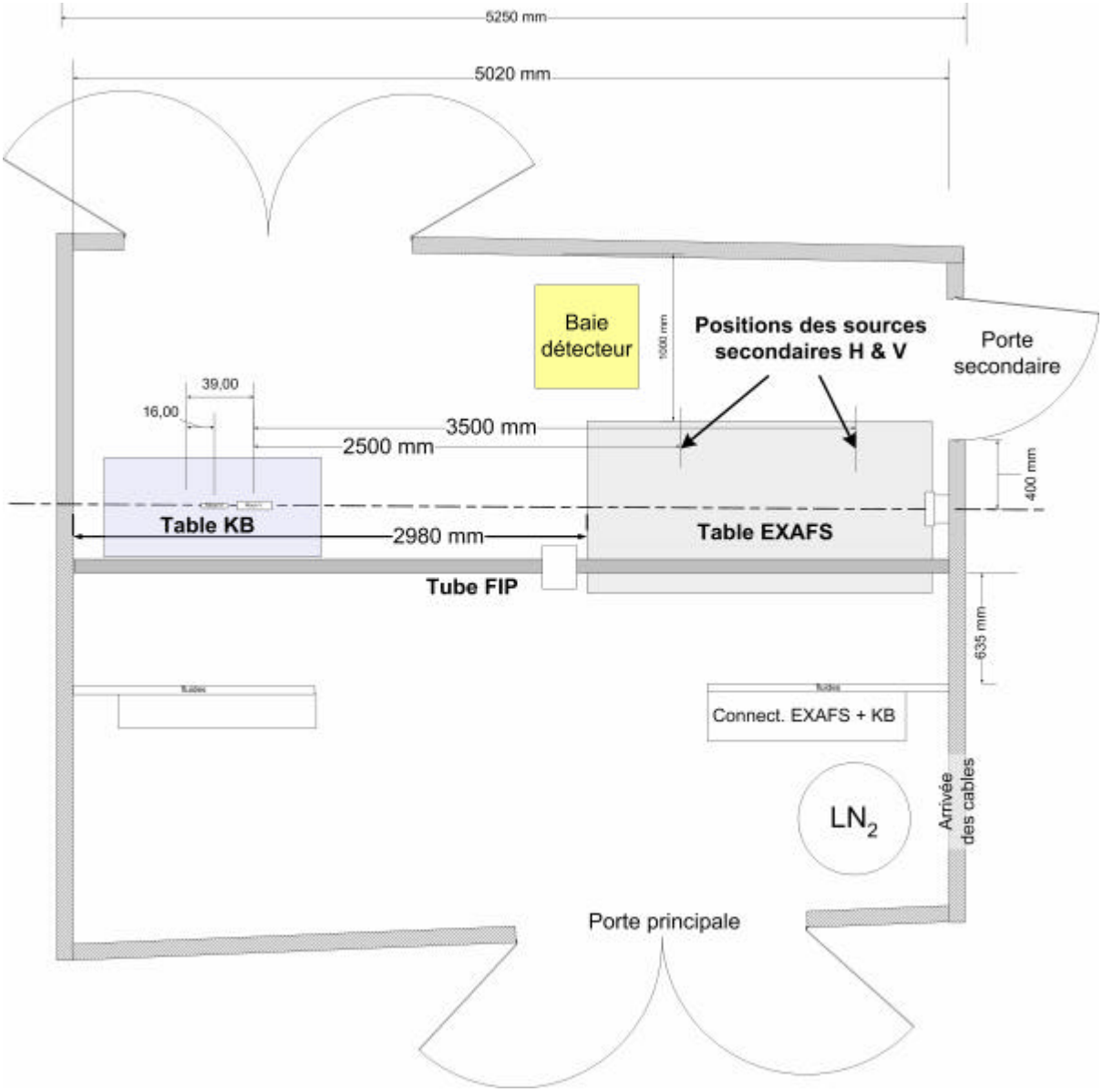

Figure 6: plan schématique de la cabane d'expérience. La table EXAFS est déplacée le plus possible en amont dans la cabane.

Bibliographie

Articles

2005

2005-1 Andreev T., Y. Hori, X. Biquard, E. Monroy, D. Jalabert ,A. Farchi , M. Tanaka, O. Oda, L Si Dang and B. Daudin, "Optical and morphological properties of GaN quantum dots doped with Tm", in press in *Physical Review B* (2005)

2005-2 Arcovito A., Lamb Don C 2, Nienhaus G. U., Hazemann J.-L., Benfatto M. and Della Longa S., "Light-Induced Relaxation of Photolyzed Carbonmonoxy Myoglobin: A Temperature-Dependent X-ray Absorption Near Edge Structure (XANES) Study", in press in *Biophyical. Journal* (2005)

2005-3 Isaure M.P., Manceau A., Geoffroy N., Laboudigue A., Tamura N., Marcus M.A., "Zinc mobility and speciation in soil covered by contaminated dredged sediment using micrometer-scale and bulk-averaging X-ray fluorescence, absorption and diffraction techniques", in press in *Geochimica et Cosmochimica Acta* (W2830)

2005-4 Panfili F., Manceau A., Sarret G., Spadini L., Kirpichtchikova T., Bert V., Laboudigue A., Marcus M.A., Ahamdach N., Libert M.F., "The effect of phytostabilization on Zn speciation in a dredged contaminated sediment using scanning electron microscopy, X-ray fluorescence, EXAFS spectroscopy and principal components analysis", in press in *Geochimica et Cosmochimica Acta* (W2853)

2005-5 Sarret G., Avoscan L., carrière M, Collins R., Geoffroy N., Carrot F., Covès J., Gouget B. "Chemical forms of selenium in the metal-resistant bacterium Ralstonia metallidurans CH34 exposed to selenite and selenate" in press in *Applied Environmental Microbiology*

2005-6 Testemale D., Argoud R., Geaymond O., Hazemann J.L., "A high-pressure/high-temperature cell for x-ray absorption and scattering techniques", accepted in *Review of Scientific Instruments*

2004

2004-1 D'Angelo P., Lucarelli D., della Longa S., Benfatto M, Hazemann J.L., Feis A., Smulevich G., Ilari A., Bonamore A. and Boffi A. "Unusual heme iron-lipid acyl chain coordination in Escherichia coliflavohemoglobin" *Biophysical Journal* **86** (2004) 3882-3892

2004-2 Giraud R., S. Kuroda, S. Marcet, E. Bellet-Amalric, X. Biquard, B. Barbara, D. Fruchard, D. Ferrand, J. Cibert and H. Mariette Ferromagnetic $Ga_{1-x}Mn_xN$ epilayers versus antiferromagnetic $GaMn_3N$ clusters, *Europhysics Letters* **65** (2004) 553-559

2004-3 Hori Y., X. Biquard, E. Monroy, D. Jalabert, F. Enjalbert, Le Si Dang, M. Tanaka, O. Oda, and B. Daudin, "GaN quantum dots doped with Eu", *Applied Physics Letters* **84** (2004) 206-208

2004-4 Manceau A., Marcus M. A., Tamura N., Proux O., Geoffroy N. and Lanson B., **"**Zn speciation in a soil of the Ohio River basin by combining x-ray fluorescence, absorption and diffraction at micrometer scales of resolution", *Geochimica et Cosmochimica Acta* **68** (2004) 2467-2483

2004-5 Marcus M. A., Manceau A., Kersten M., "Mn, Fe, Zn and As speciation in a fast-growing ferromanganese marine nodule" *Geochimica et Cosmochimica Acta* **68** (2004) 3125-3136

2004-6 Sarret G., Balesdent J., Bouziri L., Garnier J.M., Marcus M.A., Geoffroy N., Panfili F., Manceau A. "Zn speciation in the organic horizon of a contaminated soil by micro X-ray fluorescence, micro and powder EXAFS spectroscopy and isotopic dilution" *Environmental Science and Technology* **38** (2004) 2792-2801

2004-7 Testemale D., Hazemann J.L., G. Pokrovski, J. Roux, Y. Joly, "Study of the evolution of $As(OH)_3$ arsenious acid structure in supercritical conditions: an EXAFS and XANES investigation", *Journal of Chemical Physics* **121** (2004) 8973-8982

2003

2003-1 Biquard X., Proux O., Cibert J., Ferrand D., Mariette H., Giraud R. and Barbara B., **"**Local Structure and Valence State of Mn in $Ga_{1-x}Mn_xN$ Epilayers", *Journal of Superconductivity : Incorporating Novel Magnetism*, **16** (2003) 127-129

2003-2 Della Longa S., A. Arcovito, M. Benfatto, A. Congiu-Castellano, M. Girasole, J.-L. Hazemann, A. Lo Bosco, "Redox-induced Structural Dynamics of Fe-Heme Ligand in Myoglobin by X-ray Absorption Spectroscopy", *Biophysical Journal* **85** (2003) 549-558

2003-3 Manceau A., Tamura N., Celestre R.S., MacDowell A.A., Geoffroy N., Sposito G., Padmore H.A. "Molecular-scale speciation of Zn and Ni in soil ferromanganese nodules from loess soils of the Mississippi basin" *Environmental Science & Technology*, **37** (2003) 75-80.

2003-4 Martin P., M. Ripert, T. Petit, T. Reich, C. Hennig, F. D'acapito, J.L. Hazemann and O. Proux, "A Xas study of the local environments of cations in $(U,Ce)O_2$", *Journal of Nuclear Materials* **312** (1) (2003) 103-110

2003-5 Pokrovski G., J. Schott, F. Farges and J.L. Hazemann, "Iron (III)-silica interactions in aqueous solution : Insights from X-ray absorption fine Structure", *Geochimica et Cosmochimica Acta*, **67** (2003) 3559-3573

2003-6 Proux O., J.S. Micha, J.R. Regnard, F. Ernult, P. Bayle-Guillemaud, B. Dieny, A. Traverse and J.L. Hazemann, "X-ray Absorption spectroscopy study of Co/ZrO_2 discontinuous multilayers", *J. of Physics: Condens. Matter*, **15** (2003) 7237-7252

2003-7 Rose J., G. Chauveteau, R. Tabary, S. Moustier, J-L Hazemann. "Zirconium speciation in microgels: kinetics aspects". *Colloids and surfaces A: Physicochem. Eng. Aspects* **217** (2003) 159-164

2003-8 Rose J., T. J.M. De Bruin, G. Chauveteau, R. Tabary, J-L Hazemann, O. Proux, A. Omari, H. Toulhoat, J-Y Bottero. "Aqueous Zirconium Complexes for Gelling Polymers. A combined X-ray Absorption Spectroscopy and Quantum Mechanical Study", *J. Phys. Chem. B* **107** (2003) 2910-2920

Figure: Répartition des publications en fonction du domaine de recherche (2003-2005)

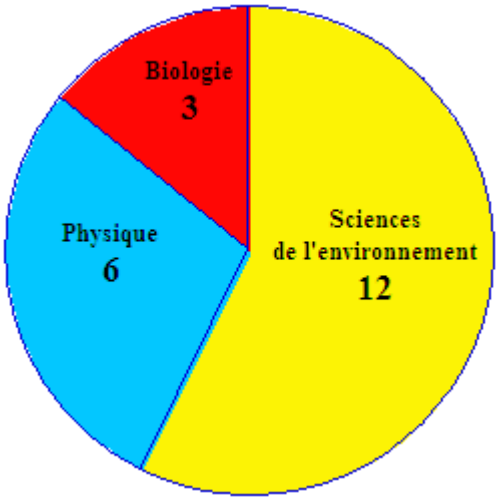

Highlights – Valorisation de la ligne

2005

2005-1 Vahé Ter Minassian, "L'heure de gloire pour FAME", *Le Journal du CNRS*, **181** février 2005

2004

2004-1 Hazemann J.-L., "FAME, un nouvel outil pour étudier les formes chimique et structurale d'éléments-traces", à paraître dans *Bulletin de Liaison de la Société Française de Minéralogie et Cristallographie* **16** (2004)

2004-2 Hazemann J.-L. et Proux O., "Principes de la spectroscopie d'absorption X", à paraître dans *Bulletin de Liaison de la Société Française de Minéralogie et Cristallographie* **16** (2004)

2004-3 Testemale D., Hazemann J.L., Pokrovski G., Joly Y., Roux J., "Structural and electronic evolution of $As(OH)_3$ molecule in high temperature and high pressure aqueous solutions by X-ray spectroscopy", à paraître dans *ESRF Highlights 2004*

Actes de colloques

2004

2004-1 Bellet E., Biquard X., Cibert J., Bougerol C., Ferrand D., Giraud R., Halley D., Kulatov E., Kuroda S., Marcet S., Mariette H., Titov A., "Properties of Ga1-xMnxN epilayers grown by molecular beam epitaxy", *27th International Conference on the Physics of Semiconductors*, Flagstaff, Arizona, EU, (26-30 juillet 2004), *to be published in Proceedings ICPS 27*

2004-2 Hori Y, Andreev T, Jalabert D, Biquard X, Monroy E, Tanaka M, Oda O, Dang LS, Daudin B, "Structural and optical properties of rare-earth doped quantum dots grown by plasma-assisted MBE", 5th International Symposium on Blue Laser and Light Emitting Diodes (ISBLLED 2004), Gyeongin, Corée du Sud, (15-19 mars 2004), *Physica Status Solidi B – Basic Research* **241** (12) (2004) 2787-2790

2004-3 Hori Y, Andreev T, Biquard X, Monroy E, Jalabert Dang LS, D, Tanaka M, Oda O, Daudin B, "Rare-earth doped GaN and InGaN quantum dots grown by plasma assisted MBE", *International Workshop on Nitride Semiconductors (IWN 2004)*, Pittsburgh, Pennsylvania (19-23 Juillet 2004), *à paraître in Physica Status Solidi*

2004-3 Morin G., S. Lebrun, F. juillot, C. Casiot, S. Belin, O. Proux and G. Calas, "Structure and reactivity of nano-crystalline As-Fe oxy-hydroxides in acid mine drainage", *Goldschmidt Geochemistry Conference*, Copenhague (5-11 juin 2004), *Geochimica et Cosmochimica Acta* **68** issue 11 suppl. 1 (2004) A102 (abstract)

2004-4 Ona-Nguema G., G. Morin, F. Guyot, O. Proux, J-L. Hazemann, M. Abdelmoula, G. Calas, "Biomineralogical processes controlling iron and arsenic mobility in anoxic systems" European Geosciences Union, 1st General Assembly, Nice (25 - 30 Avril 2004), *Geophysical Research Abstracts*, **6** (2004) 07526

2004-5 Thibault M.-H., L. Galoisy, G. Calas, J.-L. Hazemann and O. Proux, "Atomic scale determination of the insertion of Cr^{3+} in spinel and garnets: an EXAFS study of site relaxation and element clustering", *Goldschmidt Geochemistry Conference*, Copenhague (5-11 juin 2004), *Geochimica et Cosmochimica Acta* **68** issue 11 suppl. 1 (2004) A87 (abstract)

2003

2003-1 Bénard A., Rose J., Hazemann J-L, Masion A., Bottero J-Y, Vichot A., Lemarchand D., "Evolution of Pb in Portland cement during leaching", *Journal de Physique IV* **107** (2003) 143-146

2003-2 Daudin B, Gogneau N, Adelmann C, Sarigiannidou E, Andreev T, Enjalbert F, Monroy E, Fossard F, Rouviere JL, Hori Y, Biquard X, Jalabert D, Dang LS, Tanaka M, Oda O, "Structural and optical properties of GaN quantum dots", *GaN and Related Alloys – 2003 MRS Fall Meeting*, Editors: Ng HM, Wraback M, Hiramatsu K, Grandjean N *Materials Research Society Symposium Proceedings*, **798** (2003) 127-137

2003-3 Hori Y, Enjalbert F, Jalabert D, Monroy E, Dang L, Biquard X, Tanaka M, Oda O, Daudin B, "Visible red light emission from Eu-doped GaN quantum dots grown by plasma-assisted MBE", *5th International Conference on Nitride Semiconductors (ICNS-5)*, Nara, Japan (25-30 Mai 2003), *proceedings* Editor Stutzmann M, Publisher Wiley-VCH (USA)

2003-4 Isaure M.P., Manceau A., Laboudigue A., Tamura N., Marcus M.A. "Zn speciation in a soil contaminated by the deposition of a dredged sediment by synchrotron x-ray techniques", *Journal de Physique IV* **107** (2003) 657-660

2003-5 Kirpichtchikova T., Manceau A., Lanson B., Marcus M.A., Jacquet T. "Speciation and mobility of Zn, Cu and Pb in a truck farming soil contaminated by sewage irrigation", *Journal de Physique IV* **107** (2003) 695-698.

2003-6 Kuroda S., E. Bellet-Amalric, X. Biquard, J. Cibert, R. Giraud, S. Marcet,and H. Mariette "Optimization of the growth of Ga1-xMnxN epilayers using plasma-assisted MBE", *5th International Conference on Nitride Semiconductors*, Nara, Japan, (25-30 Mai 2003), *Physica Status Solidi C - conferences and critical reviews* **240** (2003) 443

2003-7 Proux O., X. Biquard, E. Lahera, J.-J. Menthonnex, A. Prat, O. Ulrich, Y. Soldo, P. Trévisson, G. Kapoujvan, G. Perroux, P. Taunier, D. Grand, P. Jeantet, M. Deleglise, J.-P. Roux and J.-L. Hazemann, "FAME: A new beamline for X-ray absorption investigations of very-diluted systems of environmental, material and biological interests", XAFS XII Sweden, june 2003, *à paraître dans Physica Scripta*.

2003-8 Rose J., Crouzet N., Trotignon L., Grimal S., Susini J., Khoury H., Salameh E., , Milodowski A., Mercier F., "Effect of leaching on the crystallographic sites of trace metals associated with natural cements (site of Maqarin, Jordan): case of Cr", *Journal de Physique IV* **104** (2003) 447-450

2003-9 Sarret G., Schroeder W.H.; Marcus M.A., Geoffroy N., Manceau A. "Localization and speciation of Zn in mycorrhized roots by X-ray fluorescence and EXAFS spectroscopy", *Journal de Physique IV* **107** (2003) 1193-1196.

Communications orales

2005

2005-1 Collet M., Noack Y., "Speciation of Zinc, Cadmium and Lead in Steel Plant Atmospheric", *XIII International Conference on Heavy Metal in the Environment*, Rio de Janeiro, Brazil (5-9 Juin 2005)

2005-2 Manceau A., "Microsight and megascience in the environmental realm at 3rd generation synchrotrons", . 2005 UK Synchrotron Radiation User Meeting, Daresbury, UK (September 13-14 2005) (**Conférence pleinière**)

2005-3 Manceau A. "Unlocking metal sequestration in soil nanoparticles", *International Clay Conference*, Tokyo August 21-27 2005) (**Conférence invitée**)

2005-4 Manceau A. "Unlocking metal sequestration in soil nanoparticles", *Symposium on 'Application of Synchrotron Science to Environmental Chemistry', Canadian Chemistry Conference Annual Meeting*, Saskatoon, Canada (May 28 - June 1 2005) (**Conférence invitée**)

2005-5 Manceau A. "Bridging the gap between fundamental and applied research in environmental science at 3rd generation synchrotrons", *Symposium on 'The Birth of a Dream: A Synchrotron Light Source in Canada. A Symposium in Honour of G. M. Bancroft', Canadian Chemistry Conference Annual Meeting*, Saskatoon, Canada (May 28 - June 1 2005) (**Conférence invitée**)

2005-6 Manceau A., Schlegel M., Rihs S., Marcus M. "Natural speciation of Mn, Ni and Zn at the micrometer scale in a clayey paddy soil using X-ray fluorescence, absorption, and diffraction", *15th Annual Goldschmidt Conference*, Moscow, Idaho, (20-25 May 2005)

2005-7 Panfili F., Manceau A., Sarret G., Laboudigue A., Bert V., Marcus M. "Changes in Zn speciation in the rhizosphere of graminaceous plants induced by phytostabilization of a contaminated sediment", *8th International Conference on the Biogeochemistry of Trace Elements* (ICOBTE). Adelaide, (April 3-7 2005)

2005-8 Schlegel M., Manceau A. "Nucleation and epitaxial growth of Zn phyllosilicate on montmorillonite", *15th Annual Goldschmidt Conference*, Moscow, Idaho, (20-25 May 2005)

2004

2004-1 Andreev T., Hori Y., Biquard X., Jalabert D., Monroy E., Tanaka M., Oda O., Le Si Dang and Daudin B., "Optical and Structural Properties of Rare Earth Doped Quantum Dots", *E-MRS 2004 Spring Conference, InN, GaN, AlN and related materials, their heterostructures and devices*, Strasbourg, France, (24-28 Mai 2004)

2004-2 Avoscan L., Sarret G., Collins R., Carriere M., Geoffroy N., Proux O., Hazemann J.L., Khodja H. and Gouget B., "Transformation of selenite and selenate by the facultative aerobe *Ralstonia metallidurans* CH34", *227th American Chemical Society National Meeting*, Anaheim, USA, (28 Mars - 1er Avril 1 2004)

2004-3 Bellet E., Biquard X., Cibert J., Bougerol C., Ferrand D., Giraud R., Halley D., Kulatov E., Kuroda S., Marcet S., Mariette H., Titov A., "Properties of Ga1-xMnxN epilayers grown by molecular beam epitaxy", *27th International Conference on the Physics of Semiconductors*, Flagstaff, Arizona (26-30 juillet 2004)

2004-4 Cacaly S., C. Maréchal, S. Cornu, F. Juillot, G. Morin, F. Guyot, "Etude cristallochimique du zinc dans des sols développés sur anomalies géochimiques naturelles", *20ème Réunion des Sciences de la Terre*, Strasbourg (20-25 septembre 2004)

2004-5 Dähn R, Scheidegger A.M., Manceau A., Baeyens B., Bradbury M.H. "Uptake mechanism of Ni(II) on montmorillonite as determined by X-ray absorption spectroscopy", *Goldschmidt Conference*, Copenhagen (5-11 June 2004)

2004-6 Le Floch M., "Physico-chemical characterisation of particulate heavy metals from municipal solid waste incinerator emissions and their contribution to ambient air quality. Case of Toulon MSWI (south of France)", *20ème Réunion des Sciences de la Terre*, Strasbourg (20-25 septembre 2004)

2004-7 Geantet C, Y. Soldo, J.L. Hazemann, "Time resolved XAFS studies on catalytic systems", *In situ and Operando Spectrocopy for Catalysis (ISOSCAT)*, Caen (18-21 Juillet 2004) (**Conférence invitée**)

2004-8 Hazemann J.L., "Fluorescence X: Expérimentation en conditions hydrothermales", *Formation Expérimentation en Sciences de la Terre* (E.N.S. Lyon), Banyuls-sur-Mer, (22-24 Novembre 2004) (**Conférence invitée**)

2004-9 Hori Y, Andreev T, Jalabert D, Biquard X, Monroy E, Tanaka M, Oda O, Dang LS, Daudin B, "Structural and optical properties of rare-earth doped quantum dots grown by plasma-assisted MBE", *5th International Symposium on Blue Laser and Light Emitting Diodes (ISBLLED 2004)*, Gyeongin, Corée du Sud (15-19 mars 2004)

2004-10 Laulhe C., F. Hippert, J. Kreisel, M. Maglione, A. Simon, "XAFS investigation of the peculiar lead-free relaxor $BaTi_{0.65}Zr_{0.35}O_3$", *Journées Couches Ferroélectriques 2004*, Besançon (18-19 Novembre 2004)

2004-11 Manceau A., Panfili F., Kirpichtchikova T., Sarret G., Lanson B., "Probing the speciation of metals at the soil-plant interface using micrometer-scale X-ray fluorescence, diffraction, and absorption techniques", *Rhizosphere 2004*, Munich (12-17 septembre 2004) (**Conférence pleinière**)

2004-12 Manceau A., Lanson B., Sarret G., "Microsight and megascience in the environmental realm at 3rd generation synchrotrons", *Users' meeting of the Advanced Light Source*, Berkeley (18-20 octobre 2004) (**Conférence invitée**)

2004-13 Menez B., J. Cauzid, J. Foriel, E. Gerard, P. Philippot, C. Rommevaux-Jestin, Y. Wang, M. Salome, A. Simionovici, A. Somogyi, P. Lopez-Garcia, M. Moreira, M. Munoz, H. Bureau, L. Avoscan, B. Gouget, J. L. Hazemann, O. Proux, "Potentialités du rayonnement synchrotron pour l'étude des interactions géomicrobiologiques", *4ème Journées Soleil Région Centre*, Orléans (6 et 7 décembre 2004)

2004-14 Morin G., S. Lebrun, F. juillot, C. Casiot, S. Belin, O. Proux and G. Calas, "Structure and reactivity of nano-crystalline As-Fe oxy-hydroxides in acid mine drainage", *Goldschmidt Geochemistry Conference*, Copenhague (5-11 juin 2004), *Geochimica et Cosmochimica Acta* **68** issue 11 suppl. 1 (2004) A102 (abstract)

2004-15 Ona-Nguema G., G. Morin, F. Guyot, O. Proux, J-L. Hazemann, M. Abdelmoula, G. Calas, "Biomineralogical processes controlling iron and arsenic mobility in anoxic systems" *European Geosciences Union, 1st General Assembly*, Nice (25 - 30 Avril 2004)

2004-16 Pokrovsky G., "Expérimentation en conditions hydrothermales", *Formation Expérimentation en Sciences de la Terre* (E.N.S. Lyon), Banyuls-sur-Mer (22-24 Novembre 2004) (**Conférence invitée**)

2004-17 Rihs S., Gaillard C., Manceau A., "Adsorption de U^{VI} sur les oxydes de manganèse" *20ème Réunion des Sciences de la Terre*, Strasbourg (20-25 septembre 2004)

2004-18 Rose J., Benard A., Bottero J-Y, "Towards improved waste and water treatment processes: the necessity of synchrotron light", *Swiss Light Source 2004 Users Meeting*, Villigen, Suisse (4-5 octobre 2004) (**Conférence invitée**)

2004-19 Rose J., Chanéac C., Prelot B., Bodiot O., Jolivet J-P., Balesdent J., Heulin T., Spalla O., Thill A., Botta A., Bergé-Lefranc J-L., Demeo M., Orsière T., Garnier J-M., Masion A., Moustier S., Bottero J-Y., Wiesner M. R., "Surface properties of industrial Fe-oxide nanoparticles: Mechanisms of bio-degradation, bio-accumulation and mutagenic effects", *Goldschmidt Geochemistry Conference*, Copenhague (5-11 Juin 2004)

2004-20 Sarret G., Manceau A., Marcus M.A.M., Saumitou-Laprade P., Willems G., Garnier J.M., Balesdent J., "Determining the Chemical Form of Metals in Soils and Plants by Synchrotron Techniques", *87th Canadian Chemistry Conference*, London, Canada (29 mai- 1er Juin 2004) (**Conférence invitée**)

2004-21 Sarret G., Saumitou-Laprade, P., Willems, G., and Manceau, A., "Accumulation et excrétion du zinc par les plantes", *Journée scientifique de l'IMBG, Zinc et Cadmium dans l'Environnement et la Santé*, Grenoble (19 Mai 2004)

2004-22 Testemale D., Hazemann J-L. and Proux O. "Local structures in supercritical water", *20ème Réunion des Sciences de la Terre*, Strasbourg (20-25 septembre 2004)

2004-23 Testemale D., "Structure of molecules in HP/HT aqueous solutions: a XAS study", *ESRF Users' meeting 2004*, Grenoble (8-13 Février 2004)

2004-24 Testemale D., JL. Hazemann, R. Argoud, O. Geaymond, "A novel high pressure and high temperature cell for x-ray studies", *4ème Forum de Technologie des Hautes Pressions*, Messigny, Dijon (1-5 Novembre 2004)

2003

2003-1 Bert V., Panfili F., Manceau A., Girondelot B., Laboudigue A. "Phytostabilisation of metal-rich dredged sediments", *Workshop COST 837 'Phytoremediation of toxic metals'*, Stockholm, (12-15 Juin 2003).

2003-2 Dähn R., Scheidegger A., Manceau A., Grolimund D. "Sorption mechanisms of radionuclides on clay mineral surfaces as determined by polarized x-ray absorption spectroscopy", *American Chemical Society Annual Meeting*, New Orleans (23-27 Mars 2003)

2003-3 Le Si Dang D., "Recent progress and physics of GaN/AlN quantum dots", *3rd conference on Physics of Light-Matter Coupling in Nanostructures (PLMCN 3)*, Acireale, Sicile (1 4 Octobre 2003) (**Conférence invitée**)

2003-4 Daudin B, Gogneau N, Adelmann C, Sarigiannidou E, Andreev T, Enjalbert F, Monroy E, Fossard F, Rouviere JL, Hori Y, Biquard X, Jalabert D, Dang LS, Tanaka M, Oda O, "Structural and optical properties of GaN quantum dots", *GaN and Related Alloys – 2003 MRS Fall Meeting*, Editors: Ng HM, Wraback M, Hiramatsu K, Grandjean N *Materials Research Society Symposium Proceedings*, **798** (2003) 127-137

2003-5 Hori Y, Enjalbert F, Jalabert D, Monroy E, Dang L, Biquard X, Tanaka M, Oda O, Daudin B, "Visible red light emission from Eu-doped GaN quantum dots grown by plasma-assisted MBE", *5th International Conference on Nitride Semiconductors (ICNS-5)*, Nara, Japan (25-30 Mai 2003)

2003-6 Isaure M.P., Manceau A., Laboudigue A., Tamura N., Marcus M.A. "Zn speciation in a soil contaminated by the deposition of a dredged sediment by synchrotron x-ray techniques" *XII International Conference on Heavy Metals in the Environment*, Grenoble, (26-30 Mai. 2003)

2003-7 Kreisel J., "The effect of high-pressure on relaxor ferroelectrics", 21st Meeting of the European Crystallographic Association. Durban, Afrique du Sud (24-29 Août 2003) (**Conférence invitée**)

2003-8 Kreisel J., "L'effet de la pression sur des ferroélectriques relaxeurs", *Journées de Couches Ferroélectriques*, Réunion de GDR, Bordeaux (18-19 Septembre 2003)

2003-9 Kuroda S., E. Bellet-Amalric, X. Biquard, J. Cibert, R. Giraud, S. Marcet,and H. Mariette "Optimization of the growth of Ga1-xMnxN epilayers using plasma-assisted MBE", *5th International Conference on Nitride Semiconductors*, Nara, Japan, (25-30 Mai 2003)

2003-10 Lanson B., Drits V.A., Manceau A. "Structure of heavy metal sorbed birnessite", *Euroclay conference*, Modena, (22-26 Juin 2003)

2003-11 Lanson B., Manceau A., Drits V. "Crystal-chemistry of poorly crystalline minerals as a tool to understand the fate of heavy metals in the environment", *NSLS Users' Meeting*, Brookhaven, (May 19-21 2003) (**Conférence invitée**)

2003-12 Della Longa S., Arcovito A., Benfatto M., Congui-Castellano A., Girasole M., Hazemann J.L. and Lo Bosco A., "XANES quantitative analysis of the redox-induced structural dynamics of the Fe-Heme-ligand in myoglobine", *12th International Conference on X-ray Absorption Fine Structure (XAFS-12)*, Malmö, Sweden, (22-27 Juin 2003) (**Conférence invitée**)

2003-13 Manceau A., "Heterogeneity, Multiplicity, Variability: The environmental clay scientist's trilogy. Brindley Lecture", *Annual meeting of the Clay Minerals Society of America*, Athens, USA, (9-12 Juin 2003) (**Conférence pleinière**)

2003-14 Manceau A. "Shining synchrotron light on the complex world of environmental materials" *8th International Conference on Synchrotron Radiation Instrumentation (SRI-2003)*, San Francisco, (25-29 Août 2003) (**Conférence pleinière**)

2003-15 Manceau A., Marcus M.A., Tamura N. "Illuminating the complex world of environmental materials with bright synchrotron light", *Workshop on x-ray microscopy*, Users meeting of the Advanced Light Source (ALS), Berkeley, (6-7 Octobre 2003) (**Conférence invitée**)

2003-16 Manceau A., Marcus M.A., Tamura N., Padmore H.A. "Full determination of heavy metal speciation in environmental systems", *12th International Conference on X-ray Absorption Fine Structure (XAFS-12)*, Malmö, Sweden, (22-27 Juin 2003) (**Conférence invitée**)

2003-17 Manceau A. "L'outil physique et mathématique au service de la protection des sols et de la réhabilitation des sites contaminés par les métaux lourds", *Réunion Annuelle de la Société Française de Physique*, Lyon, (7-10 Juillet 2003) (**Conférence invitée**)

2003-18 Manceau A., "Spéciation des métaux lourds dans les matériaux naturels par les techniques synchrotron: état de l'art et perspectives", *Atelier 'Imagerie et Synchrotron Soleil'*. (26-28 Novembre 2003), Orsay

2003-19 Marcus M.A., Manceau A., Panfili F., MacDowell A.A., "Probing Natural Systems With Combined Micro XAS, XRF and XRD", *XAS at Third Generation Sources: Highlights and Future Perspectives*, ESRF, Grenoble, (19-20 Juin 2004) (**Conférence invitée**)

2003-20 Panfili F., Manceau A., Sarret G., Kirpichtchikova T., Marcus M., Bert V., Laboudigue A., Libert M. "Direct and quantitative Zn speciation in a phytostabilized sediment" *7th International Conference on the Biogeochemistry of Trace Elements*, Uppsala, (14-19 Juin 2003)

2003-21 Pessayre S, Geantet C. Bacaud R., Sato K. and Vrinat M. "Pt doped Hydrotreating catalysts for ultradeep hydrodesulfurization of diesel fuels" *18th North American Meeting (NAM)* organisé par The North American Catalysis Society (NACS), Cancun, Mexico (1-6 Juin 2003)

2003-22 Proux O., X. Biquard, E. Lahera, J.-J. Menthonnex, A. Prat, O. Ulrich, Y. Soldo, P. Trévisson, G. Kapoujvan, G. Perroux, P. Taunier, D. Grand, P. Jeantet, M. Deleglise, J.-P. Roux and J.-L. Hazemann: FAME: A new beamline for X-ray absorption investigations of very-diluted systems of environmental, material and biological interests, *12th International Conference on X-ray Absorption Fine Structure (XAFS-12)*, Malmö, Sweden, (22-27 Juin 2003).

2003-23 Sarret G., Schroeder W.H., Marcus M.A., Geoffroy N., Manceau A. "Localization and speciation of Zn in mycorrhized roots by µSXRF and µEXAFS", *XII International Conference on Heavy Metals in the Environment*, Grenoble, (26-30 Mai. 2003)

2003-24 Thoral S., Rose J., van Geen L., Garnier J.M., Chapon V., Hazeman J-L, Heulin T., Bottero J-Y. "Oxidation of natural groundwater from Bangladesh: As-Fe interactions assessed by XAS", *XAS at Third Generation Sources: Highlights and Future Perspectives*, ESRF, Grenoble (19-20 juin 2003)

Communications par affiche

2005

2005-1 Panfili F., Manceau A., Sarret G., Laboudigue A., Bert V., Marcus M. : Changes in Zn speciation in the rhizosphere of graminaceous plants induced by phytostabilization of a contaminated sediment. *15th Annual Goldschmidt Conference*, Moscow, Idaho, 20-25 May

2005-2 Rihs S., Gaillard C., Manceau A.: Interaction of U(VI) with birnessite: a solution chemistry and EXAFS study. *15th Annual Goldschmidt Conference*, Moscow, Idaho, 20-25 May

2004

2004-1 Coulet V., Testemale D., Hazemann J.-L., Raty J.-Y., Gaspard J.-P., Bichara C., "An EXAFS analysis of the structural changes in liquid $Ge_{0.15}$ $Te_{0.85}$ eutectic alloy", *12th International Conference on Liquid and Amorphous Metals*, Metz, 11-16 juillet 2004

2004-2 Lahera E., J-J. Menthonnex, O. Proux, J-L. Hazemann, "FAME : une ligne d'absorption X dédiée principalement à l'étude des systèmes trés dilués en sciences de l'environnement", *3ème journées des Rencontres de l'Observatoire des Sciences de Univers de Grenoble* (18 novembre 2004)

2004-3 Morin G., Lebrun S., juillot F., Casiot C., Bruneel O., Belin S., Proux O., Brown G.E., Guyot F. and Calas G., "Bacterial control on the structure of As-Fe oxy-hydroxides in acid mine drainage", *2004 AGU Fall Meeting*, San-Francisco (13-17 décembre 2004), Eos Trans. AGU, **85** (47), Fall Meet. Suppl. Abstract

2004-4 Noack Y., M. Collet, M. Le Floch, "Zinc speciation in steel plant atmospheric emissions. A multi-techniques approach", *20ème Réunion des Sciences de la Terre*, Strasbourg, 20-25 septembre 2004

2004-5 Proux O., D. Testemale, J-L. Hazemann, E. Lahera, J-J. Menthonnex, "In-situ X-ray Absorption Spectroscopy experiments under hydrothermal conditions on the CRG-FAME beamline", *20ème Réunion des Sciences de la Terre*, Strasbourg, 20-25 septembre 2004

2004-6 Testemale D., J-L. Hazemann and O. Proux, "Local structures in supercritical water", *Configurational energy landscapes and structural transitions in clusters, fluids and biomolecules at the Royal Society of London*, Londres (19-20 avril 2004)

2004-7 Thibault M.-H., L. Galoisy, G. Calas, J.-L. Hazemann and O. Proux, "Atomic scale determination of the insertion of Cr^{3+} in spinel and garnets: an EXAFS study of site relaxation and element clustering", *Goldschmidt Geochemistry Conference*, Copenhague (5-11 juin 2004), *Geochimica et Cosmochimica Acta* **68** issue 11 suppl. 1 (2004) A87 (abstract)

2003

2003-1 Dähn R., Scheidegger A., Manceau A. "Uptake mechanisms of heavy metals on clay surfaces as determined by polarized EXAFS". *12'th International Conference on X-ray Absorption Fine Structure* (XAFS-12), Malmö, Sweden, (22-27 Juin 2003)

2003-2 Isaure M.P., Manceau A., Laboudigue A., Tamura N., Marcus M.A. "Zn speciation in a soil contaminated by the deposition of a dredged sediment by synchrotron x-ray techniques", *XII International Conference on Heavy Metals in the Environment*, Grenoble, (26-30 Mai 2003)

2003-3 Kirpichtchikova T., Manceau A., Lanson B., Sarret G., Marcus M.A., Jacquet T. "Speciation and mobility of heavy metals (Zn, Cu and Pb) in soil contaminated by sewage irrigation", *XII International Conference on Heavy Metals in the Environment*, Grenoble, (26-30 Mai 2003)

2003-4 Panfili F., Manceau A., Sarret G., Kirpichtchikova T., Marcus M., Bert V., Laboudigue A., Libert M. "Direct and quantitative Zn speciation in a phytostabilized sediment", *7th*

International Conference on the Biogeochemistry of Trace Elements, Uppsala, (14-19 Juin 2003)

2003-5 C E Tommaseo, A Manceau, B Lanson, G Sposito, "Structural Study Of Nickel- And Zinc-Doped Layer Type Manganese Oxides", AGU Fall Meeting, San Francisco, (8-12 Décembre 2003)

Séminaires

2003

2003-1 Geantet C. "Genesis of the active phase of an hydrotreating CoMo catalyst", *Centro de Investigaciones del Petroleo (CEINPET)*, La Havanne, Cuba (10 Juin 2003)

2003-2 Manceau A. "Le devenir des métaux lourds dans les sols: Où et comment se cachent-ils? " *DEA de Sciences de la Terre de Toulouse* (20 Novembre 2003), *ENS Lyon* (22 Mars 2003), *LGIT Grenoble* (12 Décembre 2002)

Thèses et Habilitations à Diriger les Recherches

2004

2004-1 Thoral S., "Étude des interactions Fer-Arsenic dans les eaux souterraines du Bangladesh: approche microbiologique et physico-chimique", *Thèse de l'Université Aix-Marseille III Spécialité Géosciences de l'Environnement* (2004)

2004-2 Rose J., "Dynamique et toxicité des colloïdes et contaminants: apports de la physico-chimie moléculaire", *Habilitation à Diriger des Recherches de l'Université Paul Cézanne* (2004)

2004-3 Panfili F., "Bioaccumulation du Zinc dans les végétaux. Effet de la plante sur la spéciation du métal dans le sol", *Thèse de l'Université Joseph Fourier de Grenoble (2004)*

2003

2003-1 Testemale D., "Structures locales en solution aqueuse supercritique", *Thèse de l'Université Joseph Fourier de Grenoble spécialité Physique* (2003)

- *prix Haüy-Lacroix 2004* de la Société Française de Minéralogie et Cristallographie.
- *prix Besson 2004* du réseau français de Hautes Pressions.

2003-2 Devers E., "Catalyseurs à base de métaux nobles supportés sur zircone pour l'hydrodésazotation poussée des gazoles", *Thèse de l'Université Claude Bernard Lyon 1 spécialité Chimie* (2003)

2003-3 Bénard A., "Le Plomb et le Chrome dans les Ciments : Spéciation et Modélisation du Transfert au cours de la Lixiviation", *Thèse de l'Université Aix-Marseille III Spécialité Géosciences de l'Environnement* (2003)

2003-4 Hazemann J.-L., "Mise en évidence des modifications structurales locales dans des solutions aqueuses en conditions sub et supercritiques", *Habilitation à Diriger des Recherches de l'Université Joseph Fourier de Grenoble* (2003)

Rapports d'expériences ligne CRG-FAME 2003-2004

ESRF	Experiment title: **Role of microorganisms on oxidation state and trapping mechanisms of As by iron oxides.** **Rôle des microorganismes sur l'état d'oxydation de l'arsenic et son piégeage par les oxydes de fer**	**Experiment number**: 30-02-633
Beamline:	**Date of experiment**: from: 12 june 2003 to: 17 june 2003 01 october 2003 to : 07 october 2003	**Date of report**: 10 / 03 /2004
Shifts:	**Local contact(s)**: Olivier Proux, Jean-Louis Hazemann	*Received at ESRF:*

Names and affiliations of applicants (* indicates experimentalists):
Guillaume MORIN*, François GUYOT* , sophie LEBRUN*, Georges ONA-NGUEMA* LMCP UMR7590 - Paris6&7 – IPGP, 140 rue de Lourmel 75015 Paris
Philippe BARANGER, BRGM, 3, avenue Claude Guillemin - BP 6009 - 45060 Orléans Cedex 2
Jean-Christian PERSONNÉ, Hydrosciences, UMR 5569 CNRS- Montpellier II-IRD, CC57, 34095 Montpellier cedex 05.
Violaine BONNEFOY, UPR 9043 CNRS, Lab.Chimie Bacterienne, 31 ch. Joseph Aiguier, 13402 Marseille Cedex 20

Report:

EXAFS and XANES data were recorded at the As-K edge (11 869 eV) using a Si(220) monochromator at the BM30B/FAME beamline. Data were essentially collected at 10K. Most data were recorded in fluorescence mode using a 30 elements Ge - array detector completed by a 3$\Delta\mu$ Ge filter to attenuate elastic scattering and Fe fluorescence from our Fe-rich samples. Thanks to dynamic horizontal focusing by the second monochromator crystal, we had a very high flux at 12 keV, despite FAME is a bending magnet beamline. By comparison with previous experiments we carried out on other beamlines with samples having similar chemical compositions, the flux on the sample on FAME was not more than an order of magnitude lower than that delivered by high flux undulator beamlines as ID26. Thanks to horizontal focusing, energy resolution was also very good, about 0.5 eV.
EXAFS and XANES data were recorded in step-scan mode after recording few quick-XANES spectra in order to check for unwanted photo-oxydation or reduction of the samples under the beam.

From an experimental point of view, we showed thanks to quick-XANES data that the photo-oxydation of As(III) by Fe(III) under the beam is severely slowed at liquid He temperature (Figure 1). It is also noticeable that the rate of As(III) oxidation thoroughly increases with increasing Fe(III)/As(III) ratio in the sample, as illustrated in Figure 2.

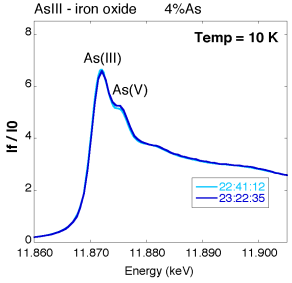

Figure 1. As K-edge XANES spectra recorded in fluorescence mode at 10K in oct 2003 at FAME. The sample consists of an iron-oxide containing 4 wt% As. The rate of As(III) photo-oxidation is enough slow at this temperature (compared to 300K, Figure 2) to record full EXAFS data in 40 mn step scans without changing the As oxidation state.

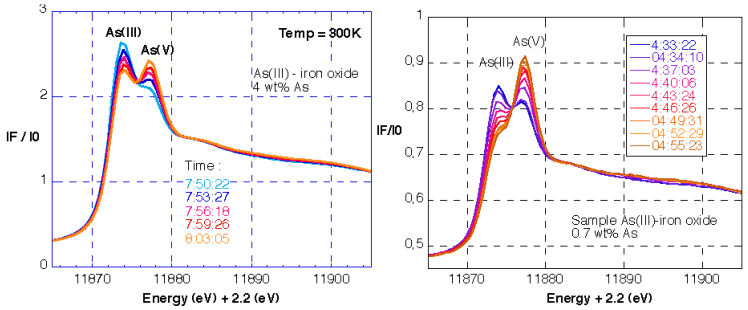

Figure 2. As K-edge quick-XANES spectra recorded in fluorescence mode at 300K on ID26 in 2002. The samples consists of iron-oxides containing 4 and 0.7 wt% As. (Left sample is the same as in figure 1). The rate of As(III) photo-oxidation under the beam increases whith decreasing As(III) concentration in the sample.

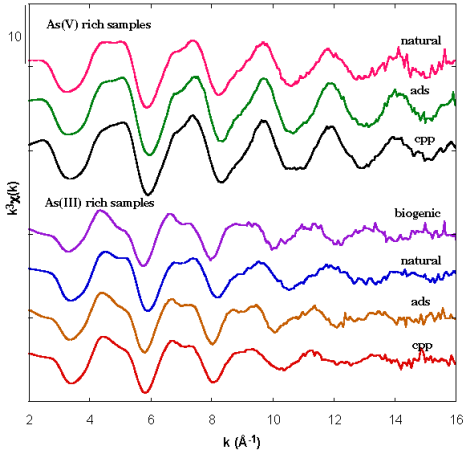

Figure 3. Representative As K-edge EXAFS spectra recorded in fluorescenece mode at 10K during the oct. 2003 run. Samples consists of iron-oxides containing 1 to 4wt% As. Although BM30B deliver a high flux on the samples, 5 to 10 scans of 40 mn in k-scan mode were necessary to get reliable S/N ratios because of the very high Fe K fluorescence background. The set of samples shown here includes natural and synthetic arsenic doped iron oxyhydroxides produced by iron and/or arsenic oxidizing bacteria in acid mine drainage environment. Arsenic coprecipitates with - and sorbs onto - bacterially produced iron-oxides, the redox state of arsenic in the solid depending on the ability of bacteria to oxidize As(III) into As(V). Natural samples are compared to synthetic ones prepared by biotic or abiotic pathways. Natural samples contain a mixtture of AsIII and AsV. This difficulty will be overcomed by using linear decomposition of the spectra.

Abstracts

Morin et al. 2004. Structure and reactivity of nano-crystalline As-Fe oxy-hydroxides in acid mine drainage. Goldschmidt Conf. Copenhague.
Lebrun et al. 2004 Mineralogy of As-Fe precipitates in acid mine drainage. the role of acidophilic bacteria. EGU Nice.
Ona-Nguema et al. 2004 Biolmineralogical processes controlling arsenic mobility in anoxic environments. EGU Nice

	Experiment title: **Study of the incorporation of Rare-earths in GaN/GaInN quantum dots**	**Experiment number:** 30.02.637
Beamline: BM30B	**Date of experiment:** from: 30/10/2003 to: 03/11/2003	**Date of report:** 05/10/2004 *Received at ESRF:*
Shifts: 12	**Local contact(s):** Xavier BIQUARD	

Names and affiliations of applicants (* indicates experimentalists):
Xavier BIQUARD*, CEA-Grenoble - DRFMC/SP2M/NRS
Thomas ANDREEV*, CEA-Grenoble – DRFMC/SP2M/NS
Yuji HORI*, NGK Insulators, Japon (currently in DRFMC/SP2M/NS)
Denis JALABERT*, CEA-Grenoble - DRFMC/SP2M/SiNaPs
Bruno DAUDIN, CEA-Grenoble – DRFMC/SP2M/NS

Report:

Overview

We have recorded room-temperature fluorescence EXAFS and XANES spectra at the Eu, Er and Tm K-edges (6.9 to 9 keV) using the 30-element energy-resolved detector, samples being kept under primary vacuum to avoid air diffusion.

Studied samples were made of 50 layers of doped GaN QDs embedded inside AlN. The QDs were doped with different amount of Eu or Er or Tm, and were grown on an Al2O3 substrate covered by MOCVD AlN as furnished by NGK.

As a lot of Bragg diffraction peaks originating form the substrate were superimposed on absorption spectra, we have systematically used quick-EXAFS scans prior to data acquisition to finely adjust the X-ray incident angle on sample to minimize the number of (annoying) Bragg peaks.

Studied samples

1°) Europium

1. 3 reference samples: metallic Eu sample N0069, bulk GaN doped with Eu (N0042) and Eu2O3 powder.
2. 2 QDs samples: sample S1425 (2.5% of Eu) that was previously studied in IHR, and sample N0066 doped with 0.6% of Eu.

2°) Erbium

1 QDs sample: N0077 doped with 3.2% of Er

3°) Thulium

1. 1 reference sample of metallic Tm N0070
2. 2 QDs samples: sample N0074 (2.3% of Tm) and sample N0073 (3% of Tm)

Results

This proposal was very successful since the good quality of the recorded EXAFS spectra have enabled us to clearly determine the localization of both Eu and of Tm in our samples. Exafs analysis was focused on determining the chemical composition of the second nearest neighbors as is illustrated in figure 1 and table 1 for Eu, and figure 2 and table 2 for Tm. These EXAFS studies (coupled with photoluminescent and cathodoluminescent ones) showed

- that Eu is incorporated substitutionnally inside GaN QDs since only Ga forms the second nearest neighbor shell
- that Tm incorporates substitutionnally at the interface between GaN QDs and AlN, in the AlN part of the interface, thus yielding 1/4th of second nearest neighbors as Ga and 3/4th as Al.

Detailed results concerning Eu were published in "GaN quantum dots doped with Eu", Y. Hori, X. Biquard, E. Monroy, D. Jalabert, F. Enjalbert, Le Si Dang, M. Tanaka, O. Oda, and B. Daudin, APL, vol 84 (2), pp 206-208 (2004)

And detailed results concerning Tm will be submitted shortly (probably to PRB), under the title "Optical and morphological properties of GaN quantum dots doped with Tm", T. Andreev, Y. Hori, X. Biquard, E. Monroy, D. Jalabert, A. Farchi, M. Tanaka, O. Oda, Le Si Dang and B. Daudin.

Second nearest neighbor shell	Eu in GaN QDs	Eu in AlN matrix
Coordination number	12	12
Bond length distortion (%)	-1.7 ± 0.3	- 0.25 ± 1.1
Debye Waller factor (10^{-3} Å^2)	8.3 ± 0.2	4.4 ± 1.2
Energy shift (eV)	-26 ± 2	-10 ± 5
r-factor (quality) of fit (%)	0,14	4

Table 1: best fit parameters for Eu

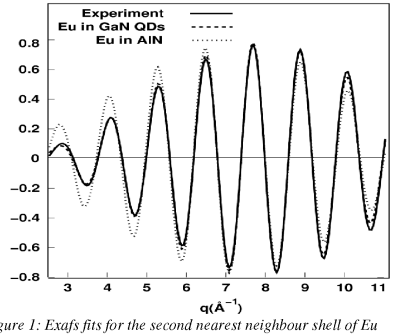

Figure 1: Exafs fits for the second nearest neighbour shell of Eu

Second nearest neighbor shell	Tm in GaN	Tm in AlN	Tm in (GaN,AlN)	
			GaN	AlN
Proportion (%)			25 ± 4	75± 4
Bond distortion (%)	-1.6 ± 0.8	0.0 ± 0.7	-1.7 ± 0.6	+1.8 ± 0.8
DW factor (10^{-3} Å^2)	13± 1	1± 1	5 ± 4	
Energy shift (eV)	-21 ± 4	-6 ± 2	-2 ± 3	
Quality of fit (%)	3,4	3,9	0,2	

Table 2: best fit parameters for Tm

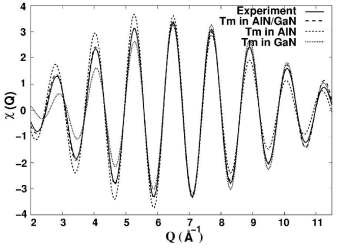

Figure 2: Exafs fits for second neighbour shell of Tm

ESRF	**Experiment title:** A XAFS spectroscopy study of local environment around gold in high T/P aqueous sulfide and chloride solutions: Implications for the mechanisms of gold deposits formation	**Experiment number:** 30 02 639
Beamline: BM30B	**Date of experiment:** from: 3 November 2003 to: 11 November 2003	**Date of report:** 5 August 2004
Shifts: 21	**Local contact(s):** Jean-Louis Hazemann, BM30B (FAME), ESRF	*Received at ESRF:*

Names and affiliations of applicants (* indicates experimentalists):

* **Jacques Schott**, Laboratoire des Mécanismes & Transferts en Géologie, LMTG-OMP-CNRS, Toulouse
* **Gleb Pokrovski**, LMTG, same address
* **Jean-Louis Hazemann**, Laboratoire de Cristallographie, ESRF-CNRS, Grenoble
* **Boris Tagirov**, Institut fur Mineralogie und Petrographie, ETH – Zentrum, Zurich, Switzerland

Report:

Experimental. The dissolution and atomic structure of gold in chloride and sulfide aqueous solutions were examined by XAFS spectroscopy at Au L_3-edge at temperatures to 400°C and pressures to 100 MPa, using an X-ray cell recently developed at the Laboratoire de Cristallographie (Grenoble). This cell allows simultaneous measurement of the absolute concentration of the absorbing element in the fluid (from edge-step height in transmission mode, fluid density and absorption cross-section of the element), and atomic environment around the absorber (from analysis of XANES and EXAFS spectra in fluorescence mode). Details about the cell operation and spectra analysis can be found in refs. 1 & 2. An improved cell design used for the present experiment utilizes a piston equipped with Viton joints and inserted into a thin-wall mono-crystalline sapphire tube. This construction avoids solutes precipitation in the colder parts of the cell. Unfortunately, multiple diffraction peaks arising from the mono-crystalline sapphire made impossible analysis of the EXAFS part of most spectra. Consequently, only gold total concentration and near-edge structure (XANES) could be accurately accessed.

Results on the gold-chloride system. Four experiments were performed in the system $HAu^{(III)}Cl_4$-NaCl-HCl±Au(metal) at 60 MPa as a function of temperature and time. It was found that below 200°C, the XANES spectra of Au in solution exhibit a strong before-edge feature (Fig. 1, A) corresponding to 2p-5d electronic transitions characteristic of tri-valent Au in the plane square $Au^{(III)}Cl_4^-$ complex reported in previous low-temperature XAFS and Raman studies[3,4]. At 200°C, this feature rapidly disappears indicating a reduction of this species, presumably into $Au^{(I)}Cl_2^-$ (ref. 4, 5). However, at higher temperature, the absorption-edge height shows rapid gold precipitation (Fig. 2). XANES spectra above 250°C display features characteristic of metallic gold (Fig. 1). It is not clear whether some gold still remains in solution in the form of Au° colloids or precipitated on the cell walls on the passage of the X-ray beam. The very narrow temporal and temperature interval of the Au(I) appearance in solution (Fig. 1 & 2) contradicts to the previous batch-reactor solubility studies which indicate that above 250°C, $AuCl_2^-$ should be the dominant species, and attain concentrations ~10 times higher than measured in our experiments [4,5]. This discrepancy might be attributed to a leak of oxygen through the Viton seals or reaction with these seals, thus destabilizing Au(I) chloride species in favor of metallic gold. Another possibility could be the beam-induced reduction of $AuCl_2^-$ into Au° (ref. 3).

Results on the gold-sulfide system. An experiment was performed in the system Au-NaOH-S by allowing a foil of metallic gold and sulfur crystals to react with a NaOH aqueous solution at elevated temperature. The complete dissolution of sulfur occurs above 100°C and produces sulfide (H_2S, HS^-) and sulfate (HSO_4^-, SO_4^{2-}) species. Fig. 3 shows that at 300°C and 60 MPa, gold rapidly dissolves, resulting in a spectrum similar to that of Au_2S (Fig. 1) and $Na_3Au(S_2O_3)_2$ (not shown) in which $Au^{(I)}$ is linearly coordinated by two sulfur atoms. This indicates that dissolved Au(I) is likely to be surrounded by two sulfide ligands in this solution by forming $Au(HS)_2^-$, as was suggested by solubility studies (c.f. ref. 6). Au concentrations attain a steady-state after about 4 hours of dissolution at 300°C (Fig. 3). At 400°C, however, a regular drop of Au concentration with time is observed. The before-edge absorption in transmission mode also shows a significant decrease which can be attributed to a loss of sulfur (the major contributor to the absorption below the Au L_3 edge in this solution). This could be due to a leak of the volatile and reactive H_2S through the Viton seals out of the cell. Nevertheless, such a leak does not occur at T≤300°C, and the absorption edge heights measured at steady-state at 300°C/60 MPa allow determination of Au concentration in solution in equilibrium with metallic gold: 0.091±0.020 mol/kg H_2O (pH=6.1, m(HS^-)=0.4, m(H_2S)=1.5, m(SO_4^{2-})=0.8). This value is in agreement with that predicted using the thermodynamic properties of $Au(HS)_2^-$ obtained from our recent batch-reactor solubility study (ref.7): m(Au)=0.27±0.15.

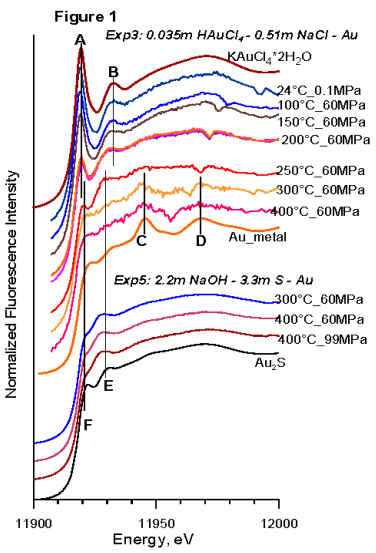

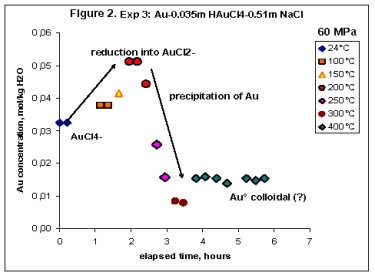

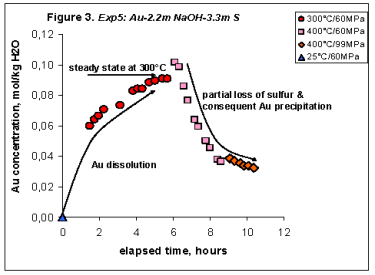

Fig. 1. Normalized near-edge fluorescence spectra of Au-bearing solids and experimental solutions at indicated conditions (concentrations are in molalities). Vertical lines show XANES features characteristic of the square $Au(III)Cl_4$ cluster (A & B), metallic gold (C & D), and linear $Au(I)S_2$ and $Au(I)Cl_2$ (E & F) configurations.

Fig. 2 & 3. Total dissolved concentration of gold as a function of time and temperature for the experiments in the systems $HAuCl_4$-NaCl-Au (Fig. 2) and Au-NaOH-S (Fig. 3) shown in Fig. 1.

Conclusions & perspectives. To our knowledge, this experiment is the first measurement of gold solubility and structure of Au(I) chloride and sulfide complexes at hydrothermal conditions using *in situ* XAFS spectroscopy. Our results demonstate the feasability of XAFS measurements of this extremely inert and weakly soluble noble metal. They bring the first undoubted spectroscopic evidence that, at least to 400°C, 1 kbar, Au(I) forms in sulfide bearing solutions linear complexes in which it is coordinated to 2 HS ligands. The ultimate goal of our future experiments will be to access, via EXAFS spectra, quantitative structural parameters of the $Au^{(I)}$ complexes dominant in natural ore-forming fluids, and to measure Au solubilities over a wide range of magmatic-hydrothermal conditions. This will be achieved using an improved cell construction (polycristalline sapphire avoiding diffraction, high-temperature joints with improved seal properties), and the high X-ray flux and sensitive detection provided by FAME or ID26 beamlines at the ESRF.

References

1. Pokrovski G.S., Zakirov I.V., Roux J., Testemale D., Hazemann JL., Bychkov A.Y., & Golikova G.V. (2002) Experimental study of arsenic speciation in vapor phase to 500°C: Implications for As transport and fractionation in low-density crustal fluids and volcanic gases. *Geochim. Cosmochim. Acta* **66**, 3453-3480.
2. Pokrovski G.S., Roux J., Hazemann JL., & Testemale D. (2004) An X-ray Absorption spectroscopy study of argutite solubility and germanium aqueous speciation in hydrothermal fluids to 500°C and 400 bar. *Chem. Geology (submitted).*
3. Berrodier I., Farges F., Benedetti M., Winterer M., Brown G.E., Jr., Deveughèle M. (2004) Adsorption mecanisms of trivalent gold on iron- and aluminum-(oxy)hydroxides. Part 1. *Geochim. Cosmochim. Acta* **68**, 3019-3042.
4. Murphy P.J., Stevens G., & LaGrange S. (2000) The effects of temperature and pressure on gold-chloride speciation in hydrothermal fluids: A Raman spectroscopic study. *Geochim. Cosmochim. Acta* **64**, 479-494.
5. Gammons C.H. & Willams-Jones A.E. (1997) The disproportionation of gold(I) chloride complexes at 25 to 200°C. *Geochim. Cosmochim. Acta* **61**, 1971-1983.
6. Shenberger D.M. & Barnes H.L. (1989) Solubility of gold in aqueous solutions from 150 to 350°C. *Geochim. Cosmochim. Acta* **53**, 269-278.
7. Tagirov B.R., Salvi S., Schott J., Baranova N.N. (2004) Experimental study of gold-hydrosulphide complexing in aqueos solutions at 350-500°C, 500 and 1000 bars using mineral buffers. *Geochim. Cosmochim. Acta* (in press).

ESRF	**Experiment title:** Toxicité de l'arsenic: mécanismes cellulaires de transfert et de résistance à l'arsenic Arsenic toxicity : Cellular mechanisms of arsenic transfer and resistance.	**Experiment number:** 30-02-667
Beamline: BM30B FAME	**Date of experiment:** from: march 3rd to 9th 2004	**Date of report:** 26-08-04
Shifts: 9	**Local contact(s):** Jean-Louis Hazemann	*Received at ESRF:*

Names and affiliations of applicants (* indicates experimentalists):

J. ROSE*[1], A. BOTTA[2], J-L BERGE-LEFRANC[2], M. AUFFAN [1*], M. COLLET*[1], P. GOSSOT*[1], A. MASION[1*], Y. NOACK*[1],

[1]CEREGE-IFR PMSE 112, Europôle de l'Arbois BP 80 13545 Aix-en-Provence France; [2]Laboratoire de Biogénotoxicologie & Mutagenèse Environnementale, Faculté de médecine, Université de la Méditerranée, 27 Bd Jean Moulin, 13385 Marseille cedex 05

Report:

Introduction

Arsenic is a significant environmental concern worldwide because millions of people are at risk of drinking water contaminated by arsenic. Epidemiological data show that chronic exposure of humans to inorganic arsenic is associated with hepatic injury, peripheral neuropathy, and increased rates of a wide variety of cancers, particularly of the skin, lung, bladder, and liver. Arsenic also produces toxic effects on the female reproductive system, including ovarian dysfunction, aberrant embryo development and lethality, and postnatal growth retardation. Interestingly, it also has proven useful for anti-cancer therapy, although the mechanisms underlying its paradoxical (antineoplastic) effects remain unclear. The predominant form of inorganic arsenic in aqueous environments is arsenate (As(V)) whereas arsenite (As(III)) occurs in anoxic environments. The mode of toxicity is strongly related to the arsenic chemical form. As(III) is known to be more soluble and toxic than As(V). In mammalian cells, As(III) can binds to sulfhydryl groups and impairs the many proteins functions. More over As(III) can interacts with DNA resulting in single-strand DNA breaks (Oremland et al, 2003). Most mammals methylate inorganic arsenic to methylarsonic (MMA) and dimethylarsinic acid (DMA). Compare with inorganic species, the methylated arsenic forms are less toxic and more readily excreted in the urine. The biomethylation of arsenic has long been considered as one major detoxification process. However recent studies have shown that methylated As(V) and As(III) can induce oxidative DNA damage. (Vahter et al, 2000; reviewed in Vahter, 2002).

Carter et al. (2003), concluded their important review on the metabolism of inorganic arsenic oxide by different questions that are still unanswered. One important point concerns the mechanism of As transport in the cell and Carter et al. (2003) indicated that we still have to *"demonstrate the displacement of the arsenic glutathione complex to form the As(III)-lipoate using in vitro system? Can we do it on biological systems?"* They also concluded that '*unfortunately it is not easy to determine an accurate oxidation state for arsenic that reflects its potential reaction"*.

The aim of our work was to access the capability of X-ray Absorption Spectroscopy to determine the arsenic speciation in situ and to answer or help answering to some of the latter questions.

Material and methods.

Human fibroblast cells were obtained after removal of skin fragments during plastic surgery operations. Cells were grown in DMEM medium containing 10% of calf serum. Cultures were performed at 37.8°C in a 5% CO_2 atmosphere. Powdered As_2O_3 was dissolved in 1 N NaOH as 1 M solution (As^{III}) then diluted with PBS and added directly to the nutritive medium. A fresh 1M As^{III} solution was prepared for each new experiment. The As concentration in the nutritive medium was 2.10^{-5} mol.l^{-1}. Cells were seeded at 1 x 10^5 cells/ml in 96 well micro-plates for 24 hours. In the report 'Nutritive medium' and 'As-fibroblast' refer to the extra-cellular medium and intra-cellular medium respectively.

XAS experiments have been conducted on the XAS CRG BM-30b French beamline (FAME) at the As K edge. The Si(111) monochromator was used. The beam was focused vertically on the sample using the 2nd mirror and horizontally with the second crystal of the monochromator. The spot size was 200*200μm. XAS spectra were recorded in the fluorescence mode with a high purity Ge multichannel fluorescence detector. We have tested various setups to keep arsenic in its initial oxidation state and to prevent any modification due to high X-ray photon flux. In a first set up, human fibroblasts contaminated with arsenic (III) were placed in 1 mm diameter quartz capillary before XAS analysis. Before selling the capillary, a setup was fixed at the entrance of the capillaries to remove air and replaced by N_2. This protocol was repeated four times to prevent the presence of oxygen in the capillaries. A second set up was tested using Borosilicate capillaries (free of As…) sealed after air removed. Both capillaries gave same results. For solid compounds (powder references compounds), samples were pressed and the pellets were placed in a vacuum chamber. Prior to XAS sample analysis we have performed spectra acquired in the continuous scanning mode (Quick-EXAFS) to test the various setups and to ensure that the extremely high photon flux did not induce changes of the oxidation state and speciation of arsenic during measurements and that oxygen was properly remove from the capillaries. Because the scans are acquired rapidly (120 s/scan), any radiation-induced modifications of the redox state of arsenic can be determined by comparing the individual data scans over the first 2 minutes. For all samples no changes were observed. After this step, XAS were collected in a step-by-step mode.

Results:

Comparison between EXAFS spectra of reference compounds and samples suggests that the arsenic atomic environment of both samples resembles the atomic environment of As2S3 (figure 1). In the low k region 'As-fibroblasts' and 'nutritive medium' EXAFS spectra are in better agreement with oscillation features of As2O3. From the Fourier transforms it clearly appears that the second peak of the RDF of the nutritive medium and the As-fibroblasts is centered at the same position with the first peak of As2S3 RDF for which As is surrounded by 3 sulfur atoms at 2.25 Å. Therefore sulfur is present around As for both samples.

Partial EXAFS spectra have been modeled. The analysis of the first coordination sphere (number and distance of atoms surrounding As) indicates that arsenic from the nutritive medium is mainly linked to sulfur atoms (>90%) and 100% of As is in the 3+ form. In the case of the As-fibroblasts results indicate that 56 %±10 of As can be involved in As-(thiol)3 molecules and that 42%±8 of As is in the 5+ form.

From the analysis of the second coordination sphere we have determined the presence of carbon atoms around As. In the case of the nutritive medium the presence of carbon is due to the formation of As-SR_3 complexes. Indeed if one R-SH molecule is linked to As therefore a As-(S)-C linkage exist for which the As-(S)-C interatomic distance is in a 2.85-3.40 Å range. The latter As--C interatomic distance range has been established by the examination of a high number of reference molecules from the CSD database (Cambridge Structural Database (*www.cmbi.kun.nl/cheminf/freeserv.shtml*) for which As-(S)-C linkages exist.

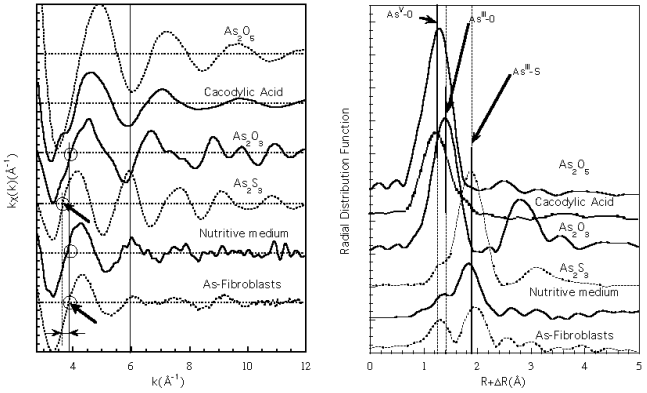

FIGURE 1. (a) Raw EXAFS data and (b) corresponding modulus of the Fourier transforms for As-fibroblasts and nutritive medium and arsenic model compounds.

In the case of the As-Fibroblasts, As-(S)-C distances decreases from 2.97 to 2.87 Å and 3.25 to 3.15 Å for As--C_1 and As--C_2 compared to the extra-cellular media. The decrease of the As-(S)-C interatomic distances can be due to a modification of the As-thiol linkage type. Arsenic can be linked to monothiol or dithiol molecule. The modification of linkage type between monothiol and dithiol has been proven in aqueous solution experiments (Carter et al, 2003). Lipoic acid (dithiol) presents the ability to displace glutathion (monothiol) linked to As. The decrease of the As-(S)-C distance between bidentate and monodentate is certainly linked to the increase of the bond strength and the change of the interatomic angles. The bond strengths are generally substantially larger for the dithiols (bidentate) than for two monothiols (monodentate) (Carter et al, 2003).

Conclusion

Even if the initial arsenic concentration was low (2.10^{-5} $mol.l^{-1}$) the use of a third generation synchrotron X-ray source enables to obtain XAS spectra with a high signal/noise ratio. Results indicate that arsenic remains in the 3+ form in the nutritive medium and that almost 90% of arsenic is linked to thiol molecules from the DMEM medium (cysteine). Only 10% of the initial arsenic is present as arsenite which suggests, if we assume that As-cysteine can not be transported though membrane cell, that only 10% of the initial concentration is toxic toward fibroblast cells. We have also determined that almost 45% of As(III) is oxidized in the intracellular medium. The fraction of As linked to sulfhydryl groups corresponds to approximately 55%. It is interesting to note that the structure of the As-thiol compounds evolves from the nutritive medium to the cell. It seems that the As is complexed to monothiol in the nutritive medium and to dithiol in the cells certainly from proteins. The structure of the As(V) fraction in cells is more difficult to interpret. The presence of MMA and DMA is not proven by XAS.

Literature

Carter D.E.; Aposhian H.V.; Gandolfi A.J.; (2003), The metabolism of inorganic arsenic oxides, gallium arsenide and arsine: a toxicochemical review, *Toxicology and Applied pharmacology*, 193, 309-33Oremland, R.S; Stolz J.F.; (2003), 'The ecology of arsenic', *science*, vol 300, 939-943.

Vahter M. (2002) 'Mechanisms of Arsenic biotransformation', Toxicology, 181-182, p211-217.

Vahter M., Concha G., Nermell B. (2000) 'Factor influencing Arsenic methylation in humans', The Journal of trace elements in experimental medicine, 13, 173-184.

Von Dollen A ., Strasdeit H. (1998) , Eur.J.Inorg.Chem, 1290,61.

4.

Four articles have been published in leading geochemistry and environmental science journals out of this long-term proposal (abstracts are copied below). Originally, we had planned to study the natural speciation of Ni, Zn, As and Pb, but only the two first elements have been investigated in detail because of beamtime constrain and of technical problems encountered in 2003 at the As K-edge, and especially at the Pb L3-edge. The technical pitfalls (mostly non-linearity of the detectors, and beam instability due to an imperfect regulation of the monochromator cooling) have been reported in our previous yearly reports, and we have been told by Jean Louis Hazemann and Olivier Proux that these problems were solved recently, in particular by the mounting of a new I0 detector. For this reason, we intend to complete this long-term program by the study of As and Pb in the coming two years.

During the last two years, great strides in our knowledge of the sequestration mechanism of zinc and nickel in soils have been made, despite the generally low concentration of these elements in the analyzed matrices and the high proportion of iron, which gives a parasitic fluorescence signal that is quite intense at the Ni and Zn K-edges. Our most advanced measurements would not have been made possible on other beamlines, at least at ESRF, and I think that all users owe a major debt of gratitude to the FAME team for their excellent technical and instrumental work, and their strong dedication and relentless efforts to maintain this beamline at a cutting-edge.

Among all the experiments, which have been performed in the last two years in the framework of this program, I think that the most novel has been, and still is, the development of polarized EXAFS on highly textured (single crystal-like) self-supporting films from the clayey fraction of natural soils and from clay standards. These experiments are technically challenging in many respects (elaboration of high quality films, quality-control by texture goniometry, availability of a focused X-ray beam for grazing-incidence measurements, high stability of the spectrometer during the scans at varying incidence angle, 30-Ge detector for Fe Kα rejection, and high flux) and have led to several groundbreaking, and even flabbergasting, results. This research work on P-EXAFS still is completely original and has been a shoo-in for acceptance in premier journals in our field. A glimpse of this accomplishment is shown below with the P-EXAFS data obtained on Zn in a clayey paddy soil from Taïwan ([Zn] = 42 ppm) and on Zn in substitution to Al in the octahedral sheet of montmorillonite ([Zn] = 85 ppm). The two samples exhibit a reversed polarization dependence, although Zn is surrounded by Al in the two samples. This difference is due to the fact that Zn occupies two distinct crystallographic sites: it is located in the octahedral sheet sandwiched between two tetrahedral Si sheets in montmorillonite, and it is located in the vacancy sites of an $Al(OH)_3$ layer in the soil sample. The two local environments, not only are highly anisotropic, but also dissimilar, thus enabling their differentiation. We believe that the new coordination chemistry of zinc discovered in the paddy soil from Taïwan is ubiquitous, and is the main sequestration mechanism of zinc in acidic to near-neutral aluminium-rich clayey soils at the earth's surface.

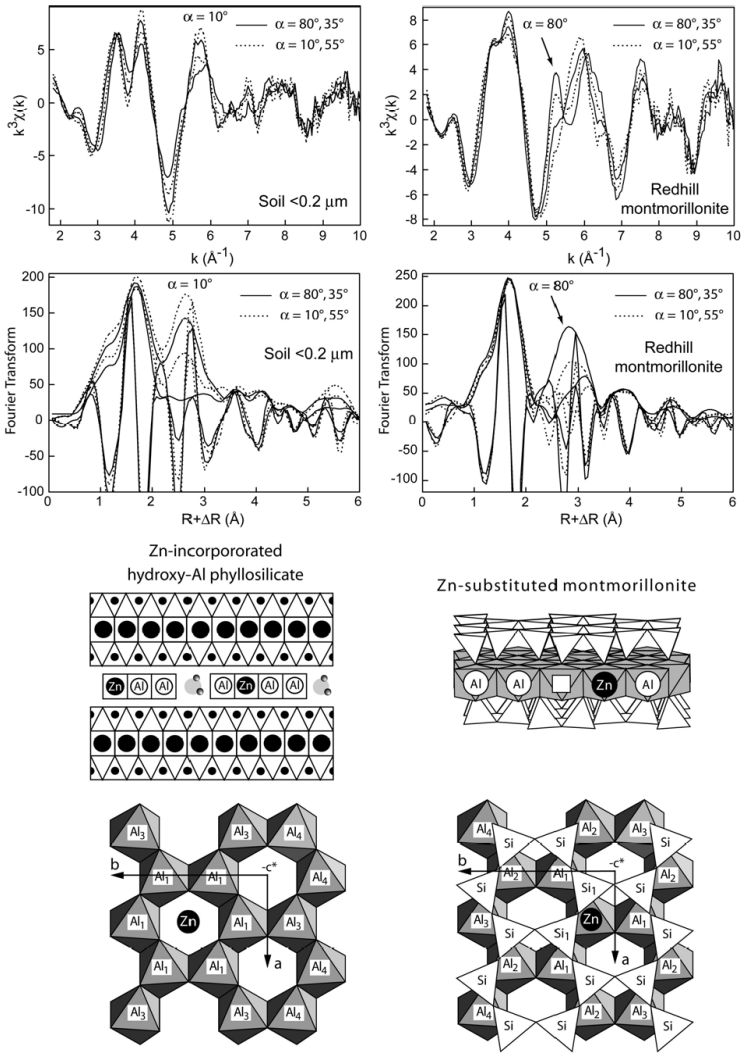

Zinc mobility and speciation in soil covered by contaminated dredged sediment using micrometer-scale and bulk-averaging X-ray fluorescence, absorption and diffraction techniques

Marie-Pierre Isaure, Alain Manceau, Nicolas Geoffroy, Agnès Laboudigue, Nobumichi Tamura, Matthew A. Marcus

Geochimica et Cosmochimica Acta, in press

ABSTRACT

The mobility and solid-state speciation of zinc in a pseudogley soil (pH = 8.2-8.3) before and after contamination by land-disposition of a dredged sediment ([Zn] = 6600 mg kg^{-1}) affected by smelter operations were studied in a 50 m^2 pilot-scale test site and the laboratory using state-of-the-art synchrotron-based techniques. Sediment disposition on land caused the migration of micrometer-sized, smelter-related, sphalerite (ZnS) and franklinite ($ZnFe_2O_4$) grains and dissolved Zn from the sediment downwards to a soil depth of 20 cm over a period of 18 months. Gravitational movement of fine-grained metal contaminants probably occurred continuously, while peaks of Zn leaching were observed in the summer when the oxidative dissolution of ZnS was favored by non-flooding conditions. The Zn concentration in the <50µm soil fraction increased from ~61 ppm to ~94 ppm in the first 12 months at 0-10 cm depth, and to ~269 ppm in the first 15 months following the sediment deposition. Higher Zn concentrations and enrichments were observed in the fine (<2 µm) and very fine (<0.2 µm) fractions after 15 months (480 mg kg^{-1} and 1000 mg kg^{-1}, respectively), compared to 200 mg kg^{-1} in the <2 µm fraction of the initial soil. In total, 1.2 % of the Zn initially present in the sediment was released to the environment after 15 months, representing an integrated quantity of ~4 kg Zn over an area of 50 m^2. Microfocused X-ray fluorescence (XRF), diffraction (XRD) and extended X-ray absorption fine structure (EXAFS) spectroscopy techniques were used to image chemical associations of Zn with Fe and Mn, and to identify mineral and Zn species in selected points-of-interest in the uncontaminated and contaminated soil. Bulk average powder EXAFS spectroscopy was used to quantify the proportion of each Zn species in the soil. In the uncontaminated soil, Zn is largely speciated as Zn-containing phyllosilicate, and to a minor extent as zincochromite ($ZnCr_2O_4$), ^{IV}Zn-sorbed turbostratic birnessite (δ-MnO_2), and Zn-substituted goethite. In the upper 0-10 cm of the contaminated soil, about 60 ± 10 % of total Zn is present as ZnS inherited from the overlying sediment. Poorly-crystalline Zn-sorbed Fe (oxyhydr)oxides and zinciferous phyllosilicate amount to about 20-30 ± 10 % each and, therefore, make up most of the remaining Zn. Smaller amounts of franklinite ($ZnFe_2O_4$), Zn-birnessite and Zn-goethite were also detected. Further solubilization of the Zn inventory in the sediment, and also remobilization of Zn from the poorly-crystalline neoformed Fe (oxyhydr)oxide precipitates, are expected over time. This study shows that land deposition of contaminated dredged sediments is a source of Zn for the covered soil and, consequently, presents environmental hazards. Remediation technologies should be devised to either sequester Zn into sparingly soluble crystalline phases, or remove Zn by collecting leachates beneath the sediment.

Mn, Fe, Zn and As speciation in a fast-growing ferromanganese marine nodule

Matthew A. Marcus, Alain Manceau and Michael Kersten

Geochimica et Cosmochimica Acta, 2004, 68, 3125-3136

ABSTRACT

The speciation of Mn, Fe, As and Zn in a fast-growing (0.02mm/yr), shallow-marine ferromanganese nodule has been examined by micro X-ray fluorescence, micro X-ray diffraction, and micro X-ray absorption spectroscopy. This nodule exhibits alternating Fe-rich and Mn-rich layers reflecting redox variations in water chemistry. Fe occurs as two-line ferrihydrite. The As is strictly associated with Fe and is mostly pentavalent, with an environment similar to that of As sorbed on or coprecipitated with synthetic ferrihydrite. The Mn is in the form of turbostratic birnessite with ~10 % trivalent manganese in the layers and probably ~8 % corner-sharing metal octahedra in the interlayers. The Zn is enriched on the rim of the nodule, associated with Mn. The Zn is completely (>90 %) tetrahedrally coordinated and sorbed in the interlayers of birnessite on vacant layer Mn sites. The Zn and Mn species are similar to ones found in soils, suggesting common structural principles, despite the differing formation conditions in these systems.

Natural speciation of Zn at the micrometer scale in a clayey soil using X-ray fluorescence, absorption, and diffraction

Alain Manceau, Matthew A. Marcus, Nobumichi Tamura, Olivier Proux, Nicolas Geoffroy, Bruno Lanson

Geochimica et Cosmochimica Acta, 2004, 68, 2467-2483.

ABSTRACT

Combined use of synchrotron-based x-ray fluorescence (SXRF), diffraction (XRD), and absorption (EXAFS) with an x-ray spot size as small as five micrometers allows us to examine noninvasively heterogeneous soils and sediments. Specifically, the speciation of trace metals at low bulk concentrations and the nature of host minerals can be probed with a level of detail unattainable by other techniques. The potential of this novel analytical approach is demonstrated by determining the Zn species in the solid phases of a pristine horizon of a clayey acidic soil (pH 4.5 – 5.0) having a Zn concentration of 128 mg/kg. The sample presents a differentiated fabric under the optical microscope with traces of localized manganiferous, ferriferous and argillaceous accumulations. The high chemical and textural heterogeneity of this soil offers an opportunity to identify new Zn species and to confirm the existence of others proposed from published least-squares fits of bulk averaged EXAFS spectra. As many as five to six Zn species were observed: sphalerite (ZnS), zincochromite ($ZnCr_2O_4$), Zn-containing phyllosilicate and lithiophorite, and Zn-sorbed ferrihydrite or Zn-phosphate, the results being less definitive for these two last species. Bulk EXAFS spectroscopy applied to the powdered soil indicated that Zn is predominantly associated with phyllosilicates, all other species amounting to less than about 10-20 % of total zinc. The role of lithiophorite in the sequestration of zinc in soils had been inferred previously, but the firm

identification of lithiophorite in this study serves as an excellent demonstration of the capabilities of combined micro-SXRF/XRD/EXAFS measurements. The micro-EXAFS spectrum collected in an area containing only phyllosilicates could not be simulated assuming a single Zn structural environment. Two distinct octahedrally-coordinated crystallographic sites (i.e., two EXAFS components) were considered: one site located within the phyllosilicate structure (isomorphic cationic substitution in the octahedral sheet) and another in the interlayer region in the form of a Zn-sorbed hydroxy-Al interlayered species. This second subspecies is less certain and further investigation of the individual EXAFS spectrum of this component is needed to precise its exact nature and the uptake mechanism of zinc in it.

Molecular-scale speciation of Zn and Ni in soil ferromanganese nodules from loess soils of the Mississippi basin

Manceau A., Tamura N., Celestre R.S., MacDowell A.A., Geoffroy N., Sposito G., Padmore H.A.

Environmental Science & Technology, 2003, 37, 75-80.

Determining how environmentally important trace metals are sequestered in soils at the molecular scale is critical to developing a solid scientific basis for maintaining soil quality and formulating effective remediation strategies. The speciation of Zn and Ni in ferromanganese nodules from loess soils of the Mississippi Basin was determined by a synergistic use of three noninvasive synchrotron-based techniques: X-ray microfluorescence (μXRF), X-ray microdiffraction (μXRD), and extended X-ray absorption fine structure spectroscopy (EXAFS). We show that Ni is distributed between goethite (α-FeOOH) and the manganese oxide lithiophorite, whereas Zn is bound to goethite, lithiophorite, phyllosilicates, and the manganese oxide birnessite. The selective association of Ni with only iron and manganese oxides is an explanation for its higher partitioning in nodules over the soil clay matrix reported from soils worldwide. This could also explain the observed enrichment of Ni in oceanic manganese nodules. The combination of these three techniques provides a new method for determining trace metal speciation in both natural and contaminated environmental materials.

The results from our experiments have been reported in an article, which is in press to *Geochimica et Cosmochimica Acta*. Its abstract is copied below. The research has been conducted partly at the ALS for the microspectroscopy part, and at ESRF on the FAME beamline for the EXAFS part on powdered samples. One of the main outcome from this study is the first identification in a natural sample of Zn-rich trioctahedral phyllosilicate. This species had been inferred in the literature by our team several years, but its existence had been questioned. Its existence is now firmly established. Frédéric Panfili defended his Ph. D. thesis in June 2004.

The effect of phytostabilization on Zn speciation in a dredged contaminated sediment using scanning electron microscopy, X-ray fluorescence, EXAFS spectroscopy and principal components analysis

Frédéric Panfili [1, 2, 5], Alain Manceau [1], Géraldine Sarret [1], Lorenzo Spadini [1], Tatiana Kirpichtchikova [1], Valérie Bert [2], Agnès Laboudigue [2], Matthew A. Marcus [3], Noureddine Ahamdach [4], Marie-Françoise Libert [5]

[1] Environmental Geochemistry Group, LGIT, University J. Fourier and CNRS, BP 53, 38041 Grenoble cedex 9, France
[2] CNRSSP, BP 537, 59505 Douai cedex, France
[3] Advanced Light Source, Lawrence Berkeley National Laboratory, University of California, Berkeley, CA 94720, USA
[4] LESTS, IRSN, BP 6, 92265 Fontenay-aux-Roses cedex, France
[5] LMTE, CEA-CADARACHE, 13108 Saint Paul lez-Durance, France

Geochimica et Cosmochimica Acta, in press

ABSTRACT

The maintenance of waterways generates large amounts of dredged sediments, which are deposited on adjacent land surfaces. These sediments are often rich in metal contaminants and present a risk to the local environment. Understanding how the metals are immobilized at the molecular level is critical for formulating effective metal containment strategies, such as phytoremediation. In the present work, the mineralogical transformations of Zn-containing phases induced by two graminaceous plants (A*grostis tenuis* and *Festuca rubra)* in a contaminated sediment ([Zn] = 4700 mg kg^{-1} , [P_2O_5] = 7000 mg kg^{-1}, pH = 7.8), untreated or amended with hydroxylapatite (AP) or Thomas basic slag (AS), were investigated after two years of pot experiment by scanning electron microscopy coupled with energy-dispersive spectrometry (SEM-EDS), synchrotron-based X-ray micro-fluorescence (µSXRF), and powder and laterally-resolved extended X-ray absorption fine structure (µEXAFS) spectroscopy. The number and nature of Zn species were evaluated by principal component (PCA) and least-squares fitting (LSF) analysis of the entire set of µEXAFS spectra, which included up to 32 individual spectra from regions of interest varying in chemical composition. Seven Zn species were identified at the micrometer-scale : sphalerite, gahnite, franklinite, Zn-containing ferrihydrite and phosphate, (Zn-Al)-hydrotalcite, and Zn-substituted, kerolite-like, trioctahedral phyllosilicate. Bulk fractions of each species were quantified by LSF of the powder EXAFS spectra to linear combinations of the identified Zn species spectra.

In the untreated and unvegetated sediment, Zn was distributed as ~50 % (mole ratio of total Zn) sphalerite, ~40 % Zn-ferrihydrite, and ~10-20 % (Zn-Al)-hydrotalcite plus Zn-phyllosilicate. In unvegetated but amended sediments (AP and AS), ZnS and Zn-ferrihydrite each decreased by 10 to 20 % and were replaced by Zn-phosphate (~30-40 %). In the presence of plants, ZnS was almost completely dissolved and the released Zn bound to phosphate (~40-60 %) and to Zn phyllosilicate plus (Zn,Al)-hydrotalcite (~20-40 %). Neither the plant species nor the co-addition of mineral amendment affected the Zn speciation in the vegetated sediment. The sediment pore waters were supersaturated with respect to Zn-containing trioctahedral phyllosilicate, near-saturation with respect to Zn-phosphate, and strongly undersaturated with respect to (Zn,Al)-hydrotalcite. Therefore, the formation of (Zn,Al)-hydrotalcite in slightly alkaline conditions ought to result from heterogenous precipitation on mineral surface.

ESRF	**Experiment title: Structure of the metal binding domain of the copper metalloprotein Atx1 and peptidic analogs in presence of Cu(I), Co(II), Cd(II) and Hg(II).**	**Experiment number:** 30-02/650
Beamline: BM30B	**Date of experiment:** from: 04.21.04 to: 04.27.04	**Date of report:** 09.01.04
Shifts: 9	**Local contact(s):** J-L Hazemann and O. Proux	*Received at ESRF:*

Names and affiliations of applicants (* indicates experimentalists):

D. Poger*, M. Ferrand*, E. Mintz and P. Delangle, CEA-Grenoble, France

C. Denauwer*, CEA-Marcoule, France

Report:

The initial aim of this experiment was the study of the coordination of some heavy metal ions (namely Cu(I), Hg(II) and Cd(II)) by the yeast metallochaperone protein Atx1, and by Atx1-derived biomimetic peptides as described in the corresponding proposal. But, due to some technical problems at the beginning of the allocated beamtime, we could only study the interactions with the Cu(I) ion. The XANES and EXAFS signals were recorded at room temperature.

So far, we have focused our study on the complexation of Cu(I) by the Atx1 protein. Some preliminary results have shed light on the glutathione-assisted Cu(I)-Atx1 interaction. Atx1 is supposed to form a homodimer in presence of glutathione, each monomer complexed to a Cu(I) ion and interacting with a glutathione. The nature of the interaction (coordination number of the Cu(I) ions and geometry of the metal sites) remains uncertain and has to be characterized. Two models (figure 1) have been hypothesised to account for the formation of the $(CuAtx1\text{-glutathione})_2$ dimer. In the first model each Cu(I) ion is 3-coordinated by 3 cysteine terminal thiolate, whereas in the second one, each Cu(I) is 4-coordinated by 2 cysteine thiolate groups (from the Atx1 proteins) and by 2 bridging thiolates (from the glutathione molecules).

Then we have used three model compounds corresponding to the three possible coordination of Cu(I) in this case: a linear 2-coordinate structure ($[Et_4N][Cu(SAd)_2]$, SAd: adamantane-1-thiolate), a planar trigonal structure ($[Et_4N]_2[Cu(SC_6H_4Cl)_3]$) and a distorted 4-coordinate one in a dicopper(I) cluster ($[Cu(SC_5H_5N)_3]_2[Cl]_2$).
As observed in figure 2, the model Cu(I) complexes exhibit a wide range in peak energies and intensities in the pre-edge region that can be correlated with the coordination number of the metal.

The dicopper(I) Atx1-glutathione homodimer exhibits a low-energy absorption peak at 8980 eV whose amplitude and feature suggest the presence of a single geometry for both copper(I) centres, and the Cu(I) ions are 3-coordinated.
The k^3-weighted experimental EXAFS spectrum of the $(CuAtx1\text{-glutathione})_2$ dimer and its Fourier transform (reported on figure 3) are compared with their fitted value computed from the CuS_3 model complex. The spectrum is dominated by the first shell contribution which is best simulated by three equivalent sulfur atoms at 2.24 Å (goodness-of-fit parameter $F = 3.9\ 10^{-2}$). This Cu-S distance is typical of a 3-coordinate Cu(I) ion, as evidenced by *ab initio* quantum mechanics calculations.

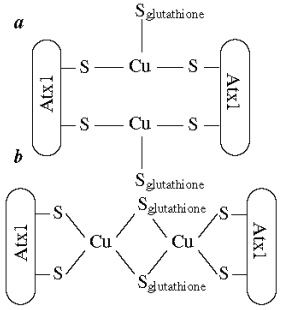

Figure 1. Models of the complexation of Cu(I) by Atx1 in solution in presence of glutathione. In model *a*, each Cu(I) ion is 3-coordinated whereas in model *b*, the ions are coordinated in a tetrahedral fashion.

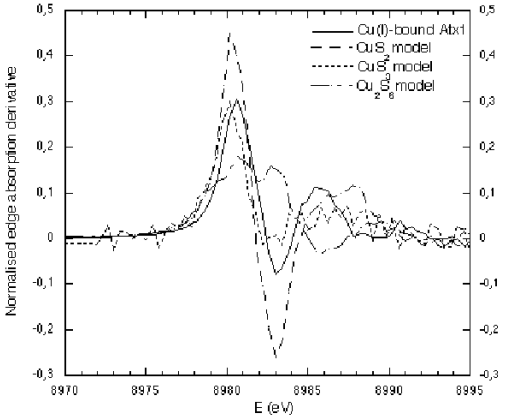

Figure 2. Normalised edge absorption derivative spectra of the Cu(I)-bound Atx1 in presence of glutathione and of the three Cu(I) model complexes of the metal site.

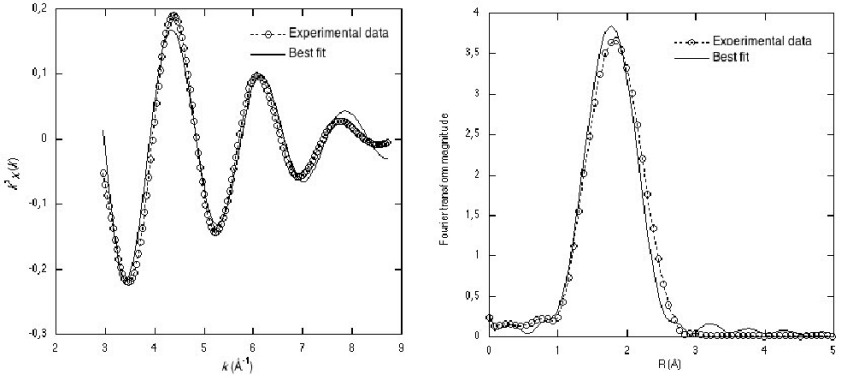

Figure 3. EXAFS spectrum (left) and Fourier transform (right) of the $(Cu(I)Atx1\text{-glutathione})_2$ dimer in solution. The best fit (with a 3-coordinated Cu(I) complex) and the experimental data are reported.

ESRF	**Experiment title:** **Resistance of bacteria to selenium oxyanions** **Résistance chez les bactéries aux oxyanions du sélénium**	**Experiment number:** **30-02-689**
Beamline: BM 30B	**Date of experiment:** from: 04/05/2004 to: 11/05/2004	**Date of report:** 31/08/2004
Shifts: 18	**Local contact(s):** Olivier Proux	*Received at ESRF:*

Names and affiliations of applicants (* indicates experimentalists):

Laure AVOSCAN*, Marie CARRIERE*, Richard COLLINS* and Barbara GOUGET*, CEA-CNRS, Laboratoire Pierre Süe-Saclay, 91191 Gif sur Yvette, France

Géraldine SARRET*, Groupe de Géochimie de l'Environnement, LGIT/IRIGM, Université Joseph Fourier BP 53, F-38041, Grenoble cedex 9, France

Introduction

The purpose of our study is to improve the understanding of mechanisms of bacterial uptake and subsequent internal reduction of Se oxyanions. *Ralstonia metallidurans* CH34, a soil bacterium characteristic of metal-contaminated biotopes, is known to resist to a wide range of metals as well as the oxyanions selenite (SeO_3^{2-}) and selenate (SeO_4^{2-}). As other soil micro-organisms, its resistance to selenite is based on the reduction of the oxidized form, highly soluble, toxic and bioavailable in the environment, to the elemental form Se(0), extremely insoluble, strongly resistant to oxidation and therefore, less toxic and mobile. In addition, *R. metallidurans* CH34 is a good model for genetic studies since its genome is entirely sequenced.

Microbiology experiments are carried out at the Pierre Süe Laboratory at Saclay to characterize the capacity of resistance and accumulation of the bacteria exposed to both Se oxyanions, and to determine the kinetics of accumulation in various culture conditions.

A first Se K-edge XANES experiment was performed on BM32 in 2001 in which *R. metallidurans* CH34 was shown to resist high selenite concentration and accumulate it after subsequent reduction to elemental selenium in the monoclinic form (ROUX et al., 2001).Two other XANES experiments were carried out on BM30B in 2003. The aims were on one hand to obtain spectra of various references in order to characterize the organic Se compounds synthesized by the bacteria and on the other hand, to focus on the kinetics of selenite and selenate reduction by this bacterial strain (experiments LS2141 and 30-02-626). Our results showed that *R. metallidurans* CH34 reduced selenite more quickly at high cell density (optical density at 600 nm: OD_{600nm}=3). Selenite was present as minor species in the cells from the start of the experiment and a transient organic Se compound was found. This suggest that two reactions with similar kinetics take place: an assimilatory pathway leading to organic Se, and a slow detoxification pathway leading to Se(0). Then, selenite uptake strongly increased and Se(0) was largely predominant, suggesting an activation of selenite transport and bioreduction systems. In addition, *R. metallidurans* CH34 was able to reduce selenate to selenite and then to organic selenium as major product. Elemental Se was detected, but represented less than 25% of total selenium (experiment report 30-02-626 ; Sarret et al., subm. to AEM).

In the present experiment, we studied the kinetics of reduction of both selenite and selenate species by 3 mutant strains, in comparison with the wild-type strain. These mutant strains, selenite-resistant, were developed in the Jacques Covès group in Grenoble. The mutated gene and the corresponding protein putatively involved in selenite transport are being studied by this group.

Materials and methods

Three mutated strains, called RM6, RM7 and RM8 and resistant up to 15 mM of selenite, were cultured in the same conditions as *R. metallidurans* CH34. Two experiments were conducted in parallel in order to test the influence of the bacterial population. For the first experiment, RM7 and RM8 were exposed to 10 mM of selenite added to the culture medium at the beginning of the exponential growth phase (OD_{600nm}=0.3). For the second experiment, RM6, RM7 and RM8 were exposed to 10 mM of selenite or 5 mM of selenate, added to the culture medium at the beginning of the stationary phase (OD_{600nm}=3). The kinetics of the reactions were followed by samplings made at regular interval during 6 days. For each sampling, the bacteria and the culture medium were separated by centrifugation. Total Se concentrations in each fraction were determined by ICP-MS.

Se K-edge XANES spectra were recorded in fluorescence mode using a 7-element solid state Ge detector (Canberra). The monochromator was a Si(220) double crystal. To avoid photoreduction of Se during the measurements, acquisitions were conducted using a cryostream. XANES spectra were calibrated by setting the maximum of the white line of hexagonal (gray) elemental Se at 12.6592 KeV, and normalized using two polynomial functions. The spectra were then simulated by linear combinations fitting (LCF) using Se reference compound spectra. Given total Se concentration in each sample, the percentages of each Se species were reported to the biomass determined by protein content.

Results

I. Reference spectra

Table 1 details the Se model compounds used to simulate XANES spectra with a linear combination fitting program.

Compound	monoclinic red elemental Se	seleno diglutathion	seleno-DL-cystin	seleno cystein	methyl seleno L-cystein	selenourea	selenite	selenate
	Se(0)	SeS_2	R-SeH	R-Se-Se-R	R-Se-R	Se=C	Se(IV)	Se(VI)
Max of the white line (keV)	12.6592	12.6598	12.6601	12.6601	12.6608	12.6638	12.6638	12.667

***Table 1**: Se model compounds and the position of the maximum of the white line*

II. Accumulation and bioreduction of selenite by selenite-resistant mutant strains

Interestingly, accumulation experiments showed that the selenite-resistant mutant strains accumulated significantly less selenium added as selenite in the culture medium than the wild-type strain *R. metallidurans* CH34. However, the mechanism of selenium reduction seemed to be unchanged. Figure 1 presents the percentages of the major species obtained after exposure of RM7 to 10 mM of selenite added at OD 0.3: selenite is detected during the first 6 hours of experiment and rapidly reduced to organic Se (as alkyl Se) and elemental Se. Figure 2 presents the same results normalized using total selenium contents in the bacteria and compared to the results obtained with *R. metallidurans* CH34 exposed to 2 mM of selenite added at OD 0.3.

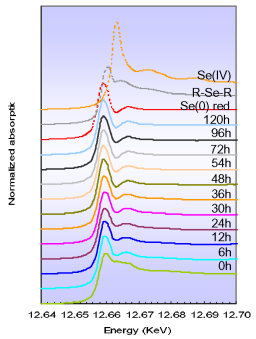

Proportions of Se species (%)

Time, h	Se(0)	SeS_2	R-Se-Se-R	R-SeH	R-Se-R	C=Se	Se(IV)	Se(VI)
0	53	-	-	-	39	-	12	-
6	53	-	-	-	41	-	6	-
12	65	-	-	-	35	-	-	-
24	66	-	-	-	33	-	-	-
30	70	-	-	-	30	-	-	-
36	78	-	-	-	22	-	-	-
48	91	-	-	-	9	-	-	-
54	94	-	-	-	6	-	-	-
72	94	-	-	-	6	-	-	-
96	93	-	-	-	6	-	-	-
120	95	-	-	-	5	-	-	-

***Figure 1**: Se K-edge XANES spectra for mutated strain RM7 exposed to 10 mM selenite added at the beginning of exponential phase (OD 0.3), and proportions of Se species determined by linear combination fitting using reference spectra (tab.1). The uncertainty is estimated at ± 10% for organic species, and ± 5% for Se(IV) and Se(VI).*

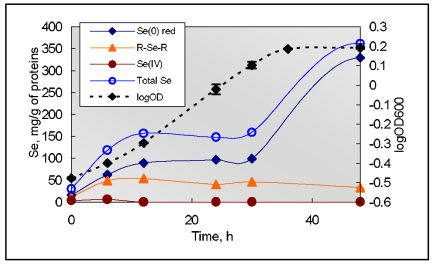

***Figure 2**: Growth curve of the mutated strain RM7 and the concentrations of the various Se species present in the mutated strain exposed to 10 mM selenite added at OD 0.3, calculated from the XANES results and from the total Se concentrations.*

Figure 3 shows the results obtained with RM6 exposed to 10mM of selenite added at OD 3. Like with *R. metallidurans* CH34, at high cell density, the kinetic of selenite reduction was accelerated. The same results were obtained with the other mutated strains.

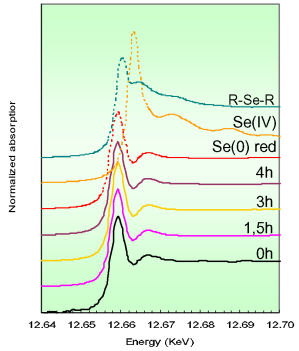

Proportions of Se

Time, h	Se(0)	SeS_2	R-Se-Se-R	R-SeH	R-Se-R	Se=C	Se(IV)	Se(VI)
0	88	-	12	-	-	-	-	-
1.5	100	-	-	-	-	-	-	-
3	100	-	-	-	-	-	-	-
4	100	-	-	-	-	-	-	-

***Figure 3**: Se K-edge XANES spectra for mutated strain RM6 exposed to 10 mM selenite added at the start of stationary phase (OD 3), and proportions of Se species determined by linear combination fitting using reference spectra. The uncertainty is estimated at ± 10% for organic species, and ± 5% for Se(IV) and Se(VI).*

III. Accumulation and bioreduction of selenate by selenite-resistant mutant strain

Results obtained after exposure of RM8 to 5 mM of selenate added at OD 3 are presented figure 4 and figure 5. The accumulation of selenium by the mutated strain was quite similar as the wild-type strain (<2%). It can be noticed that in these conditions, right after the addition of selenate in the culture medium, selenate is present in the bacteria in the same proportions as organic Se. Selenite is present as a minor species during the first 6 hours of exposure. Then, organic Se becomes the predominant species and selenate proportions decrease. Elemental Se is only detected at 24h. A similar mechanism of selenate reduction had been observed with the wild-type strain CH34. For the other mutated strains RM6 and RM7 exposed to selenate, data are still in process.

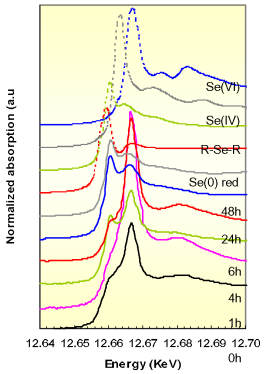

Proportions of Se

Time, h	Se(0)	$Se\ S_2$	R-Se-Se-R	R-SeH	R-Se-R	Se=C	Se(IV)	Se(VI)
0	-	-	-	-	51	-	9	45
1	-	-	-	-	17	-	27	91
4	-	-	-	-	69	-	-	31
6	-	-	-	-	24	-	-	83
24	17	-	-	-	73	-	-	9
48	-	-	14	-	59	27	-	-

***Figure 4**: Se K-edge XANES spectra for mutated strain RM8 exposed to 5 mM selenate added at the beginning of stationary phase, and proportions of Se species determined by linear combination fitting using reference spectra. The uncertainty is estimated at ± 10% for organic species, and ± 5% for Se(IV) and Se(VI).*

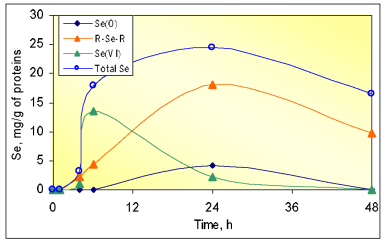

***Figure 5**: The concentrations of the various Se species present in the mutated strain RM8 exposed to 5 mM selenate, calculated from the XANES results (Fig. 4) and from the total Se concentrations*

Conclusions and perspectives

These results show that the sensitivity of the beamline BM30B allowed us to probe even the lowest Se concentration samples. BM30B proved to be particularly well suited to the study of diluted samples containing Se concentrations in the micromolar range. This experiment proved as well that even if the mutated strains of *R. metallidurans* CH34 accumulated far less selenium added as selenite in the culture medium than the wild-type strain (2% of the selenite added at zero time compared to 100%, respectively), the mechanism of selenium reduction seemed to be the same. For experiments with selenate, the major species was organic Se after an entrance of selenate during the first hours. Like for the wild-type strain, we noted the presence of selenite and elemental Se in the bacteria. The mutated protein seems to be highly implicated in selenite transport through the bacterium.

Bibliography

- Roux M., Sarret G., Pignot-Paintrand I., Fontecave M., and Covès J. (2001) Mobilization of Selenite by *Ralstonia metallidurans* CH34. Appl. Environ. Microbiol. 67(2), 769-773.
- Sarret G, Avoscan L, Carrière M, Collins R, Geoffroy N, Covès J, Gouget B (submitted to Appl. Environ. Microbiol.)

ESRF	**Experiment title:** **Kinetics of oxydoreduction of iron in silicate glasses and liquids.**	**Experiment number**: 30-02-676
Beamline: BM30B	**Date of experiment**: from: 12May2004 to:17May 2004	**Date of report**:
Shifts: 15	**Local contact(s)**: Dr. Jean-Louis HAZEMANN, BM30B, ESRF	*Received at ESRF:*

Names and affiliations of applicants (* indicates experimentalists):

* Véronique Magnien, Physique des Minéraux et des Magmas, IPGP-CNRS, Paris

* Daniel Neuville, Physique des Minéraux et des Magmas, IPGP-CNRS, Paris

*Laurent Cormier, LMCP, Paris

*Pascal Richet, Physique des Minéraux et des Magmas, IPGP-CNRS, Paris

*Jacques Roux, Physique des Minéraux et des Magmas, IPGP-CNRS, Paris

Report:

The aim of our experiment was to use X-ray absorption spectroscopy to determine the kinetics of iron redox reactions in silicate glasses and melts. Especially it is interesting for us to derive information concerning implied mechanisms in order to control vitrification processes and the temperature-induced structural changes in glass or nuclear industry. XANES techniques are well adapted to answer to this goal because they present a two-fold advantage in that they allow not only to determine the redox coordination states of iron with the pre-edge feature but also to realize in situ measurements.

For this reason, we used a set-up of microfurnace developed by Richet et al.(1993), which is made of a Pt wire with a hole which can be heated from ambient up to 2000K. A small amount of powder is placed in the hole (1mm) and heated in different temperature stages. On each stages, several XANES were recorded according to time in order to follow oxidation reaction. Several compositions with different redox states (well characterized by chemical, Mössbauer spectroscopy and electron microprobe analyses) were investigated during these experiments, especially :

- Pyrox : 50% mole SiO2, 10% FeO, 20%CaO, 20%MgO
- PyroxNa : 50% mole SiO2, 5% Na2O, 10% FeO, 17,5%CaO, 17,5%MgO
- PyroxLi : 50% mole SiO2, 5% Li2O, 10% FeO, 17,5%CaO, 17,5%MgO

Those experiments were complementary of those carried out on ID24 in March 2004. Indeed, the studied compositions were in both cases Ca, Mg – bearing iron silicates, but contrary to ID24, BM30 exhibits a relatively large spot, which offers the possibility to work on powder then to study redox kinetics for temperatures near glass transition (whereas the investigated temperature on ID24 were higher than 1273K).

The two first shifts were used to align the beamline and set-up the experiment. No significant problem have emerged during theses experiments. Nevertheless, we can note three remarks. At first, during the XANES acquisition, all the engines managing displacements of the table, monochromator or the detector must move simultaneously. So some problems of synchronisation have been encountered which have deteriored the quality of spectra. This was ponctually solved by the change of temporization of some engines.

Moreover, some difficulties in the loading of the sample could be encountered due to the high amount of iron, then a very small amount of powder should be introduced.

Finally, for relatively high temperatures (above Tg) and very small granulometry, redox kinetics seem to be extremely fast and the set-up is not adapted for the following of fast reaction, acquisition time being too long. It could be improved by a change in the granulometry of our sample to slow down redox kinetics.

To conclude, we have observed the oxidation of these three compositions from 673K to 1073K.

Results:

Despite the fact that the major part of spectra was under treatment, some interesting and promising results could be extracted. In the following figure, three XANES spectra obtained at 781K according to time for PyroxNa could illustrated our results. By comparison, the spectra at room temperature is shown too.

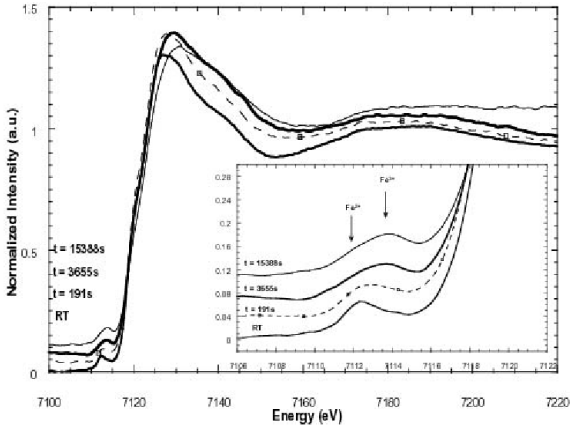

Here we observe a change in the pre-edge of the XANES spectra as a function of time, especially the progressive increase of a contribution at high energy to the detriment of that at low energy, caracterising the oxidation of our sample with time. Same features are observed for the majority of samples and temperatures. Moreover slight differences between composition could be observed, indeed redox kinetics in PyroxLi seem to be faster than in the others and those for Pyrox slower. Then those promising results let consider not only some estimates of the time required for the oxidation process and some interpretation on implied mechanisms, but a first basis of interpretation of the influence of composition on redox kinetics, especially the influence of the amount or the type of alkalin element. Besides they illustrate also the use of BM30B beamline with this large beam for the study of redox kinetics, especially near glass transition.

Some additional experiments near glass transition are necessary in order to investigate other compositions, as alumino and borosilicate glasses. Those information should be essential to complete the understanding of redox mechanisms and the influence of composition.

ESRF	**Experiment title:** Speciation of zinc in hyperaccumulating plants	**Experiment number:** 30 02 672
Beamline: BM 30B	**Date of experiment:** from: May, 1, 2004 to: May, 5, 2004	**Date of report:** August, 5, 2004
Shifts: 15	**Local contact(s):** Olivier Proux	*Received at ESRF:*

Names and affiliations of applicants (* indicates experimentalists):
Géraldine Sarret* and Nicolas Geoffroy*
LGIT, Maison des Géosciences, Univ. Joseph Fourier, BP 53, 38041 Grenoble Cedex

Report:

Introduction

Certain plant species have the ability to survive and reproduce on soils containing high concentrations of metals, and to store large amounts of metals in their aerial parts (more than 10000 µg/g d. w. for Zn). These plants present a great interest for phytoremediation, a soft method in which plants are used for the cleanup of metal-polluted soils. The project aimed at better understanding the molecular mechanisms underlying the immobilization of metals as non-toxic forms in such plants. The Zn and Cd hyperaccumulator *Arabidopsis halleri* is a good model for such studies since its genome is close to *A. thaliana*, the well known genetic model for higher plants, and the molecular tools developed for *A. thaliana* (genetic map, gene ships, putative genes involved in metals homeostasis…) can be used for *A. halleri* (Becher *et al.*, 2004, Weber *et al.*, 2004).
In a previous experiment, we showed that the major accumulation form of zinc is Zn malate in *A. halleri*, whereas this metal occurs as Zn phosphate in the non-tolerant and non- hyperaccumulating species *A. lyrata* (Sarret *et al.*, 2002). The localization of the metal strongly differs in the two species: Zn occurs predominantly in the leaf cells of *A. halleri*, and in the veins of *A. lyrata* (Sarret *et al.*, in preparation). In both species, the base of the trichomes (epidermal hairs) also contain high concentrations of Zn.

We have realized some interspecific crossings between *A. halleri* and *A. lyrata*. in order to segregate the tolerance and hyperaccumulation traits since they are genetically independent in *A. halleri* (Macnair *et al.*, 1999). The first progeny (F1) was tolerant but did not accumulate Zn (Figure 1), and the second generation obtained by back cross (F1 × *A. lyrata*) presented a continuum of phenotypes from non-tolerant to tolerant and from non-accumulators to moderately accumulators, the two traits being independent. Four individuals with contrasted phenotypes were selected : non tolerant non accumulator: BC121, moderately tolerant and accumulator: BC75, non tolerant and moderately accumulator: BC 273, and tolerant but not accumulator: BC5, see Figure 1).

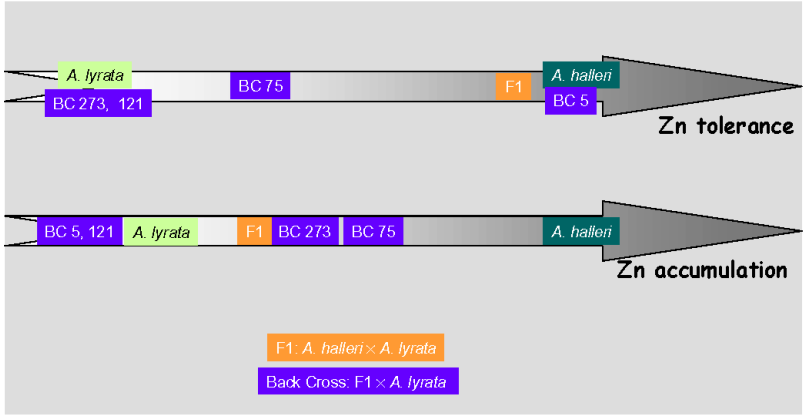

Figure 1: Degree of Zn tolerance and Zn accumulation for the plants studied.

Objectives of this experiment and Methods

The main purpose of this experiment was to determine the relationships between the chemical form of Zn and the tolerance and accumulation phenotypes. Another objective of this experiment was to test various sample conditionnings for the leaf samples (hydrated versus dehydrated, spectrum recorded at room temperature versus 100K). In this purpose, leaves of *A. halleri* were freeze-dried, ground and pressed as pellets, and the spectra were recorded at room temperature and at 100K using a He cryostat. The same leaves were plunged them in liquid nitrogen, ground and pressed as pellets in a cold room (-15°C), and transferred into the cryostat. The EXAFS spectra were recorded on the frozen-hydrated pellets at 100K.

Zinc concentrations ranged between 150 and 3000 mg kg^{-1} (dry weight) for *A. lyrata,* F1 and BC progenies, and reached 1.2 % for *A. halleri*. Spectra were recorded both in transmission and fluorescence mode, using a photodiode and a 13-element Ge detector. Normalized EXAFS spectra were first treated by linear combination fits, using a library of Zn spectra, and then by FEFF simulations in order to determine the structural parameters.

Results

The spectra for the freeze dried plant and frozen hydrated tissue recorded at 100K were identical, so freeze-drying does not seem to alter Zn speciation. At the opposite, some spectral modifications were observed for the spectrum recorded at room temperature, which are probably due to some radiation damage of the high intensity beam. Therefore, EXAFS spectra on plant materials should be recorded at low temperature. All spectra presented in this report were recorded at 100K on freeze-dried samples since spectra for frozen hydrated powders were much more noisy because of the high water content.

Figure 2 shows that the Zn K-edge EXAFS spectra for *A. lyrata*, F1, and the 4 back-crosses are strictly identical, and correspond to Zn phosphate (Zn is in tetrahedral coordination with d(Zn-O) = 1.98 Å, and the second shell contains P). These spectra contrast with *A. halleri* spectrum, corresponding to Zn malate (Zn is in octahedral coordination d(Zn-O) = 2.02 Å, and the second shell contains C). This finding is consistent with the results obtained on the localization and speciation of Zn at the micrometer scale: in a parallel experiment

performed on beamline 10.3.2 at the ALS (Berkeley) using µ-XRF and µEXAFS, we found that Zn distribution was identical in the leaves of all these plants, Zn being stored in the veins and in the trichomes (Fiigure 3). The chemical form was Zn phosphate in both locations. In *A. halleri*, Zn was also present as Zn phosphate in the trichomes, but occured as Zn malate in the leaf cells.

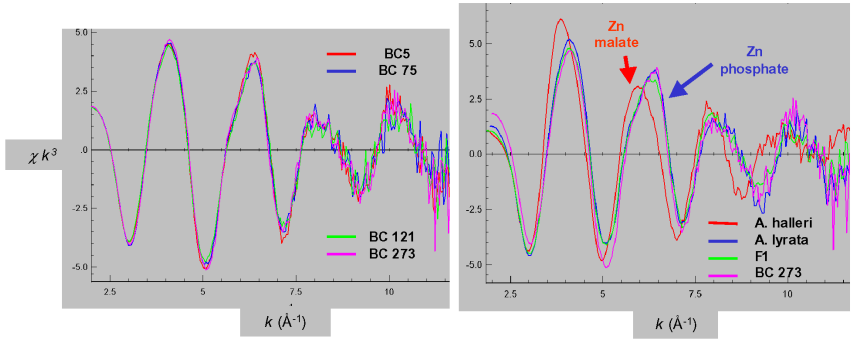

Figure 2: Comparison of the Zn K-edge EXAFS spectra for the leaves of the F1 and back cross progenies with parent plants.

These results are not surprising for F1, BC5 and BC121 since these plants do not accumulate Zn, but they are rather unexpected for the moderately accumulators BC75 and BC273, for which a mixture of Zn malate and Zn phosphate was expected. Moreover, Zn speciation does not change as a function of the degree of tolerance of the plants.

The results show that Zn accumulation can be realized by a mechanism different from the overexpression of Zn transmembrane transporters and the sequestration of Zn in the vacuoles as Zn malate: Zinc can also be stored as Zn phosphate in the veins. A F2 progeny (F1 × F1) is currently being produced. We expect that this progeny will contain real accumulators, and we wish to determine the chemical form of Zn in these plants in order to verify this hypothesis. The fact that no differences in Zn speciation were observed between tolerant and non-tolerant plants suggests that this trait is not determined by the accumulation form of Zn.

Conclusions and Perspectives

The identification of the accumulation forms of Zn by powder EXAFS on diluted samples realized on FAME, and the localization and speciation of Zn by µXRF and µEXAFS at the micrometer scale realized at the ALS provided complementary and consistent informations.

Following this esperiment, we wish to study plants of the F2 progeny, and to start the study of the accumulation forms of cadmium in *A. halleri*. This study is part of a National Research Project funded by the CNRS (ECCO), aiming at better understanding the molecular and genetic mechanisms responsible for Zn and Cd tolerance and hyperaccumulation in this species.

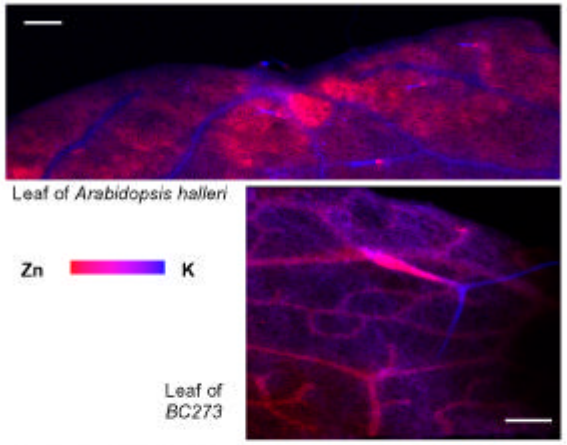

Figure 3: µXRF map showing the distribution of zinc in the leaves of *A. halleri* and BC 273 (non-tolerant, moderately accumulator). Bar = 100 µm. The metal is present in the leaf cells and trichomes in the former, and in the veins and trichomes in the latter.

Scientific production related to this experiment

CONFERENCE (INVITED SPEAKER):

Sarret G., Manceau A., Marcus M.A.M., Saumitou-Laprade P., Willems G., Garnier J.M., Balesdent J., Determining the Chemical Form of Metals in Soils and Plants by Synchrotron Techniques, 87th Canadian Chemistry Conference, London, Canada (May 29 - June 1, 2004).

CONFERENCE (ORAL COMMUNICATION):

Sarret G., Saumitou-Laprade, P., Willems, G., and Manceau, A., Accumulation et excrétion du zinc par les plantes, *Journée scientifique de l'IMBG* "Zinc et Cadmium dans l'Environnement et la Santé", 19 Mai 2004, Grenoble.

ARTICLE

Sarret G., Marcus M.A.M., Saumitou-Laprade P., Willems G., relationships between Zn chemical form and Zn tolerance and accumulation traits: an EXAFS study of *Arabidopsis halleri* and *Arabidopsis lyrata* interspecific crosses. *In preparation*

References

Becher M, Talke IN, Krall L, Kramer U (2004). Plant Journal **37**: 251-268.

Macnair MR, Bert V, Huitson SB, Saumitou-Laprade P, Petit D (1999). Proceedings of the Royal Society of London **B 266**: 2175-2179.

Sarret G, Saumitou-Laprade P, Bert V, Proux O, Hazemann JL, Traverse A, Marcus MAM, Manceau A (2002). Plant Physiol. **130**: 1815-1826.

Weber M, Harada E, Vess C, von Roepenack Lahaye E, Clemens S (2004). Plant Journal **37**: 269-281.

ESRF	**Experiment title:** ***In vitro* study of Cd/U toxicity to renal epithelial cells Intracellular competition with Zn**	**Experiment number:** 30-02-662
Beamline: BM 30B	**Date of experiment:** from: 23/06/2004 to: 26/06/2004	**Date of report:** 15/10/2004
Shifts: 9	**Local contact(s):** Olivier Proux and Vivian Nassif	*Received at ESRF:*

Names and affiliations of applicants (* indicates experimentalists):

Marie CARRIERE*
Barbara GOUGET* CEA/DSM/DRECAM/LPS
Laure AVOSCAN* CEA Saclay
Richard COLLINS* Bât 637
Hicham KHODJA* F-91191 Gif sur Yvette, France

Aims of the experiment and scientific background

Nephron, the functional unit of kidney, is composed of different segments. Among these segments the glomerulus acts as filtering unit, the proximal and distal tubules as reabsorptive units. Each segment consists in distinct cell types. Epithelial cells are responsible for blood toxins filtration, water and solutes reabsorption leading to the production of concentrated urine. Their transport capacities make them frequent targets for xenobiotic toxics such as **heavy metals**.

Because of its industrial use, **cadmium** (Cd) has become ubiquitous in the biosphere and enters the food chain, thus contaminating animals. Following oral exposure, Cd is absorbed through the gastrointestinal tract and transported via the blood circulation to target tissues. **Kidneys** are one of the major sites of Cd accumulation and many studies have investigated Cd uptake, transepithelial transport and toxic effects on kidneys.

For our experiments, cell lines dog and rat were used, from distal and proximal tubular origins. Quantification of metal uptake as well as intracellular trace and major elements contents were monitored using nuclear microprobe and ICP-MS analysis. Our results proved the ability of proximal as well as distal renal cells to accumulate large amounts of Cd (1000 ppm of Cd per dry weight, as a function of toxic metal concentration and time of exposure) and a strong competition between Cd and the endogen Zn was demonstrated. The aim of the present experiment was to determine the local structure of intracellular Cd and Zn after cadmium exposure. X-ray absorption spectroscopy (EXAFS) of lyophilized cells at the Cd and Zn K-edges was performed on BM30B.

Experimental method

MDCK (dog, distal tubule) and NRK52E (rat, proximal tubule) cultured cells were continuously grown at 37 °C, 5% CO_2 in DMEM (Dulbecco's Modified Eagle's Medium) cell culture medium supplemented with 10% (v/v) fetal calf serum. For metal exposure, cells were grown in 175 cm^2 flasks. The cells were washed twice with serum free cell culture medium, and 0-1 mM Cd was administered as $CdCl_2$ solutions diluted in serum free culture medium. Following 0-24 h incubation periods, cells were rapidly washed with PBS/EDTA 2 mM and trypsin was used to detach cells from their support. After centrifugation, the pellet was frozen and then lyophilized by highering temperature from –10 °C to 20 °C in 3h under a 0.37 mbar vacuum. The samples were dispersed in boron nitride and pressed as 5-mm diameter pellets. The amount of sample was calculated to give a jump of one across the K-edges. Zn and Cd K-edges EXAFS spectra were recorded in fluorescence mode using a 30 elements solid state Ge detector (Canberra). The monochromator was a Si(220) double crystal. To avoid evolution of samples during the measurements, acquisitions were conducted using a cryostream. At least 6 spectra for each sample were recorded and averaged to improve the statistics. The EXAFS oscillations were isolated from the raw, averaged data by removal of the pre-edge background, approximated by a first-order polynomial, followed by μ_0-removal *via* spline fitting techniques (SEDEM and Athena). Curve-fitting amplitudes and phases will be calculated in a second step.

Results

We expected to elucidate the intracellular speciation (XANES and EXAFS) of Cd accumulated in renal epithelial cells exposed to 20 or 50 µM $CdCl_2$ concentrations during 1-24 h. The local structure of the endogen Zn after exposure of the cells to Cd should allow to confirm the hypothesis that Cd substitutes to Zn on metallothionein. 3 shifts of experiments were conducted at the Zn K-edge and 6 shifts at the Cd K-edge. Data are still under process. However, the first results prove that the sensitivity of the beamline BM30B is particularly well suited to the study of diluted samples containing Cd or Zn concentrations as low as 100 ppm. Spectra for intracellular endogen Zn and for Cd accumulated for longer than 2 h could be recorded without any difficulty.

Fig. 1 shows the Zn K-edge XANES spectra (A) and the corresponding EXAFS oscillations (B) of MDCK cells exposed (MCd20-8h) or not (MCd0) to 20µM $CdCl_2$ for 8h compared to the metallothionein (MT). XANES and EXAFS signals obtained for MCd0 and MCd20-8h at this edge are strictly identical: the Zn local structure after Cd intoxication remains stable. The comparison of EXAFS oscillations obtained with cells and with the protein of reference (MT) clearly shows that the Zn local structure in our samples is similar to that of Zn in the metallothionein, with a probable slight contraction of the distances. In comparison to the XANES spectrum obtained for Zn-metallothionein (MT), the white line intensity is strongly decreased and double for cellular samples. The average position of the edges for cells and MT is comparable: the Zn valence may be the same.

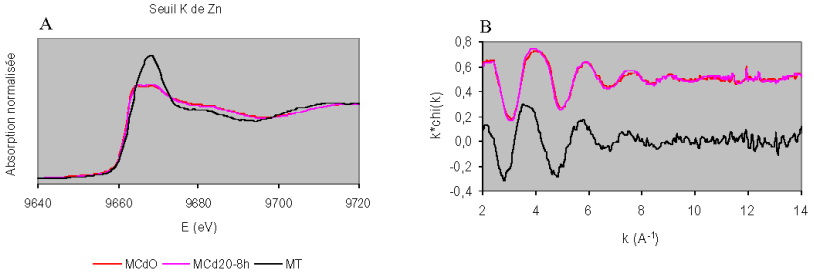

Fig. 1: Zn K-edge XANES spectra (A) and the corresponding k-weighted EXAFS spectra (B) of MDCK cells exposed to 20µM $CdCl_2$ for 8h (MCd20-8h) compared to cells not exposed to Cd (MCd0) and Zn-metallothionein (MT).

Fig. 2 shows the Cd K-edge XANES spectra (A) and the corresponding EXAFS oscillations (B) of MDCK cells exposed to 20µM $CdCl_2$ for 4, 6 or 8 h (MCd20-4, 6, 8 h respectively) compared to references (CdCl, CdO, CdS). The spectra for our reference metallothionein could not be recorded at this edge since its content in Cd was too low compared to the detection limit. An enriched Cd-metallothionein will be analysed during the next experiment. Metallothionein is a protein able to fix 7 atoms of Cd by Cd-S bonds and the reference Cd-S is used here for the comparisons.

Examination of our data confirms the evolution of the Cd local structure in MDCK cells in course of the exposure to the toxic. After 4 h of Cd exposure, the local structure of Cd in cells is similar to that of Cd-S (EXAFS) with a possible mixture of Cd-Cl and Cd-S (XANES). At time 6 h, the local order is strongly comparable to that of Cd-O (the amplitudes and the frequency of oscillations are similar). After 8 h, the Cd local structure is once again comparable to Cd-S.

On the contrary, as shown in Fig. 3, at 50 µM $CdCl_2$ the local order of Cd accumulated in NRK52E cells is similar to Cd-S whatever the time (2 or 4 h). When cells were exposed to 20 µM $CdCl_2$ for 8 h, the data seem to be relative to a mixture of Cd-S, Cd-Cl and Cd-O. The results should be confirmed after modelization of the Fourier transforms obtained from these data.

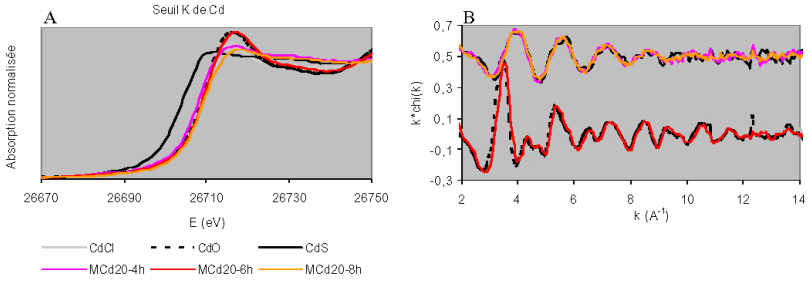

Fig. 2: Cd K-edge XANES (A) and the corresponding k-weighted EXAFS spectra (B) of MDCK cells exposed to 20 µM $CdCl_2$ for 4, 6 or 8 h (MCd20-4, 6 or 8 h) compared to references (CdCl, CdO, CdS).

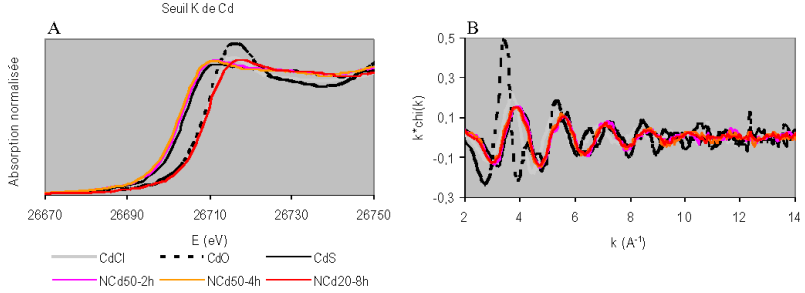

Fig. 3: Cd K-edge XANES (A) and the corresponding k-weighted EXAFS spectra (B) of NRK52E cells exposed to 20 or 50 µM $CdCl_2$ for 2, 4 or 8 h (NCd50-2 or 4h, NCd20-8h) compared to references (CdCl, CdO, CdS).

Conclusions and perspectives

Fitting of the measured data using a structural model of shells has not been processed yet. However, the first results obtained from XANES spectra and examination of EXAFS oscillations are promising. They should be confirmed by analysis of more samples ranging the whole course of Cd intoxication for both cell lines.

Bibliography

- Investigation of cadmium toxicity on renal epithelial cells using nuclear microprobe analysis. H. Khodja, M. Carrière, L. Figard, F. Carrot, B. Gouget, *Nuclear Instruments and Methods in Physics Research B* 210 (2003) 359-63.
- In vitro study of metal toxicity to renal epithelial cells. B. Gouget, L. Figard, F. Carrot, S. Lemaout, R. Gobin, H. Khodja, *In: Metal Ions in Biology and Medicine*, Vol. 8, p.101-105, 2004.
- Transient induction of metallothionein isoform 3 (MT-3), *c-fos, c-jun and c-myc* in human proximal tubule cells exposed to cadmium. Garrett SH, Phillips V, Somji S, Sens MA, Dutta R, Park S, Kim D, Sens DA, *Toxicology Letters*, 126 : 69-80, 2002.

ESRF	**Experiment title: XAS Study of highly diluted $ZnBr_2$ in supercritical fluids (H_2O, methanol, ethyl acetate)**	**Experiment number**: 30.02.682
Beamline: BM30b	**Date of experiment**: from: 10/06/2004 to: 17/06/2004	**Date of report**: 15/10/2004
Shifts: 18	**Local contact(s)**: Hazemann Jean-Louis	*Received at ESRF:*

Names and affiliations of applicants (* indicates experimentalists):

*Proux Olivier, CNRS - Laboratoire de Géophysique Interne et Tectonophysique, Grenoble

*Testemale Denis, Swiss Norvegian BeamLine

*Hazemann Jean-Louis, CNRS - Laboratoire de Cristallographie, Grenoble

Experimental details.

High pressure / high temperature XAFS spectroscopy analysis of $ZnBr_2$ solutions were performed at Br K-edge, using an X-ray cell recently developed at the Laboratoire de Cristallographie (Grenoble) [1]. This cell allows simultaneous measurement of the absolute concentration of the absorbing element in the fluid (from edge-step height in transmission mode), and the determination of the atomic environment around the absorber (from analysis of XANES and EXAFS spectra in fluorescence mode). The $ZnBr_2$ concentration was 0.033mol/l for the water solution, 0.085 and 0.0085mol/l for the methanol solutions.

$ZnBr_2$ aqueous solution

The comparison of the obtained EXAFS oscillations (figure 1) and those from the previous experiments [2,3] clearly shows that:

- Br ions are largely hydrated under normal conditions (max. of the oscillations for low k values at ~2.5 $Å^{-1}$)
- ions pairs are formed in hydrothermal conditions (max. of the oscillations for medium k values at ~6 $Å^{-1}$)

Previous results obtained on $ZnBr_2$ aqueous solutions have shown that ion pair formation start around 125°C for a 0.17mol/l concentration [3]. For a 5 times lower concentration, this evolution appears between 200 and 300°C.

$ZnBr_2$ methanol solution

The evolutions of the edge heights (figure 2) are similar for temperature lower than 150°C. For the 0.0085mol/l concentration, the normalized edge heights seems to follow the pure methanol density, the drop of the height around 250°C might be linked to the strong decrease of the methanol density in this temperature range (no data was found for pure methanol in the supercritical area but $?_c$=0.273g/cm^3 at 78.5 bars and 239.6°C). For the 0.085mol/l concentration, the decrease of the edge heights appears around 200°C; this might be due to the deposition of solid salts out of the beam path as result of precipitation.

The comparison of the modulus of the Fourier Transform of the EXAFS oscillations (figure 3) are similar for both concentrations. The only evolution is a decrease of the intensity of the FT *vs* temperature, simply due to the increase of the thermal disorder. Contrarily to the aqueous case, it seems that no ion-pairing occurs in the $ZnBr_2$ methanol solution.

Conclusion and perspectives

The main objective of this experiment was to study very diluted solutions, in order to get rid of any clustering effect at ambient conditions and thus be sensitive only to the evolution of ion pairing. The very good quality of the data shows the feasibility of such XAS measurements. Precise simulations are under progress in order to quantify these effects and to understand why a precipitation seems to occur (from the edge height evolution) until no ion pairs are clearly seen on the EXAFS data.

The goal of our future experiments will be to study the $ZnBr_2$ methanol solution at the Zn K-edge and $ZnBr_2$ salt in a non-polar solvent (ethyl acetate).

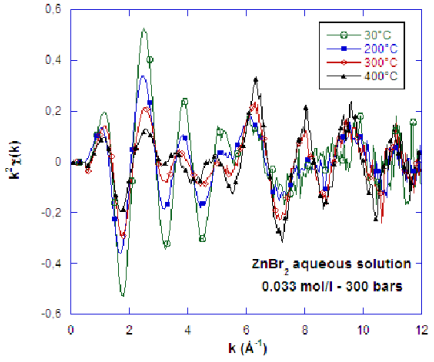

Figure 1 : $k^2?(k)$ EXAFS signals obtained at the Br K-edge in the fluorescence mode for the $ZnBr_2$ aqueous solution (concentration: 0.033 mol/l) at different temperatures (pressure: 300 bars).

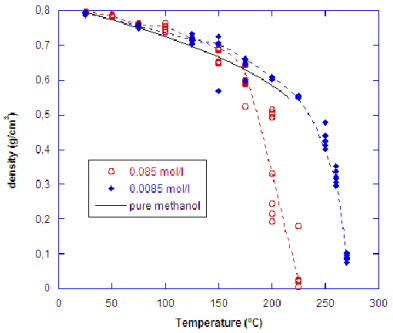

Figure 2: Absorption edge heights measured in the transmission mode for the $ZnBr_2$ methanol solutions at the Br edge, for two concentrations, 0.085 and 0.0085 mol/l, *vs* temperature (pressure: 100 bars). Heights have been normalized to pure methanol density at 25°C and are then compared to the solvent density (solid line).

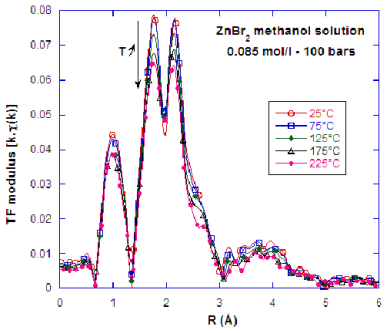

Fig. 3 : modulus of the k?(k) Fourier Transform signals obtained at the Br K-edge in the fluorescence mode for the $ZnBr_2$ methanol solution (concentration: 0.085 mol/l) at different temperatures (pressure: 100 bars).

References

[1] Argoud R. *et al.* "High pressure / high temperature cells for in situ structural investigations in geothermal conditions", *proceedings of the Réunion des Sciences de la Terre, Strasbourg* (2004)

[2] Simonet V. *et al.* "X-ray absorption spectroscopy studies of ionic association in aqueous solutions of zinc bromide from normal to critical conditions", *J. Chem. Phys.*, **117** (2002) 2771-2781

[3] Simonet V. *et al.* "Structure of aqueous ZnBr2 solution probed by X-ray absorption in normal and hydrothermal conditions", *J. Chem. Phys.*, **116** (2002) 2997-3006

ESRF	**Experiment title:** Thermal behaviour of xenon and krypton in uranium dioxide	**Experiment number:** 30 02 658
Beamline: BM30B	**Date of experiment:** from: 30-06-2004 to: 06-07-2004	**Date of report:** 30-08-2004
Shifts: 18	**Local contact(s):** O. Proux	*Received at ESRF:*

Names and affiliations of applicants (* indicates experimentalists):
*Philippe MARTIN, *Philippe GARCIA, *Carole VALOT, *Catherine SABATHIER, Michel RIPERT, Gaelle CARLOT
DEN/DEC/SESC/LLCC, CEA Cadarache, 13108 St Paul-lez-Durance, France

Frederico GARRIDO CNRS/CSNSM Orsay, France

Report:

The aim of this experiment was to study the thermal behaviour of xenon and krypton in uranium dioxide. the samples were polished UO_2 pellets implanted with Xe or Kr at a fluence of 10^{17} at.cm^{-2}. The heat treatments performed in a reducing atmosphere (Ar+10% H_2) at CEA Cadarache were : 800°C, 1000°C, 1200°C, 1400°C and 1500°C, with two hold times for each temperature: 2 and 12 hours.

All the measurements were performed at the Xe (34.56 keV) and Kr (14.32 keV) K edges with a 13 element fluorescence detector because at the experiment date the beamline's 30 element detector was not available. Acquisition was indeed longer than expected so the choice was to focus on Xe implanted samples. The measurements were performed at 11 K using a He cryostat. On one case, the He level in the experiment chamber dropped and some Xe K edge spectra were recorded at a higher temperature. The XAFS spectra obtained were completely flat: no EXAFS oscillation. On the same sample, once the He level reached its normal value, EXAFS oscillations were clearly observed. This accidental result demonstrates that when studying samples at the xenon K edge, experiments must be performed at or below 11 K.

The only results obtained from the fitting procedure that are presented here are those relative to the Xe implanted UO_2 samples, because previous experiments have enabled us to validate it. As regards Kr spectra, more effort is required in order to satisfactorily model and eliminate multi-excitation processes [1]. Figure 1 shows two Kr K edge XANES spectra of an as implanted sample and a sample annealed for 2 hours at 1200°C. A strong white line with weak EXAFS oscillations is seen in both cases. As described in [1,2] such features are characteristic of the presence of pressurised Kr inclusions. As expected, Kr atoms precipitate to form pressurised bubbles in UO_2. Based on a comparison of our results with those obtained by Di Cicco *et al.* [1], a Kr pressure in excess of 2.0 GPa is expected.

As regards the xenon spectra, our previous experiments [3] have enabled us to analyse these results in greater detail. Numerical values are obtained with Athena/Artemis software [4] using FEFF8.2 calculations.

The Fourier transform of k-weighted EXAFS spectra for an as implanted sample and two annealed ones ($2 \leq k \leq 7.5$ Å^{-1}) are shown in Figure 2. The narrow k interval is due to the poor signal to noise ratio relative to the as implanted sample.

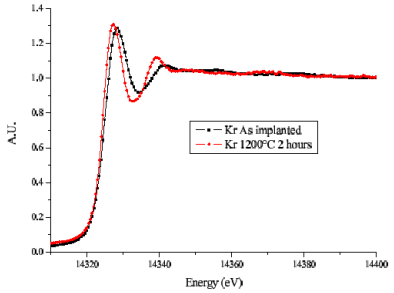

Figure 1 : XANES spectra obtained at the Kr K edge.

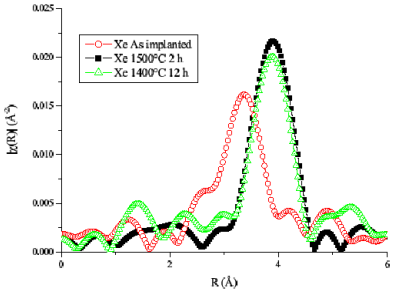

Figure 2 : Fourier transforms of the Xe K edge EXAFS spectra.

For each sample, only one coordination shell is clearly observed. For the as implanted sample the peak is broader and distance is shorter than for the two annealed samples. In each case, the peak is attributed to the presence of other surrounding Xe atoms. It is impossible to fit the experimental data by modelling Xe-U or Xe-O bonds. These results illustrate the fact that Xe is insoluble in UO_2 and readily forms aggregates (bubbles). A similar Xe-Xe distance appears to be observed for both annealed samples which could indicate a stabilisation of Xe aggregates. Furthermore, results of a PIXE analysis on sibbling samples have revealed xenon losses of 27% and 25% for the 1400°C and 1500°C samples respectively.

At 11 K, xenon precipitates in a cubic face centred crystal with a cell parameter of 6.20 Å. In this structure, the first coordination shell comprises 12 Xe atoms at 4.38 Å. Using the xenon equation of state, the pressure in the aggregates can be evaluated using the distance determined from the EXAFS fit. From the as-implanted spectrum, one can infer that each Xe atom is on average surrounded by 2.4±0.7 Xe atoms at a distance of 3.98±0.02 Å. The analysis of the spectra relative to the annealed samples reveals the presence around each Xe atom of 6±0.7 Xe atoms at 4.39±0.02 Å. One of the effects of the thermal treatments is clearly to reduce the pressure in the xenon aggregates. At these temperatures, inclusions would therefore be expected to contain xenon in a gaseous state.

These experimental results are highly relevant to the modelling of rare gas diffusion in UO_2. Indeed, by estimating the size distribution and concentration of gas bubbles resulting from these annealing conditions, it is then possible to estimate the fraction of gas atoms precipitated in bubbles. The remaining xenon atoms are then free to migrate in the bulk of the solid whence release is possible.

These experiments have demonstrated that the FAME beam line is particularly well suited for this subject. It is therefore planned to extend current research to the stability of rare gas bubbles under irradiation. This topic will make up the main part of our next application for beam time.

[1] A. D. Cicco, A. Filipponi, J. Itie and A. Polian, Physical Review B 54, 9086 (1996).
[2] A. Polian, J.P. Itie, E. Dartyge, A. Fontaine and G. Tourillon, Physical Review B 39, 3369 (1989).
[3] P. Martin, M. Ripert, G. Carlot and P. Garcia, ESRF BM8 experimental report ME 353, Febuary 2003 (2003).
[4] M. Newville, Synchrotron Radiation 8, 322 (2001).

ESRF	**Experiment title:** ÉTUDE EXAFS DE FILS ET BOITES QUANTIQUES DE SEMICONDUCTEUR III-V. XAFS STUDY OF III-V SEMICONDUCTORS QUANTUM WIRES AND QUANTUM DOTS	**Experiment number**:
Beamline:	**Date of experiment**: from: 18/06/03 to: 21/06/03	**Date of report**: 15/10/04
Shifts:	**Local contact(s)**: Dr. X. Biquard	*Received at ESRF:*

Names and affiliations of applicants (* indicates experimentalists):

Dr. Hubert RENEVIER*

Dr. Maria Grazia PROIETTI*

Dr. Jorge M. GARCIA

Dr. Michel GENDRY

Dr. Jean Michel GERARD

Dr. Luisa GONZALEZ

Dr. Cristelle MONAT

Report:

Preliminary measurements on a serie of GaN/AlN Quantum Dots (QDs) samples, were carried out at the CRG beamline FAME (BM30) (ref. n. 3002-636). EXAFS spectra were recorded in fluorescence mode at the Ga K-edge, with the polarization vector perpendicular to the surface, that is to the growth plane, along the [001] direction.

The samples consist of GaN/AlN QDs grown onto SiC substrates by MBE in the Modified Stransky-Kranstanov regime [1]. The QDs layer is capped by an AlN spacer layer. The sequence GaN QDs/AlN spacer is repeated 3, 10 and 78 times, as shown in Table I. The spacer layer thickness is about 7nm for samples s1582, s1580 and s1581 and 11nm for sample E242. The equivalent GaN thickness is 6ML for the first three samples and 4ML for the last one.

Depending on the AlN spacer, a strain driven correlation mechanism between each QDs layer and the layer underneath, can take place. In that case the QDs tend to pile up getting larger and more homogeneous in size. Samples S1580 and S1581 are supposed to be correlated whereas sample E242 is not.

The EXAFS analysis has been carried out by using the FEFF8 code, to generate theoretical phases and amplitudes, taking into account beam polarization. The Artemis package was used to fit theoretical signals to the experimental data. As an example, we show the best fit curves for sample E242 in Fig.1 and Fig. 2, compared to the experiment.

The *r*-spectra were filtered out in the range 0.5-3.3 Å and the fit performed in *k*-space. Six single scattering paths (SS) and four multiple scattering (MS) paths were found to be relevant in this range:

- $(Ga\text{-}N)_{//}$, in-plane, I shell path, corresponding to the three Ga-N bonds of the tetrahedron that are nearly in-plane ;
- $(Ga\text{-}N)_{\perp}$, out of plane, I shell path, corresponding to the fourth Ga-N bond of the tatrahedron, lying along c axis;

plane lattice parameter);

- $(Ga\text{-}Ga)_{\perp}$ II shell, out-of-plane path, corresponding to 6 Ga atoms at a distance that is a combination of *a* and *c*, $\{1/3\ a^2 + 1/4\ c^2\}^{1/2}$;
- (Ga-N), III shell path, corresponding to one N atom along c direction;
- (Ga-N), IV shell path, corresponding to 6 N nearly in-plane atoms;

The further MS paths consisted of triangular paths Ga-N-N and Ga-N-Ga.
(note: "in-plane" refer to the surface or growth plane)

We performed the fit by letting the lattice parameter *a* and *c* vary but mantaining the hexagonal cell symmetry, i.e. expressing all the interatomic distances of coordination shells, higher than the I one, as a function of a and c. The Ga-N first shell distances were let free to vary independently of a and c since, as it is well known, the Vegard's law is far from being valid for semiconductor alloys, in which the bond-bending mechanism is dominant compared to bond-stretching. The best fit parameters are shown, for the whole set of samples in Table I, where we also report, as a reference, the bulk and pseudomorphic values for GaN.
Starting from the fit results, we calculated the ε_{xx} $[(a_{sample}-a_{GaN})/a_{GaN})]$ and ε_{zz} values, $[(c_{sample}-c_{GaN})/c_{GaN})]$, that we sketch in Fig. 3 as ε_{xx} vs ε_{zz} and in fig. 4 as a function of the layers number.

We observe the following findings:

- the Ga-N first shell in-plane and perpendicular-to-plane distances show to be very close to each other, within the fit errors (0.01Å), in agreement with previous studies [2];
- the $(Ga\text{-}Ga)_{//}$ and $(Ga\text{-}Ga)_{\perp}$ II shell distances look to be diffferent, as expected due to the strain effect;
- the $(Ga\text{-}Ga)_{//}$,i.e. *a*, tends to contract as a function of the GaN layers number, approaching the AlN lattice parameter (3.11Å);

In Fig. 3 we compare the GaN elastic behaviour, i.e. ε_{zz}=- $2\varepsilon_{xx}(C_{13}/C_{33})$, with the experiment. We see that a subelastic trend looks to show. It could be related to the strong piezoeletric effect which tends to compensate the effect of strain, giving lower c values than expected from elasticity [3].

Nevertheless, the ε_x values look to be too high. We must note that the errors on $a_{//}$ are very large (0.06 Å), giving a corresponding large error on ε_x, as shown on Fig. 4. This is mostly due to the lack of data with the beam polarization parallel to the surface that would allow a much more precise determination of $a_{//}$. In addition, the quality of our XAFS spectra is quite poor, the *k*-space range had to be limited to about 10 $Å^{-1}$ due to the presence of numerous Bragg peaks and the signal-to-noise ratio should also be improved. Note that the GaN equivalent thickness is quite low, ranging down to only 6ML for the sample with one QDs layer.

	R1 (Ga-N) (Å)	$R2_{\perp}$ $(Ga\text{-}Ga)_{\perp}$ (Å)	$R2_{//}$: *a* $(Ga\text{-}Ga)_{//}$ (Å)	*c* (Å)	*c/a*
1L (S1582)	1,93	3,18	3,16 *(3,15)*	5,22	1,65
3L (S1580)	1,92	3,16	3,11 *(3,156)*	5,21	1,67
10L (S1581)	1,92	3,16	3,08 *(3,152)*	5,23	1,7
78L (E242)	1,92	3,16	3,08	5,24	1,7
GaN/AlN pseud.	*not available*	3,184	3,11	5,26	1,69
GaN bulk theor.	1,947	3,18	3,18	5,193	1,63

Table I: Best fit results for the measured samples. The statistical errors on the values reported range from 0.01 Å for R1 to about 0.06Å for $R2_{\perp}$, $R2_{//}$ and c. The values reported in parenthesis have been obtained by diffraction measurements

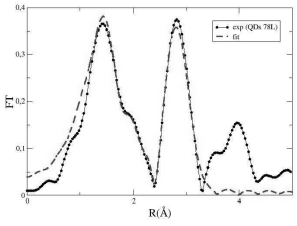

Fig. 2: *R-space best fit results for sample E242*

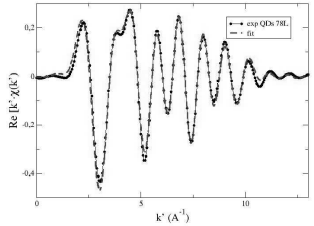

Fig. 1: *k-space best fit results for sample E242*

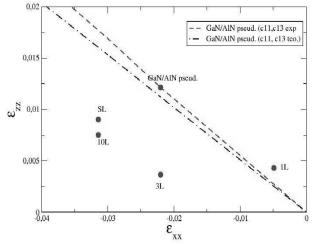

Fig. 3: ε_{zz} *as a function of* ε_{xx} *for the different samples (1L, 3L, 10L, 78L(SL))*

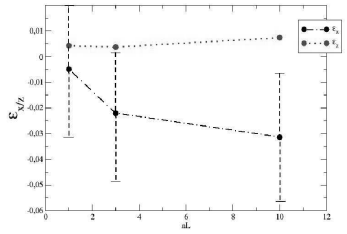

Fig. 4: ε_{zz} *and* ε_{xx} *as a function of the layers number*

In Table I we also show the $a_{//}$ values deduced by X-ray diffraction measurements on the same samples that show to be higher than the EXAFS values. This suggests, as expected, that EXAFS is probing different region of the samples with a uniform weight, that is not the case for diffraction. In particular the wetting layer, that is known to be, in the case of GaN SK growth, a quite consistent part of the total GaN amount (about 2MLs), and it is expected to be pseudomorphic to AlN.

Summarizing, we believe that these preliminary measurements show that EXAFS can provide use valuable information about a system that is being intensively studied and the structural properties of which have not yet been elucidated.

References :

[1] N. Gogneau, D. Jalabert, E. Monroy, T. Shibata, M. Tanaka and B. Daudin, J.Appl. Phys., **94,** 2254 (2003)
[2] F. D'Acapito, f. Boscherini, S. Mobilio, A. Rizzi, R. Lantier, Phys. Rev. B **66**, 205411 (2002)
[3] J. Gleize et *al*., Phys. Rev. B 63,073308 (2001)

ESRF

ESRF	**Experiment title:** Spéciation des éléments traces métalliques (Cr et Ni) dans les sols réunionnais : rôle des « nano-minéraux ».	**Experiment number:** 30-02-664
Beamline: BM30B	**Date of experiment:** from: 13 July 2004 to: 16 July 2004	**Date of report:** 15/10/04
Shifts: 9	**Local contact(s):** Vivian NASSIF (e-mail: nassif@polycnrs-gre.fr)	*Received at ESRF:*

Names and affiliations of applicants (* indicates experimentalists):

Dr Emmanuel DOELSCH[1]*, Dr Isabelle BASILE-DOELSCH[2]*, Dr. Armand MASION[3], Dr. Jérome ROSE[3]*

1. CIRAD-CA, Programme écosystèmes cultivés, Equipe REGARD, Station de La Bretagne, BP 20, 97408 SAINT DENIS Messagerie Cedex 9, Ile de la Réunion, France.
2. IRD-La Réunion (LSTUR) BP 172, 97492 Sainte-Clotilde cedex, Ile de La Réunion, France.
3. Géosciences de l'environnement – CEREGE Europole Méditerranéen de l'Arbois BP 80 13545 Aix en Provence Cedex 04, France.

Report:

L'utilisation du pouvoir épurateur des sols dans le cadre du recyclage de déchets organiques (ex : boues de station d'épuration, effluents agro-industriels, …) est un enjeu scientifique, technologique et économique majeur. Sa réussite repose sur la préservation optimale des milieux terrestres et aquatiques tout en garantissant l'innocuité des productions végétales. C'est pourquoi des normes d'épandage ont été établies afin de limiter la contamination des sols en éléments traces métalliques (ETM) et en polluants organiques (ex : décret n°97-1133 du 8 décembre 1997 relatif à l'épandage de boues de station d'épuration). Toutefois, ces normes qui ne tiennent pas compte des contextes géologiques, pédologiques et climatologiques sont souvent inadaptées aux conditions rencontrées dans les régions de l'hémisphère Sud. De par sa localisation, l'Île de la Réunion est à ce titre un exemple particulièrement intéressant que nous utilisons comme site d'étude.

Le substrat volcanique sur lequel se sont développés les sols réunionnais engendre des teneurs en Cr supérieures à celles imposées par la législation avant tout épandage. Il apparaît donc fondamental de déterminer la spéciation de ces éléments dont la toxicité a été démontrée afin d'évaluer leur mobilité et biodisponibilité potentielles.

Le but de notre projet est de caractériser la spéciation du Cr dans les différentes fractions organo-minérales d'un andosol (fractions obtenues après séparation physique densimétrique) naturellement riche en ETM (Cr= 462 ppm**).**

L'expérience a été conduite du 13 au 16 juillet 2004 sur la ligne française FAME (XAS CRG BM-30b). Pour l'analyse du chrome, un moniochromateur du type Si (220) a été utilisé. Les spectres d'absorption ont été enregistrés en fluorescence par un détecteur (Ge) 13 éléments (le détecteur 30 éléments étant en réparation) lorsque les échantillons étaient dilués et en transmission lorsque les échantillons étaient concentrés (espèces de référence).

Tout d'abord, il est important de souligner que l'asservissement du second cristal du monochromateur par la mise en place d'un système piezoélectrique améliore très nettement la qualité des spectres en diminuant le bruit de fond. Le spectre de la chromite (fig.1) enregistré avec un temps de comptage de 2 secondes par point atteste de l'excellente qualité des spectres (spectre acquis en moins de 30 minutes). Des structures fines sont visibles jusqu'à 14,5 Å-1 sans perturbation liée au bruit.

Pour une telle étude, il était important d'enregistrer tout d'abord les spectres (XANES et EXAFS) de références minéralogiques représentatives des minéraux constitutifs des sols réunionnais.

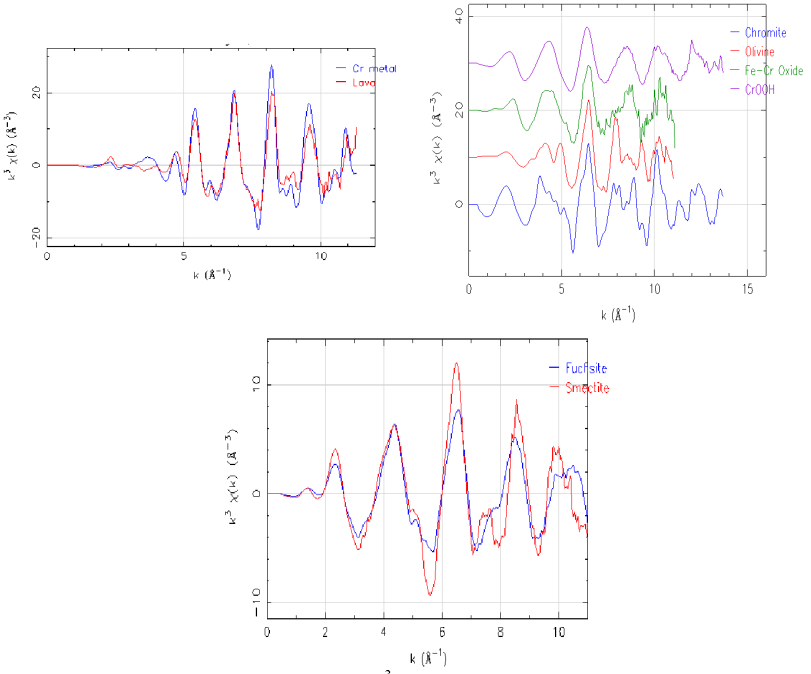

Figure 1 : spectres EXAFS ($k^3\chi(k)$) des références minéralogiques.

Comme les roches mères réunionnaises sont d'origine volcaniques, nous avons étudié le Cr au sein de 2 laves aux teneurs contrastées : lorsque les laves sont riches en Cr(~1000 ppm), il est présent sous forme d'inclusion de spinelle (ech. Chromite) au sein des olivines qui forment des phénocristaux (ech. Olivine). Si les laves sont pauvres en Cr (<500 ppm), les olivines sont absentes et le spectre EXAFS (ech. lava) est très proche de celui du Cr métal. Enfin, pour compléter la gamme des références minéralogiques, nous avons enregistré des spectres d'un oxyde Fe-Cr, de CrOOH, de la fuchsite (variété de muscovite) et d'une smectite riche en Cr (cf. Figure 1).

L'acquisition des spectres EXAFS des différentes fractions organo-minérales de l'andosol ont été enregistrés au seuil K du Cr. Mais, comme le montre la Figure 2, les seuils LII de Ce et le seuil LIII de Nd sont présents.
La résolution des détecteurs de fluorescence (200 eV au mieux) ne permet pas de séparer les raies de fluorescence de Ce, Nd (env. 5200 eV) et Cr (5400 eV et 5900 ev).

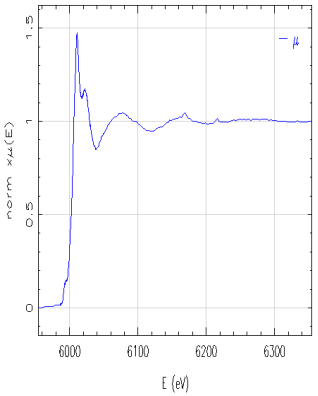

Figure 2 : spectre d'absorption de l'andosol

Comme le montre la Figure 3, la présence de ces éléments, même en quantité très faible par rapport au Cr, risquent de poser des problèmes pour l'interprétation des spectres EXAFS.

Malgré, la présence de Ce et Nd, nous sommes actuellement en train d'étudier ces spectres en les comparant avec ceux des références minéralogiques. Ceci est facilité par la connaissance fine que nous avons de la minéralogie de chacune des fractions.

Enfin, par rapport au projet initial, nous devons souligner que par manque de temps, il nous a été impossible d'étudier ces mêmes échantillons au seuil K du Ni. Etant donné la résussite des expériences conduites au seuil K du Cr et ceci malgré les faibles concentrations de nos échantillons, une nouvelle demande de temps de faisceau pourrait être déposer prochainement.

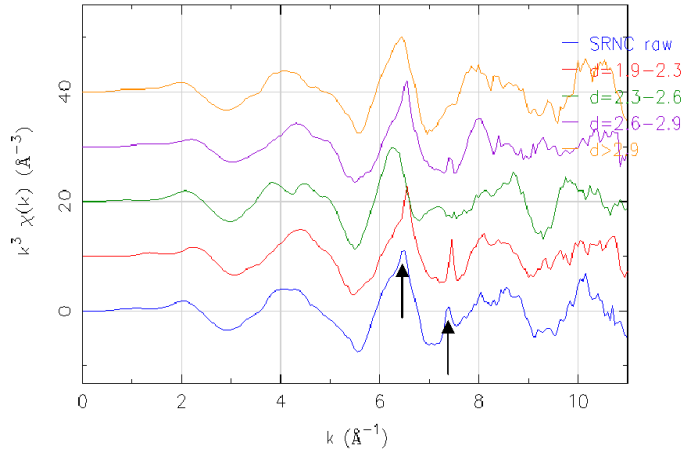

Figure 3 : spectres EXAFS ($k^3\chi(k)$) de l'andosol brut (SRNC raw) et des différentes fractions organo-minérales séparées par densimétrie (d=1,9-2,3 ; d=2,3-2,6 ; d=2,6-2,9 et d>2,9).

ESRF	**Experiment title:** **Spéciation des métaux au sein d'aérosols émis par des unités sidérurgiques et incinérateurs : cas d'As et Cd** Speciation of metal in aerosol emitted by metallurgic plants and incinerators : As and Cd case	**Experiment number:** **30-02-668**
Beamline: BM30B FAME	**Date of experiment:** from: JULLY 16TH to 19th 2004	**Date of report:** 26-09-04
Shifts: 9	**Local contact(s):** Jean-Louis Hazemann	*Received at ESRF:*

Names and affiliations of applicants (* indicates experimentalists):
Yves NOACK[1*], Francois BERHO[2], Daniel BORSCHNECK[1], Magali COLLET[1*], Olivier DONARD[3], Jérome Rose[1*]
1-Géosciences de l'environnement – CEREGE Europole Méditerranéen de l'Arbois BP 80 13545 Aix en Provence Cedex 04 France; 2- LECES - BP 40223 57282 MAIZIERES LES METZ CEDEX; 3- LCBIE - Université de Pau -Helioparc - 2 Av Président Angot - 64000 Pau

Report:

Introduction

Le problème de la pollution atmosphérique est au cœur des préoccupations des citoyens. Cette inquiétude est à l'origine de la mise en place de nouvelles réglementations et contrôles imposés par les autorités. Ainsi, il est demandé aux industriels émetteurs d'aérosols, d'évaluer l'impact sanitaire des poussières. Or, Il a été clairement démontré, en particulier pour les métaux que ce sont les formes chimiques d'un élément qui gouvernent ses propriétés toxicologiques, ses modes de transfert, et de bio-accumulation dans l'environnement. Dès lors, il devient nécessaire, tant d'un point de vue sanitaire qu'environnemental d'obtenir une caractérisation fine des formes chimiques des espèces métalliques émises par les principaux émetteurs industriels.

Dans ce contexte général, un programme est mené par le CEREGE avec l'appui de Sollac et de l'ADEME sur l'étude de la spéciation des éléments métalliques des aérosols d'une zone industrielle. Les émetteurs ciblés dans le cadre du projet sont deux étapes représentatives de l'élaboration de l'acier (usine d'agglomération pour la filière intégrée et aciérie électrique pour la filière électrique) et une importante Usine d'Incinération d'ordures ménagères (UIOM de Toulon). Lors de cette expérience, la spéciation du cadmium a été étudiée sur des aérosols d'usine d'agglomération. Une étude sur cet élément avait déjà été effectuée en 2003, mais du fait des très faibles teneurs en cadmium et d'un rapport signal/bruit relativement élevé, (le système piézoélectrique n'étant pas encore installé), les temps d'acquisition étaient très longs, et ne permettant de passer que très peu d'échantillons. L'expérience EXAFS menée en juillet 2004 s'inscrit donc dans la continuité de cette étude.

L'expérience a été conduite du 16 au 19 juillet 2004 sur la ligne française FAME (XAS CRG BM-30b). Pour l'analyse du cadmium, un cristal Si (220) a été utilisé. Les spectres d'absorption ont été enregistrés en fluorescence par un détecteur (Ge) 13 éléments (le détecteur 30 éléments étant en réparation) lorsque les échantillons étaient dilués et en transmission lorsque les échantillons étaient concentrés (espèces de référence). Les poussières d'usine d'agglomération ont été prélevées en cheminées après le système de filtration et avant leur rejet dans l'air, selon la norme XP-X4-051. Les poussières issues de l'aciérie (filière intégrée) ont été recueillies à la trémie du dépoussiéreur. Les concentrations en cadmium variaient entre 500 et 1000 ppm. Les spectres ont été enregistrés de –100 à 800 eV autour du seuil d'excitation du Cd avec un pas d'environ 1 eV. Une dizaine de spectres a été enregistrée sur chaque échantillon pour une bonne représentation statistique.

L'asservissement du second cristal par la mise en place d'un système piezoélectrique améliore la qualité des spectres en diminuant le bruit de fond et en augmentant la résolution. La comparaison entre les spectres EXAFS d'espèces de référence enregistrés en 2003 et 2004 montre clairement que le système piézoélectrique entraîne une nette amélioration du signal dans le cas du chlorure de cadmium (Figure 1) et du carbonate de cadmium (Figure 2).

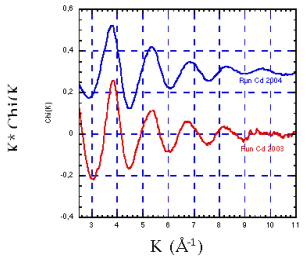

Figure n°1 : Comparaison des spectres EXAFS pour le CdCl2 avant (Run 2003) et après (Run 2004) la mise en place du système piezoélectrique.

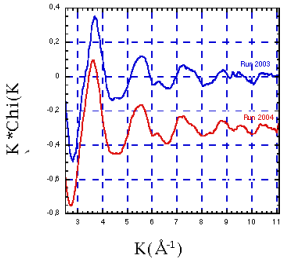

Figure n°2 : Comparaison des spectres EXAFS pour le CdCO3 avant (Run 2003) et après (Run 2004) la mise en lace du système piezoélectrique.

Lors de l'acquisition, les spectres d'absorption des échantillons présentaient deux glitches importants à 12 et 13 angströms dus à la présence d'harmoniques parasites. Ces glitches ne nous ont pas permis d'analyser les spectres EXAFS pour des valeurs de k supérieures à 11.5 $Å^{-1}$. Malgré ce problème la qualité des spectres enregistrés cette année nous a pleinement satisfait.

Les premiers résultats portant sur l'étude de la spéciation du cadmium dans les poussières issues de l'usine d'agglomération montrent une forte ressemblance avec l'espèce CdCl2 (figure n°3), alors que les poussières d'aciérie présentent une spéciation du cadmium se rapprochant plutôt d'une espèce carbonatée (figure n°4) pouvant indiquer que le cadmium présente une spéciation spécifique de chaque émetteur. Ces résultats sont en accords par les extractions chimiques séquentielles appliquées à ces mêmes échantillons. Elles permettent, d'étudier le comportement des métaux lourds, notamment leur

solubilité et donc leur potentiel de toxicité, lors de lixiviations successives d'un échantillon. Aussi, pour les poussières d'agglomération, les résultats ont montré que le cadmium est très facilement soluble et se rapproche donc d'un sel ou d'un sulfate. Le cadmium contenu dans les poussières d'aciérie présente deux phases de solubilités principales conduisant à penser qu'il est associé à une phase très soluble (sel ou sulfate) et une autre carbonatée.

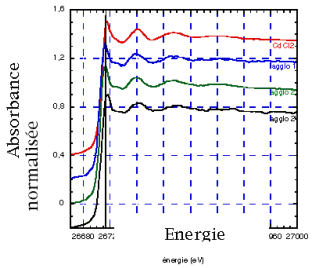

Figure n°3: Comparaison des spectres d'absorption de poussières d'usine d'agglomération avec CdCl2.

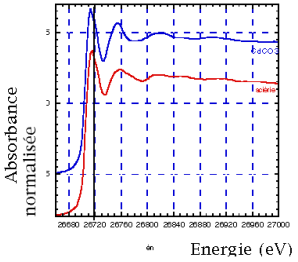

Figure n°4 : Comparaison des spectres d'absorption de poussières d'aciérie avec CdCO3.

Ces premiers résultats indiquent que le cadmium se trouve donc sous des formes relativement solubles et mobiles et que la spéciation varie en fonction du type d'émetteur industriel. Les modélisations des spectres EXAFS sont en cours.